Université d'Ottawa · University of Ottawa

Université d'Ottawa · University of Ottawa

FACULTÉ DES ÉTUDES SUPÉRIEURES ET POSTDOCTORALES

FACULTY OF GRADUATE AND POSTDOCTORAL STUDIES

Xiaohong WANG

AUTEUR DE LA THÈSE - AUTHOR OF THESIS

M. A. Sc. (Mechanical Engineering)

GRADE - DEGREE

Department of Mechanical Engineering

FACULTÉ, ÉCOLE, DÉPARTEMENT - FACULTY, SCHOOL, DEPARTMENT

TITRE DE LA THÈSE - TITLE OF THE THESIS

Free Vibration and Stability of Complete Orthotropic Toroidal Shells

D. Redekop

DIRECTEUR DE LA THÈSE - THESIS SUPERVISOR

CO-DIRECTEUR DE LA THÈSE - THESIS CO-SUPERVISOR

EXAMINATEURS DE LA THÈSE - THESIS EXAMINERS

R. Singhal

X. Wang

J.-M. De Koninck, Ph.D

LE DOYEN DE LA FACULTÉ DES ÉTUDES SUPÉRIEURES ET POSTDOCTORALES

DEAN OF THE FACULTY OF GRADUATE AND POSTDOCTORAL STUDIES

FREE VIBRATION AND STABILITY OF COMPLETE ORTHOTROPIC CIRCULAR TOROIDAL SHELLS

X.H. Wang

A thesis submitted to the

Faculty of Graduate and Postdoctoral Studies

in partial fulfillment of the requirements

for the degree of

MASTER OF APPLIED SCIENCE

in Mechanical Engineering

UNIVERSITY OF OTTAWA

Your file Votre référence
ISBN: 0-494-01634-5
Our file Notre référence
ISBN: 0-494-01634-5

Abstract

This study makes contributions in the areas of vibration and stability analysis of complete orthotropic circular toroidal shells. It is conducted in four main parts. A literature survey is first carried out indicating the new and continuing uses of toroidal shells in engineering structures. Secondly, theory is developed for the free vibration analysis of toroidal shells using the differential quadrature method. Numerical results are determined using the method for shells with small bend to cross-section radius ratios, and compared with finite element results. Thirdly, theory is developed using the Rayleigh-Ritz method for the free vibration analysis of toroidal shells having large bend to cross-section radius ratios. A parametric study of such shells including orthotropic and ring-stiffened isotropic ones is conducted using the finite element method. Finally, theory is developed using the Rayleigh-Ritz method for the linearized buckling analysis of toroidal shells with large bend to cross-section radius ratios. Numerical results are found for orthotropic and ring-stiffened isotropic shells using the finite element method. All theoretical work is carried out within the confines of the first-order Sanders-Budiansky shell theory. The work ends with an appropriate set of conclusions.

Acknowledgements

I am most grateful and indebted to my supervisor, Dr. D. Redekop, for his invaluable suggestions that led to my selection of this thesis, his penetrating vision that guided me moving forward, his enthusiasm toward this research area that made me feel this research enjoyable, and his patient, continuous encouragement.

I would like to thank all the members of the Department of Mechanical Engineering who made contributions towards my studies and research.

Special thanks go to my parents and brothers and sisters for their encouragement during my study.

The financial support provided by the Natural Sciences and Engineering Research Council of Canada is gratefully acknowledged.

Contents

List of Tables

List of Figures

Nomenclature

$a_k\pi$	circumferential distance of the *k*th stiffener
A_1, A_2	Lamé parameters
A_k	cross sectional area of the *k*th ring stiffener
$\overline{A}_k$	nondimensional cross sectional area of the *k*th ring stiffener, defined by $\overline{A}_k = \dfrac{A_k}{r^2}$
e_k	the distance between the centroid of the cross-section of the *k*th stiffener and the shell mid-surface
E , E_k	Young's modulus for isotropic toroidal shell, and the *k*th stiffener, respectively
$\overline{E}_k$	nondimensional modulus of elasticity of the *k*th stiffener, defined by $\overline{E}_k = \dfrac{E_k}{E}$
E_ϕ, E_1	Young's moduli in the meridional (ϕ) directions for orthotropic material
E_θ, E_2	Young's moduli in the circumferential (θ) directions for orthotropic material
G, G_k	shear modulus for isotropic toroidal shell, and the s *k*th stiffener, respectively
$\overline{G}_k$	nondimensional shear modulus of the *k*th stiffener, defined by $\overline{G}_k = \dfrac{G_k}{G}$
$G_{\phi\theta}, G_{12}$	shear moduli for orthotropic toroidal shell
G_{ij}	sub-geometry-matrix of the shell

h	thickness of toroidal shells
i, j, k	Cartesian unit vector
I_k	second moment of area of *k*th stiffener
$\overline{I}_\eta$	in plane, nondimensional moments of inertia of the *k*th stiffener, defined by $\overline{I}_\eta = \dfrac{I_{\eta k}}{r^4}$
$\overline{I}_z$	out of plane, nondimensional moments of inertia of the *k*th stiffener, defined by $\overline{I}_z = \dfrac{I_{zk}}{r^4}$
J_k	torsional constant of *k*th stiffener
$\overline{J}_k$	nondimensional torsional constant of *k*th stiffener, defined by $\overline{J}_k = \dfrac{J_k}{r^4}$
K_{ij}	sub-stiffness-matrix of the shell
K_{kij}	sub-stiffness-matrix of *k*th stiffener
M_{ij}	sub-mass-matrix of the shell
m	circumferential harmonic
M, N	truncation integers
$M_\phi, M_\theta, M_\eta, M_{\phi\theta}, \overline{M}_{\theta\eta}$	bending stress resultants
$N_\phi, N_\theta, N_\eta, N_{\phi\theta}, \overline{N}_{\theta\eta}$	membrane stress resultants
p	external pressure
q_1, q_2	orthogonal coordinate system
Q_ϕ, Q_θ	transverse shear resultants

r	radius of cross-section
$\mathbf{R}$	radius vector
R_1, R_2	principal radii of curvatures
R	bend radius
t	time
$T_{\max}$	maximum kinetic energy
u, v, w	displacement components
u_k, v_k, w_k	displacement components of the shell at the position $\eta = a_k\ \pi$ of the kth stiffener
u_n, v_n, w_n	unknowns Ritz coefficients
u_k^s, v_k^s, w_k^s	displacement components of kth stiffener
$\ddot{u}, \ddot{v}, \ddot{w}$	acceleration components
U, V, W	displacement components
$\overline{U}$	strain energy of the shell
$\overline{U}_k$	strain energy of kth stiffener
$\overline{V}$	potential energy of the shell
$\overline{W}$	work done by the external pressure
x, y, z	Cartesian coordinates
α_1, α_2	Lamé parameters
γ	radius ratio, defined as r/R
$\varepsilon_\phi, \varepsilon_\theta, \varepsilon_\eta, \varepsilon_{\phi\theta}, \varepsilon_{\theta\eta}$	strain components of toroidal shell

ζ	parameter, defined as $\zeta = 1 + \gamma \cos\theta$;
η	circumferential angular coordinate, defined by ϕ / γ
θ	meridional angular coordinate
$\kappa_\phi, \kappa_\theta, \kappa_\eta, \kappa_{\phi\theta}, \kappa_{\theta\eta}, \kappa_1, \kappa_2$	curvature components of toroidal shell
λ	frequency parameter, defined by $\lambda = \rho r^2 h \omega^2$
$\bar{\lambda}$	critical buckling parameter, defined by $\bar{\lambda} = p/2$
μ_m	parameter, defined as $\mu_m = m\pi \gamma / \varphi$
ν	Poisson's ration of isotropic toroidal shell
$\nu_\phi, \nu_\theta, \nu_1, \nu_2$	Poisson's ration of orthotropic toroidal shell
ξ_1, ξ_2	orthogonal coordinate system
Π	total potential energy of the shell
ρ	mass density
$\bar{\rho}$	nondimensional constant of radius ratio, defined as R/r
$\bar{\rho}_k$	nondimensional mass density of the kth stiffener
ϕ	circumferential angular coordinate
ϕ_θ, ϕ_η	rotation of the toroidal shell
φ	the shell angular length (Fig. 4-1)
ω	natural frequency
Ω	frequency parameter, defined by $\Omega = \rho h \omega^2$

Chapter 1

Introduction

1.1 Toroidal shells

Shells are familiar enough in nature. They have many useful properties. When suitably designed, even very thin shells can support large loads. Thin-walled curved structural elements in the form of general shells have become very common in engineering practice.

Toroidal shells are one of the typical thin-walled structures. They have been playing an important role in engineering structures for a long time. Many factors, including cost and weight economy in construction, development of new materials and processes and the growth of increasingly powerful methods of analysis, have contributed to the increase in the uses of toroidal shell structures. Their applications to satellite antenna support structures, diver's oxygen tanks, nuclear reactors and underwater structures, submarine reinforcement, oil rigs, storage vessels, spacecraft, rocket fuel tanks, etc. are noteworthy. They are also quite useful and efficient for pressure vessel applications. Segments of toroidal shells are frequently used as transitions between cylindrical tanks and shallow spherical or flat caps. Toroidal shapes have been regarded as superior substitutes to the existing, highly imperfection-sensitive, standard shapes. Especially, for some applications the toroidal shapes give the optimum configurations, like the vacuum vessels used for fusion reactors, the Tokamak breeder reactor vessel, the Stanford Torus, the support structure for underwater drilling rig, the circular pipes as the reinforcement for submarines, the energy absorbing devices for a nuclear waste transport packaging and the toroidal shell roof used in the Gatesheads Sage Music Centre. A summary of some applications of toroidal shells with the shell geometries and the material properties is given in Table 1-1. In this table the R represents the bend radius of the toroidal shell, r the cross-sectional radius and h the wall thickness.

With present trends in engineering towards higher temperatures and pressures, problems associated with the design and safety assessment of toroidal shells structures have become correspondingly more complex and challenging. It is an essential part of the analysis to determine their vibration and stability characteristic under various conditions.

There are many numerical methods available for shell vibration and stability analysis, such as, finite difference method (FDM), finite element method (FEM), boundary element method (BEM), differential quadrature method (DQM), Rayleigh-Ritz method (RRM), etc. Among these methods, the FDM is a purely mathematical technique. The equations of motion have to be known for the structure that is to be investigated. By contrast, the FEM does not require knowledge of the differential equations of motion, once the element stiffness, geometry and mass matrices are defined. The BEM, also commonly known as the boundary integral equation (BIE) method, is an efficient alternative to the FEM, particularly for problems requiring the resolution of high stress gradients, such as those found near stress concentrations and cracks. The DQM is a powerful numerical method for the study of vibration and stability of the structures. The basis of DQM is the representation of the derivatives of a function $f(x)$ by a weighted sum of the function values at sampling points in the domain. The RRM is extremely useful for the analyses of stiffened shell structures and structures with simple boundary conditions.

In this study the first-order Sanders-Budiansky [Sanders, 1959] [Budiansky, 1968] linear thin shell theory is used as a main tool of study. The theoretical solutions are developed using the DQM and RRM, and numerical results found using the DQM and FEM. The fundamental principles of each of these methods are described in the following.

1.2 Shell theories

Essentially, a structural shell is a body bounded by two curved surfaces, with the behavior of the shell being governed by the membrane and bending properties of an appropriate reference surface. The transformation of the three-dimensional elasticity equations into an approximate system of two-dimensional shell equations is an essential feature of any shell theory. In a shell, the membrane and the bending behavior are coupled. The coupled deformations in the form of stretching and curvature change of the reference surface are required in predicting the strains existing throughout the shell space. Both the theory and analysis of shells have always presented challenges to the researchers in this area. The so-called "thin shell theory" is firmly established in the literature and is used extensively in analytical solutions and numerical analysis [Novozhilov, 1959] [Flügge, 1967] [Kraus, 1967].

The most common shell theories are those based on linear elastic concepts. Linear shell theories adequately predict stresses and deformations for shell exhibiting small elastic deformation, that is, deformations for which it is assumed that the equilibrium equation conditions for deformed elements are the same as if they were not deformed. Additionally it is necessary that Hooke's law applies. The nonlinear theory of elasticity forms the basis for the finite deflection and stability theories of shells. Large-deflection theories are often required when dealing with shallow shells, highly elastic membranes, and to derive the linearized theory to solve buckling problems.

The shell theory of Sanders is considered one of the most accurate first-order theories. The basic assumptions and conditions for validity of the Sanders theory are discussed by Sanders [1959]. This theory is adapted for the current study. The details of this theory are discussed in chapters 3, 4 and 5.

1.3 Differential quadrature method

The DQM is a relatively new numerical technique for solving differential equations. This approach, which transforms governing equations of differential form to matrix form by using weighting matrices, is a computationally efficient method. The DQM requires small amount of computer capacity and is able to provide accurate results. It expresses a derivative at a point as a weighted linear sum of the function values at all the discrete sampling points. The determination of the weighting functions plays an important role in DQM analysis.

The first step in the DQM approach is the definition of a grid of sampling points covering the domain, including the boundary. Then the three displacement components at each of the sampling points of the grid together with the frequency or the buckling load parameters constitute the unknowns of the problem. The second step in the DQM approach is the replacement of all derivatives with series of terms that contain the product of the displacement functions at the sampling points and the weighting coefficients. The weighting coefficients are determined a priori for some appropriately chosen set of test or trial functions. The details of this approach are given in chapter 3.

1.4 Rayleigh-Ritz method

The RRM has proven to be a popular and powerful technique based on the stationarity of the total potential with respect to kinematically admissible variations in the displacements.

The RRM [Guarracino, Walker, 1999] for solids and structures consists of the following main steps:

(1) Write the functional of the total potential energy of the system.

(2) Choose a trial function for the displacement field; the function must satisfy the geometrical boundary conditions but it may or may not satisfy the mechanical boundary conditions (i.e. regarding stresses or resultants). This shape function is defined for the entire domain and must be dependent on a finite number of parameters (Ritz coefficients).

(3) Insert the trial function into the potential energy functional and integrate over the domain of the structure.

(4) Minimize the obtained function with respect to the parameters to get a linear system of equations in the unknowns.

(5) The solution of the linear system defines the value for the parameters of the shape functions and thus provides the approximate solution to the problem of elastic equilibrium at hand.

This method is easily extended to cover problems of vibration and stability.

1.5 Finite element method

The FEM has become one of the most powerful techniques in applied mechanics. It is used to solve physical problems in engineering analysis and design.

The FEM combines several mathematical concepts to produce a system of linear or nonlinear equations and has two characteristics that distinguish it from other numerical procedures:

(1) The method utilizes an integral formulation to generate a system of algebraic equations.

(2) The method uses continuous piecewise smooth functions for approximating the unknown quantity or quantities.

In this method a mathematical model is generated by subdividing the actual structure into a finite number of small regions called elements. Within an element displacements and stresses are approximated using polynomial shape functions. An element is connected to adjacent elements at a finite number of points called nodes. Interaction among elements is solely through the forces they exert at the nodes. Element material properties and geometry are used to generate the stiffness of the entire structure, discretized at the nodes. Known loads acting on the structure are represented as forces, also at the nodes. The solution requires using these known loads and stiffnesses to solve for unknown displacements. The displacements are then used to find element results such as force per unit length, stress, strain, etc.

Various commercial computer codes based on the theory of finite elements are available. One software ADINA [ADINA, 2003] is used to carry out the FEM analysis in the current study. The nine-node shell element is used in vibration and linearized buckling analysis of toroidal shells. Results obtained from ADINA are presented in chapters 3, 4 and 5 and used to validate the results from other numerical methods, as well as to provide main results.

1.6 Orthotropic materials

With structural materials becoming more complex in engineering practice, there is a demand for shells made of anisotropic, orthotropic, or transversely isotropic materials. In this study there is an emphasis on orthotropic shells. These shells have different elastic properties in three mutually perpendicular directions, and have three planes of symmetry with respect to the elastic properties. There are generally five parameters for an orthotropic thin shell as opposed to two parameters in an isotropic thin shell. In general, orthotropic materials are more efficient than isotropic ones, not only because they have a higher stiffness to weight ratio, but also because they are less sensitivity to initial imperfections [Jones, 1975].

1.7 Objective of this thesis

The objective of this study is to develop theory and present numerical results for the problems of vibration and stability of complete orthotropic toroidal shells. The first-order Sanders-Budiansky [Sanders, 1959] [Budiansky, 1968] thin shell theory is used as the theoretical basis. Numerical results are obtained using the DQM and/or the FEM. The theory for the vibration and stability of stiffened toroidal shells using the RRM is also presented.

In Chapter 2, a literature survey is presented which includes the description of previous work on vibration and buckling of toroidal and other shells. It is carried out indicating the new and continuing uses of toroidal shells in engineering practice. The DQM, RRM and FEM are also discussed in this chapter.

Chapter 3 presents a free vibration study of complete orthotropic toroidal shell with small bend to cross-section radius ratios. Numerical results from the DQM and FEM are presented and compared with previously published results.

Chapter 4 is focused on the free vibration analysis of orthotropic and stiffened isotropic toroidal shells with large bend to cross-section radius ratios. The RRM is applied to derive the expressions for stiffness matrix and the mass matrix. Numerical results are presented from the DQM for unstiffened shells and from the FEM for stiffened shells.

The stability of complete orthotropic toroidal shells with large bend to cross-section radius ratios is studied in Chapter 5. The RRM is applied to derive expressions for the stiffness and the geometric matrices. Numerical results are obtained using the FEM and compared with previously published results. The performance of shells with various stiffener arrangements is also studied.

In Chapter 6 conclusions are presented as well as some suggestions for further research.

Chapter 2

Literature survey

2.1 Introduction

A shell is a continuum that is bounded by two curved surfaces which are separated by a distance referred to as the thickness. When the thickness is about ten percent or less of the principal radii of curvatures of the bounding surfaces, the shell is said to be thin. As discussed in chapter 1, the most common shell theories are those based on linear elasticity concepts. The various linear shell theories can be classified into four basic categories:

(1) First-order-approximation shell theory

(2) Second-order-approximation shell theory

(3) Specialized theories for shells

(4) Membrane shell theory

The shell theories of the first three categories mentioned above are generally referred to as "bending" theories of shells because their development includes the consideration of the flexural behavior of shells. If in the study of equilibrium of a shell, all flexural expressions are neglected, the resulting theory is a so-called "membrane" theory of shells [Baker et al, 1972].

The shell theory of Sanders [1959] is considered one of the most accurate first-order theories and is thus adopted for the current study. The details of this theory are given in the next three chapters.

2.2 Vibration of shells

Vibration problems in structures of various shapes and configurations have been extensively studied in the past hundred years or so. Two very early studies on the subject of shell structures, by Rayleigh and Love [Soedel, 1993] respectively, dealt with the subject of vibration.

Two distinguished monographs on shell vibration analysis are those of Leissa [1973] and Soedel [1993]. Leissa's monograph is dedicated to the organization and summarization of knowledge existing in the field of shell vibrations. He compared results obtained from the popular shell theories including those of Love and Timoshenko, Byrne and Flügge, Vlasov, Reissner, Berry and Naghdi, Sanders, Donnell, and Flügge. In Soedel's book, details are given about the fundamental thin shell theories and their applications. He also provided some significant new material, which reflects the latest developments in this field.

2.3 Vibration of toroidal shells

With structures becoming more complex, the toroidal shells have gained in popularity. Research on toroidal shells began a half century ago. Clark [1950] established the theory of thin elastic toroidal shells. Later in a series of studies, Sanders and Liepins [1963] investigated the toroidal membrane under uniform pressure. Their approach was improved by Rossettos and Sanders [1965] who used both the nonlinear membrane theory and the bending theory. Liepins [1965] studied the free vibrations of prestressed toroidal shells. His research was based on the linearized shell theory and applied Fourier series expansions in the circumferential direction and finite difference approximations in the meridional direction. Balderes and Armenakas [1973] first investigated the free vibration of ring-stiffened isotropic toroidal shells using the Love-Reissner shell theory. The frequencies together with the corresponding mode shapes were obtained for a range of shell parameters and ring properties. Using a toroidal shell with holes as an example, Gavelya and Kononenko [1975] calculated the Green's matrices used to determine the stress-strain state of shells in 1973. Kosawada et al [1985] presented the free vibration of thin and thick toroidal shells with circular cross-section. They used the stationary condition of the Lagrangian of the toroidal shell for the equations of motion and the boundary conditions. These equations were solved exactly by a power series expansion.

Yamada et al [1989] presented the solution to the free vibration problem of a toroidal shell with elliptical cross-section using the transfer matrix approach. They demonstrated that this approach was a very useful approach for solving vibration problems of shells of revolution numerically. Leung and Kwok [1994] studied a 90-degree-bend curved pipe based on Donnell-Mushtari-Vlasov [Niordson, 1985] thin shell theory, Fourier's series and Galerkin's method. Redekop [1994] determined the natural frequencies of a short curved pipe for shear diaphragm supports based on the Mushtari-Vlasov-Donnell assumptions. Huang et al [1997] used the linear elastic Sanders shell theory to solve the problem of the free vibration of a curved pipe with rigid diaphragm end supports. Redekop and Xu [1999] studied the vibration of toroidal panels using the differential quadrature method.

A new application for toroidal shells is in satellite antenna support structures which consist of inflatable toroidal shells. Studies of this application include those of Lewis and Inman [2001] who studied the structural dynamics and vibration suppression via piezoelectric actuators of an inflatable torus. Park et al [2001] studied the integration of smart materials into dynamics and control of inflatable space structures. In their study, an experimental investigation of vibration testing and control of an inflated thin-film torus was presented.

Ming et al [2002] studied experimentally the free vibrations of a 90^0 elbow pipe under different boundary conditions. Solutions based on the linear Sanders thin shell theory were also given. Salley and Pan [2002] presented the modal characteristics of curved pipes (sectorial toroidal shells). Finite element procedures were employed to investigate the dynamic behavior of curved pipes, specifically resonance frequencies and mode shapes. Experimental and theoretical procedures were employed to verify finite element results in their study. Li and Cook [2002] investigated fiber overwrapped toroidal vessels using membrane theory. These shells were used as an attractive alternative storage container of the compressed air used in breathing apparatus for divers. In a study by Jha and Inman [2002], the piezoelectric patches were attached to an inflated toroidal shell and used as actuators and sensors. Based on Sanders linear shell theory, a study of the stiffness and mass effects of the piezoelectric patches was performed using a frequency response function. Jha et al [2002] studied the free vibration analysis of an inflated toroidal shell using the shell theory of Sanders, which included the effect of pressure.

Tzou and Wang [2003] studied the vibration control of toroidal shells with parallel and diagonal piezoelectric actuators. In this study, dynamics and control effectiveness of toroidal shell panels laminated with distributed piezoelectric sensor layers were presented. Jiang and Redekop [2003] presented the static and vibration analysis of orthotropic toroidal shells of variable thickness by the differential quadrature method. In this study, solutions based on the Sanders-Budiansky shell equations were developed. The semi-analytical differential quadrature method in which Fourier series were written in the circumferential direction was adopted.

2.4 Stability of shells

The stability of structural members must be considered in the design analysis. Elastic buckling of shells is a stability phenomenon in which large deflections appear perpendicular to the shell surface at a critical pressure value. The buckling of shells is studied in this work.

Due to the extensive use of shells very intensive research has been carried out on the stability of shells since the 1930s. In his popular monograph, Yamaki [1984] presented results for studies on the elastic stability of circular cylindrical shells. He presented both theoretical and experimental results on the buckling, postbuckling and initial-post-buckling problem under typical single or combined loadings for various boundary conditions. In this book, the difference between the Donnell theory, the modified theory, and Sanders theory were discussed in detail.

In a monograph by Bushnell [1985] computerized buckling of shells was considered. A mixture of theoretical, analytical, and numerical procedures was presented. Samuelson and Eggwertz [1992] edited a shell stability handbook for calculation of the carrying capacity of shell structures with respect to buckling. This book provides many useful results of the carrying capacity for engineering practice.

Teng [1996] provided a review of recent research advances and trends in the area of thin shell stability. In particular, he emphasized three topics; imperfections in real structures, buckling of shells under local/non-uniform loads, and the use of computer buckling analysis in the stability design of complex thin shell structures.

2.5 Stability of toroidal shells

The first study of the stability of externally-pressurised closed toroidal shells with circular cross-sections was by Sobel and Flügge [1967]. In their study, the theory was based on the assumption of a precritical membrane state. Nonlinear theory was applied in many other studies, dealing with instability due to symmetric or asymmetric deformations of tori. Kosheleva and Myachenkov [1971] studied the stability of toroidal shells with localized loadings using the finite difference method based on Mushtari thin shell theory. Nordell and Crawford [1971] studied experimentally seven epoxy toroidal shell models which were subjected to hydrostatic pressure.

There are further extensive studies concerned with the stability analysis of toroidal shells, which included those of Bushnell, Panagiotopoulos, Skrzypek and Bielski, Wang and Zhang. In Bushnell's study [1981] there is a study of straight and curved pipe models subjected to external or internal pressure, simulated by thermal loading. Panagiotopoulos [1985] presented a finite element solution for the stress and stability of toroidal pressure vessels under hydrostatic pressure. Skrzypek and Bielski [1988] studied the optimal design of elastic toroidal shells subject to buckling under external pressure based on geometrically nonlinear theory of finite displacements, but small strains. Wang and Zhang [1991] studied the stability of toroidal shells under hydrostatic pressure using the Sanders's non-linear stability equations. Bielski [1992] considered the influence of geometrical imperfections in the meridional shape and thickness of elastic toroidal shells on buckling pressure and post-buckling behavior. They observed that the ovalization imperfection showed greater sensitivity.

Galletly and his co-workers conducted extensive research work on the stability of toroidal shells. Galletly and Blachut [1995] studied the stability of complete circular and non-circular toroidal shells. The numerical results were obtained using BOSOR 5 program and compared with experimental results. [Galletly[a], Galletly[b] 1996] studied the buckling of complex toroidal shell structures with regard to a proposed innovation in the design of submersibles. The stress distributions, elastic-plastic buckling pressures and mode shapes were determined using the variational finite-difference BOSOR5 program. In another work they studied the elastic buckling of complete toroidal shells of elliptical cross-section subjected to uniform internal pressure and presented the numerical results using BOSOR and INCA FEM programs [Galletly, 1998a]. Also, Galletly [1998b] presented results for the elastic buckling of imperfect circular toroidal shells under external pressure. In this study, the effects of axisymmetric initial geometric imperfections on reducing the critical buckling pressure for a perfect shell were investigated and various other types of imperfection were studied. Galletly [1999] studied the buckling of imperfect elastic elliptic toroidal shells subjected to uniform external pressure. In this study, the effects of axisymmetric initial geometric imperfections on the buckling pressures of externally pressurized steel elastic toroidal shells of elliptical cross-section were determined.

Redekop [1997] studied the elastic instability of a thin curved pipe under three-point bending based on Donnell-type linearized stability equation. Blachut and Jaiswal [1999] studied the instabilities in torispheres and toroids under suddenly applied external pressure. They found that under suddenly applied pressure, a geometrically perfect torisphere fails by indirect axisymmetric snapping, and that the critical pressure at which snapping occurs was smaller than the static bifurcation buckling pressure. Blachut and Jaiswal [2000] presented results on buckling of toroidal shells with elliptical cross-section under external pressure. They presented the results of a numerical study into the buckling resistance of geometrically perfect and imperfect steel toroidal shells with non-circular cross-sections which showed that toroids with an elliptical cross-section can be much stronger than ones with a circular cross-section.

More recent research works concerned with toroidal shells are those of Naboulsi and Blachut. Naboulsi et al [2000] presented a static-dynamic analysis of toroidal shells. Blachut [2002] investigated the collapse of externally pressurized toroids. This study discussed the load carrying capacity of toroidal shells with closed circular cross-section and loaded by static external pressure.

2.6 Stiffened shells

Stiffened shell structures have found widespread applications in aerospace and marine engineering owing to their superior strength to weight ratio, better durability, excellent damage tolerance and other qualities. Various stiffener arrangements are used to achieve greater strength with relatively small amounts of material so as to satisfy the objective of minimum weight.

The early studies on the elastic buckling of stiffened shells using the Rayleigh-Ritz approach were carried out by Kendrick [1953]. Galletly et al [1958] carried out the experiments to verify the Kendrick's results.

Baruch and Singer [1963] studied the effect of eccentricity of stiffeners on the elastic buckling capacity of simply supported cylindrical shells under hydrostatic pressure. Balderes and Armenskas [1973] investigated the free vibrations of ring-stiffened toroidal shells using the Runge-Kutta method. Baig and Yang [1974] carried out a buckling analysis of orthogonally stiffened waffle cylindrical shells using the method of energy minimization.

Omurtag and Aköz [1993] proposed a study of a compatible cylindrical shell element for stiffened cylindrical shells based on a mixed finite element formulation. Wang et al [1994] studied the buckling of cylindrical shells with internal ring supports under lateral pressure and hydrostatic pressure using RRM. Tian et al [1999] carried out the elastic buckling analysis of ring-stiffened cylindrical shells under general pressure loading based on the RRM. Raj et al [1995] compared the effect of ring stiffeners on vibration of cylindrical and conical shell models by both theoretical and experimental methods. Araar and Jullien [1996] studied the buckling of cylindrical shells under external pressure for a proposed new shape of self-stiffened shell. Yamazaki and Tsubosaka [1997] used a stress analysis technique for plate and shell built-up structures with junctions and applied it to the minimum weight design of stiffened structures using a finite element formulation.

Kwon and Cunningham [1998] compared finite element models for a stiffened shell subject to underwater shock. Samanta and Mukhopadhyay [1999] studied large deflection of shallow and deep stiffened shells.

Ross and Etheridge [2000] carried out a theoretical and an experimental investigation into the buckling and vibration of prolate hemi-ellipsoidal tube-stiffened domes under external water pressure. Prusty and Satsangi [2001] studied the analysis of stiffened shell for ships and ocean structures using an eight-noded isoparametric element for the shell and a three-noded beam element for the stiffener. Spagnoli [2001] considered different buckling modes in axially stiffened conical shells by a linear eigenvalue finite element analysis. Rikards et al [2001] studied the buckling and vibrations of composite stiffened shells and plates based on the first-order shear deformation theory.

More recent research works related to the stiffened shell are those of Abramovich et al [2002]. They considered the influence on buckling of geometrical imperfections of stiffened shells under combined loading. Yaffe and Abramovich [2003] performed a study of dynamic buckling of cylindrical stringer stiffened shells. Das et al [2003] presented solution for the buckling and ultimate strength of stiffened shells under combined loadings. Samanta and Mukhopadhyay [2004] studied the free vibration of stiffened shells using finite elements. Ruzzene [2004] considered the dynamic buckling of periodically stiffened shells.

2.7 Differential quadrature method

The DQM first introduced by Bellman and his associates [Shu, 2000] in the early 1970s is an efficient numerical method for rapid solutions of linear and non-linear partial differential equations. Bert et al [1988] applied this method to structural problems involving fourth order partial differential equations. Since then, many researchers have applied this method in many areas of engineering. In a very good review, Bert and Malik [1996a] presented a comprehensive summary of the chronological development and the application of the DQM up to 1996. They also studied the free vibration of thin cylindrical shells using this method [Bert, Malik, 1996b].

In a very comprehensive monograph, Shu [2000] systematically described both the theoretical analysis and the application of the DQM. It is shown in this book that the weighting coefficients of the polynomial-based, Fourier expansion-based, and exponential-based differential quadrature methods can be computed explicitly.

Wu and Liu [2000] gave the axisymmetric bending solution of shells of revolution by applying the generalized differential quadrature rule. Wu and Lee [2001] studied the free vibration analysis of laminated conical shells with variable stiffness using the DQM. The first-order shear deformation shell theory was used to account for the effects of transverse shear deformations in their study.

Jiang and Redekop [2002] studied the polar axisymmetric vibration of a hollow toroidal shell with circular cross-section and uniform thickness using the DQM. Jiang and Redekop [2003] also studied the static and vibration analysis of orthotropic toroidal shells of variable thickness based on the Sanders-Budiansky shell theory by applying the semi-analytical DQM.

Choi and Chou [2003] studied the free vibration analysis of non-circular curved panels using the Love's hypothesis and gave results in an orthogonal curvilinear co-ordinate system using the DQM. Wu et al [2003] studied the bending of cylindrical barrel shells by applying the generalized DQM. Redekop [2004] presented a solution to the free vibration problem of hollow bodies of revolution using the DQM. In this study, the three-dimensional theory of elasticity is used to set up an accurate solution for the natural frequencies of vibration of a hollow body of revolution of arbitrary geometry.

2.8 Rayleigh-Ritz method

The RRM is a very powerful technique that can be used to predict the natural frequencies and buckling loads of shell structures together with corresponding mode shapes. Many researchers have adopted this approach in their research work.

Wang et al [1994] studied the buckling of cylindrical shells with internal ring support using this method. The solution presented allowed any combination of end conditions and any number of internal supports. Ip et al [1996] studied the vibration of orthotropic thin cylindrical shells with free ends using this approach. Tian et al [1999] presented an elastic buckling analysis of ring-stiffened cylindrical shells under general pressure loading via the RRM. By means of a nondimensional formulation, generic buckling solutions for shells with various end conditions, stiffener distributions and under various pressure distributions were obtained in this study. Chakraverty et al [1999] provided a good review of recent research on the vibration of structures using boundary characteristic orthogonal polynomials in the RRM.

Young [2000] considered the free vibration of shells arbitrarily deep in one direction using the RRM. Grigolyuk and Lopanitsyn [2002] studied the axisymmetric postbuckling behaviour of shallow spherical domes using this approach. Lee et al [2002] carried out a study on the free vibration of joined cylindrical-spherical shell structures using this method. Hu et al [2002] studied the vibration of twisted laminated composite conical shells using the RRM. Hu et al [2004] studied the vibration of angle-ply laminated plates with twist using the RRM.

The literature on the RRM indicates that this approach is very popular in shell vibration and stability analysis. There are few if any studies related to toroidal shells using this approach. The application of this approach to toroidal shells is a major challenge and forms a major part of the current study.

Chapter 3

Free vibration of a complete orthotropic circular toroidal shell -- small R/r ratio

3.1 Introduction

Toroidal shells have in recent years been adapted for many uses, such as fusion reactor vessels, satellite antenna support structures, protective devices for nuclear waste containers, circumferential reinforcement for submarines, rocket fuel tanks, and diver's oxygen tanks. Vibration analyses are an important part of the design process for such shells. Analytical solutions are useful either in the form of a primary solution or as a means of supplementing results determined using the FEM.

Toroidal shells are shells of revolution. Development of theory for general shells of revolution has the advantage that not only toroidal shells can be analyzed but also other shell forms such as the spherical and cylindrical. For this reason theory in this chapter is initially derived for shells of revolution, and then specialized for toroidal shells. For maximum generality orthotropic materials are assumed.

The recent literature on the vibration of shells of revolution includes work dealing mainly with isotropic shells. Tan [1998] developed a substructuring technique and considered applications to thin cylindrical, spherical, and hyperbolical shells. Leissa and Kang [1999] used the RRM for the analysis of thick shells, and considered applications to truncated conical shells and spherical shell segments. Redekop [2004] used the DQM for bodies of revolution of arbitrary thickness, and considered cylindrical and hemispherical applications. Studies of orthotropic shells have typically been dedicated to shells of a specific geometry, e.g. Ip et al [1996], who considers a thin cylindrical shell.

In this chapter the differential equations based on the Sanders-Budiansky theory are developed for the linear vibration analysis of an orthotropic thin shell of revolution. Solutions to the equations are set up using the DQM approach. Examples are given for complete toroidal shells (Fig. 3-1), which unlike partial toroidal shells (curved pipes) [Ming et al, 2002], have received little recent attention. The method is validated by comparing results for a complete isotropic toroidal shell with previously published results [Balderes, Armenakas, 1973]. A parametric study for complete isotropic and orthotropic toroidal shells with small R/r ratio is then conducted. FEM results are given along with the DQM. The chapter ends with an appropriate set of conclusions.

3.2 Geometry

The mid-surface of an arbitrary thin shell is described by a radius vector **R** = **R** (q_1, q_2), where q_1, q_2 form an orthogonal coordinate system. The Lamé parameters of the shell are depicted by α_1, α_2, and the curvatures by κ_1, κ_2. For a shell of revolution the radius vector takes the form **R** = $\bar{r}\sin\phi\,\mathbf{i} + \bar{r}\cos\phi\,\mathbf{j}$ + z**k**, where $q_1 = \phi$ is the circumferential angle, $\bar{r} = \bar{r}(q_2)$, $z = z(q_2)$, and **i, j, k** are the unit vectors [Dym, 1977].

The geometric parameters for a specific shell of revolution may readily be derived from the radius vector [Soedel, 1993]. For example for a toroidal shell of circular cross-section (Fig. 3-2) the parameters are given by

$$q_1 = \phi; q_2 = \theta;\ \alpha_1 = R\zeta;\ \alpha_2 = r;\ \kappa_1 = \frac{\cos\theta}{R\zeta};\ \kappa_2 = 1/r \qquad (3.1)$$

where ϕ is the circumferential angle, θ is the meridional angle, measured clockwise from the positive horizontal, R is the bend radius, r is the radius of the cross-section, and

$$\gamma = r / R;\ \zeta = 1 + \gamma \cos\theta;\ \bar{r} = \bar{r}(\theta) = R\zeta;\ z = z(\theta) = r\cos\theta.$$

For a complete toroidal shell the meridian forms a closed curve, and boundary conditions need not be considered. The present method can easily be extended to shells of revolution with incomplete meridian by specifying appropriate boundary conditions at the ends of the meridians of such shells.

3.3 Sanders-Budiansky shell theory

To determine the vibration characteristics of the toroidal shells the first-order linear version of the Sanders-Budiansky [Sanders, 1959] [Budiansky, 1968] shell theory is used, in conjunction with the D'Alembert principle and orthotropic constitutive relations. This approach has recently been successfully applied to a general shell [Redekop, 2004]. The equations of motion in this theory, expressed in terms of the stress and moment resultants are

$$\begin{aligned}
&a_1 N_\phi^\bullet + a_2 N_\phi + a_3 N_\theta + a_4 N_\phi' + a_5 N_{\phi\theta} + a_6 M_\phi^\bullet + a_7 M_\phi + a_8 M_\theta \\
&+ a_9 M_{\phi\theta}' + a_{10} M_{\phi\theta} + \alpha_1 \alpha_2 \rho h \ddot{u}_1 = 0 \\[1ex]
&a_{11} N_\phi + a_{12} N_\theta' + a_{13} N_\theta + a_{14} N_\phi' + a_{15} N_{\phi\theta} + a_{16} M_\phi + a_{17} M_\theta' + a_{18} M_\theta \\
&+ a_{19} M_{\phi\theta}^\bullet + a_{20} M_{\phi\theta} + \alpha_1 \alpha_2 \rho h\ \ddot{u}_2 = 0 \\[1ex]
&a_{21} N_\phi + a_{22} N_\theta + a_{23} M_\phi^{\bullet\bullet} + a_{24} M_\phi^\bullet + a_{25} M_\phi' + a_{26} M_\phi + a_{27} M_\theta^\bullet + a_{28} M_\theta'' \\
&+ a_{29} M_\theta' + a_{30} M_\theta + a_{31} M_{\theta\phi}^\bullet + a_{32} M_{\theta\phi}'^\bullet + a_{33} M_\theta^{\bullet}{}' + a_{34} M_{\phi\theta} + \alpha_1 \alpha_2 \rho h \ddot{u}_3 = 0
\end{aligned} \tag{3.2}$$

where for convenience the following notations are defined

$$( )^{\bullet} = \frac{\partial}{\partial \phi}( ); \; ( )' = \frac{\partial}{\partial \theta}( )$$

In equations (3.2), ρ is the mass density, h is the shell thickness, $\ddot{u}_1, \ddot{u}_2, \ddot{u}_3$ are the acceleration components, and the a_i, $i = 1, \ldots, 34$ are known functions of the Lamé parameters and curvatures, listed in Appendix A1.

For an orthotropic material the constitutive relations [Raymond et al, 2000] are taken as

$$\begin{aligned} &N_\phi = b_1 \varepsilon_\phi + b_2 \varepsilon_\theta; \quad N_\theta = b_3 \varepsilon_\phi + b_4 \varepsilon_\theta; \; N_{\phi\theta} = b_5 \varepsilon_{\phi\theta} \\ &M_\phi = b_6 \kappa_\phi + b_7 \kappa_\theta; \; M_\theta = b_8 \kappa_\phi + b_9 \kappa_\theta; \; M_{\phi\theta} = b_{10} \kappa_{\phi\theta} \end{aligned} \tag{3.3}$$

where b_i, $i = 1, \ldots, 10$ are constants representing known material properties, the $\varepsilon_\phi, \varepsilon_\theta, \varepsilon_{\phi\theta}$ are the strain components, and the $\kappa_\phi, \kappa_\theta, \kappa_{\phi\theta}$ are the changes in curvature. For an orthotropic material with Young's moduli E_ϕ, E_θ, Poisson's ratios $\nu_{\phi\theta}, \nu_{\theta\phi}$ and shear modulus $G_{\phi\theta}$ the constants are given by

$$\begin{aligned} &b_1 = E_\phi h/(1 - \nu_{\phi\theta}\nu_{\theta\phi}); && b_6 = E_\phi h^3/12(1 - \nu_{\phi\theta}\nu_{\theta\phi}) \\ &b_2 = \nu_{\theta\phi} E_\phi h/(1 - \nu_{\phi\theta}\nu_{\theta\phi}); && b_7 = \nu_{\theta\phi} E_\phi h^3/12(1 - \nu_{\phi\theta}\nu_{\theta\phi}) \\ &b_3 = \nu_{\phi\theta} E_\theta h/(1 - \nu_{\phi\theta}\nu_{\theta\phi}); && b_8 = \nu_{\phi\theta} E_\theta h^3/12(1 - \nu_{\phi\theta}\nu_{\theta\phi}) \\ &b_4 = E_\theta h/(1 - \nu_{\phi\theta}\nu_{\theta\phi}); && b_9 = \nu_{\theta\phi} E_\theta h^3/12(1 - \nu_{\phi\theta}\nu_{\theta\phi}) \\ &b_5 = G_{\phi\theta} h; && b_{10} = G_{\phi\theta} h^3/12 \end{aligned} \tag{3.4}$$

For an isotropic shell with Young's modulus E and Poisson's ratio ν one has the simplifications $E_\phi = E_\theta = E$, $\nu_{\phi\theta} = \nu_{\theta\phi} = \nu$, $G_{\phi\theta} = E/2(1+\nu)$. Transverse shear resultants are defined through

$$Q_\phi = a_{35} M_\phi^\bullet + a_{36} M'_{\phi\theta} + a_{37} M_{\phi\theta} + a_{38} M_\theta$$

$$Q_\theta = a_{39} M'_\theta + a_{40} M^\bullet_{\phi\theta} + a_{41} M_{\phi\theta} + a_{42} M_\phi \tag{3.5}$$

where the a_i, i = 35,...,42 are known functions of the geometric and material properties given in Appendix A1. In the Sanders-Budiansky theory, the kinematic relations are given by

$$\varepsilon_\phi = c_1 u_1^\bullet + c_2 u_2 + c_3 u_3$$

$$\varepsilon_\theta = c_4 u_1 + c_5 u'_2 + c_6 u_3$$

$$\varepsilon_{\phi\theta} = c_7 u'_1 + c_8 u_1 + c_9 u_2^\bullet + c_{10} u_2$$

$$\kappa_\phi = c_{11} u_1^\bullet + c_{12} u_1 + c_{13} u_2 + c_{14} u_3^{\bullet\bullet} + c_{15} u_3^\bullet + c_{16} u'_3$$

$$\kappa_\theta = c_{17} u_1 + c_{18} u'_2 + c_{19} u_2 + c_{20} u_3^\bullet + c_{21} u''_3 + c_{22} u_3 \tag{3.6}$$

$$\kappa_{\phi\theta} = c_{23} u'_1 + c_{24} u_1 + c_{25} u_2^\bullet + c_{26} u_2 + c_{27} u_3^\bullet + c_{28} u'_3 + c_{29} u_3^{\bullet\prime}$$

where the c_i, $i = 1,\ldots,29$ are known functions of the Lamé parameters and curvatures, given in Appendix A2.

Adopting a semi-analytical approach the displacement components of the mth circumferential harmonic are represented by

$$u_1 = u(\theta)\cos m\phi \sin \omega t$$

$$u_2 = v(\theta)\sin m\phi \sin \omega t \tag{3.7}$$

$$u_3 = w(\theta)\sin m\phi \sin \omega t$$

where the u, v, w represent the displacement functions for the mth harmonic mode dependent on θ only, ω is the natural frequency, and t is the time.

The displacement components (3.7) are substituted into the kinematic relations (3.6) and combined with the constitutive relations (3.3) and the equations of motion (3.2). Factoring out the product $\alpha_1\alpha_2$ one obtains three governing equations of the form

$$\begin{aligned}
&e_1u''+e_2u'+(e_3+m^2e_4)u+me_5v'+me_6\,v+me_7w'' \\
&+me_8w'+(m^3e_9+me_{10})\,w=\Omega\,u \\
&me_{11}u'+me_{12}u+e_{13}v''+me_{14}v'+(e_{15}+m^2e_{16})v+me_{17}w''' \\
&+me_{18}w''+(e_{19}+m^2e_{20})\,w'+(e_{21}+m^2e_{22})w=\Omega v \\
&me_{23}u''+me_{24}u'+(m^3e_{25}+me_{26})\,u+e_{27}v'''+e_{28}v'' \\
&+(e_{29}+m^2e_{30})v'+(m^2e_{31}+e_{32})\,v+e_{33}w''''+e_{34}w''' \\
&+(e_{35}+m^2e_{36})w''+(e_{37}+m^2e_{38})\,w'+(e_{39}+m^2e_{40}+m^4e_{41})\,w=\Omega w
\end{aligned} \tag{3.8}$$

where the e_i, i = 1,…,41 are known functions of the Lamé parameters, curvatures, the material properties given in Appendix A3, and $\Omega=\rho h\omega^2$. The set of differential equations (3.8) contains as the unknowns the displacement components and the natural frequency parameter of the mth harmonic.

The m = 0 case, i.e. the axisymmetric circumferential harmonic, is a special case which can easily be extracted from the theory for the general harmonic described in the preceding. In the development of the special axisymmetric case the displacement u_ϕ, the resultants $N_{\phi\theta}$, $M_{\phi\theta}$, Q_ϕ, and all derivatives with respect to ϕ are set to zero. The solution of the equation set (3.8) using the DQM is now considered.

3.4 Differential quadrature method

The first step in the DQM approach [Shu, 2000] is the definition of a grid of sampling points covering the domain, including the boundary. The present problem having been reduced to one dimension mathematically, according to (3.7), requires only a grid along an arbitrary meridional line. The three displacement components at each of the sampling points of the grid together with the frequency parameter constitute the unknowns of the problem.

The second step in the DQM approach is the replacement of derivatives with series of terms that contain the product of displacements at the sampling points and weighting coefficients. This step converts the problem from one of differential equations to one of linear equations. The r-th derivative of a generic function of a single variable $f(x)$ at the sampling point x_i is represented as

$$\left.\frac{d^r f(x)}{dx^r}\right|_{x_i} = \sum_{h=1}^{M} A_{ih}^{(r)} f(x_h) \tag{3.9}$$

where the $A_{ih}^{(r)}$ are the weighting coefficients of the r-th order derivative in the x direction for the i-th sampling point, $f(x_h)$ is the value of $f(x)$ at the sampling point position x_h, and M is the number of sampling points in the x direction.

In the DQM, the weighting coefficients are determined a-priori for a preselected grid, with the aid of selected trial functions. For the present problem where there is completeness of geometry in the meridional direction it is convenient to use a Fourier basis for the weighting coefficients, and to use equally spaced points. For such a scheme, explicit formulas for the weighting coefficients $A_{ih}^{(r)}$ are available [Shu, 2000].

Use of the quadrature rule (3.9) for the derivatives in the governing differential equations (3.8) for the domain leads to transformed DQM vibration equations. Enforcement of the equations at the sampling points leads to a set of simultaneous linear equations of the form

$$[K](U) = \lambda [M](U) \tag{3.10}$$

where the unknowns (U) are the values of the displacement functions at the sampling points, λ is the eigenvalue, related to ω, and $[K]$, $[M]$ are the known 'stiffness' and 'mass' matrices. Standard matrix eigenvalue extraction routines may be used to solve the equation (3.10).

The lengthy derivation of the governing equation following the procedure described herein allows for an analysis of thin shells of revolution of arbitrary smooth meridian. For the analysis of toroidal shells the appropriate values of the Lamé coefficients and curvatures are inserted at the solution stage, i.e. on enforcing the domain equations at the sampling points. While the approach is demonstrated herein for toroidal shell of complete meridian it can easily be extended to segmental shells by the specification of appropriate boundary conditions at the ends of meridional lines.

3.5 Finite element method

The commercial FEM program ADINA [ADINA, 2003] is used to provide an alternate solution to the vibration problem. Both natural frequencies and mode shapes may be determined, and isotropic and orthotropic materials are considered. An isoparametric nine-node fifty-four degree-of-freedom shear-deformation shell element is used for the vibration analysis of the toroidal shells. Selections in meshing options are made to give elements that are nearly square in plan at the crowns. The modeling accounted for the full geometry, with no account made of any symmetry. For isotropic material one must define E and ν (two constants). For orthotropic material one must define E, G in two directions and ν (five constants).

3.6 Validation

The DQM solution is validated by comparing results for a complete toroidal shell with results obtained previously using the Runge Kutta Method (RKM) by Balderes and Armenakas [1973]. The shell has the following geometric and material parameters

$$R = 1.0m;\ r = 0.2m;\ h = 0.004m; \tag{3.11}$$

$$E = 0.207e12Pa;\ \nu = 0.3;\ \rho = 7800kg/m^3$$

and is analyzed for completely free support conditions. Results for the first six natural frequencies ω_i together with their circumferential mode number m are given in Table 3-1. The DQM results labeled DQM1, DQM2, DQM3, and DQM4 are respectively for grids containing 10, 20, 30, and 40 sampling points. The FEM results are the converged values determined using the nine-node shell element of the ADINA program.

The DQM results in Table 3-1 indicate that the method has rapid convergence, with 20 grid points sufficient to give four figure accuracy for this completely free shell. There is especially close agreement between the DQM and FEM results, with maximum differences in the converged values less than 0.2%. The agreement with the RKM results is not as close, but within 0.6%. The good agreement between the three sets of results indicates the near equivalence of the underlying shell theories for the three methods.

3.7 Results

Free vibration characteristics are determined for four cases of complete isotropic toroidal shells as described in Table 3-2. A previous study of these shells, to determine stability characteristics, was carried out by Sobel and Flügge [1967]. The shells labeled

A, B, C, and D are of relatively small *R/r* ratio, varying from 4.0 to 1.3. The thickness ratio *r/h* of the shells is either 100 or 200.

Table 3-3 gives the results of a convergence study for the first two natural frequencies for the four cases. It is noted that for some grid choices the DQM may skip an eigenvalue. A check of results for various grids is advisable, just as in the FEM it is appropriate to consider the results from several different meshes.

In Table 3-4 are presented the results for the first six natural frequencies for cases A-D as obtained using the FEM and DQM. The FEM results are the converged values obtained using the nine-node shell element, whereas the DQM results are values obtained generally from grids containing 30 or 40 mesh points. The results are for an isotropic material as described in equations (3.11). Also presented in the table are the circumferential mode numbers obtained from the DQM solution for each of the frequencies.

For these shells either the axisymmetric or the 2nd circumferential harmonic produces the lowest frequency. Cases A and B differ only in the wall thickness, and it is seen that there is an increase in the frequencies for the thicker shell. Cases A, C, D have the same wall thickness ratio *r/h* and bend radius *R* but vary in the radius ratio *R/r*. It is seen that as the *R/r* ratio decreases there is a decrease in the value of the lowest natural frequency, but an increase in the value of the other frequencies.

Shells with the orthotropic materials are considered next. The properties of three different orthotropic materials labeled M1, M2 and M3 are given in Table 3-5. The '1', '2' represent the circumferential and meridional direction (Fig. 3-2) respectively and '3' is the direction perpendicular to the shell mid-surface. E_1, E_2 are the Young's moduli in

1 and 2 directions, respectively. ν_{ij} are the Poisson's ratio for transverse strains in the *j*-direction when stressed in the *i*-direction (*i*, *j* = 1,2,3). G_{23}, G_{13}, G_{12} are shear moduli in the 2-3, 3-1, and 1-2 planes respectively. For orthotropic material, there are two orthogonal planes of material property symmetry. Symmetry will exist relative to a third mutually orthogonal plane. There are only nine independent material parameters, because of the symmetry conditions $\nu_{12}E_2 = \nu_{21}E_1$. In a thin shell theory in which shear deformation effects are not considered, only five parameters are required.

In Tables 3-6 to 3-8 are presented the results for the first six natural frequencies ω_i together with their circumferential mode number *m* for cases A-D when the shells consist of an orthotropic material. The results were determined using 50 or 60 mesh points in the DQM. Results are given for shells consisting of the three orthotropic materials described in Table 3-5.

In Table 3-6 are given the results for material M1 [Wang, 1999] for which the Young's modulus of the circumferential direction is about two times larger than the modulus in the meridional direction ($E_1 = 2.14E_2$). There is generally agreement between the results of the DQM and FEM within less than 3%, but the slightly larger differences of 4% and 8% are noted in case C and case D respectively. It is also noted that in case C, the DQM has skipped an eigenvalue. This is believed a characteristic of the eigenvalue extraction routine.

Table 3-7 presents the results for material M2 [Lahtinen, Pramila, 1996] for which the Young's modulus of the circumferential direction is about seventeen times larger than the modulus of the meridional direction ($E_1 = 17.6E_2$). It is observed that the results of the DQM and FEM are very close for the axisymmetric circumferential harmonic mode.

For the other circumferential harmonics, the two results agree mostly within 7%, but larger differences of up to 12% are noted in case D.

In Table 3-8 are presented the results for material M3 [Jiang, Redekop, 2003] for which the Young's modulus of circumferential direction is over one hundred times larger than the modulus in the meridional direction ($E_1 = 105E_2$). In this table, it is indicated that for the results of the DQM and FEM, there is general agreement for cases C and D within 8%, but for cases A and B, the difference up to 11% is noted. It is also observed that there is excellent agreement of the two results for the axisymmetric circumferential harmonic mode.

The trends observed earlier for isotropic shells with regard to changes in wall thickness and radius ratio are observed again for these orthotropic shells. For the orthotropic shells also either the axisymmetric or the 2nd circumferential harmonic contains the lowest frequency. There is generally good agreement of the FEM and DQM results, but for a few frequencies differences of up to 11% are noted. As well for cases C and D the sixth apparent root is registered only by one of the two methods. Further study of the issue of missing roots is indicated, but adoption of an analysis program employing two methods clearly is one way of overcoming the difficulty. The results show that the material of M2 produces higher natural frequencies than those of materials of M1 and M3 because of its greater stiffness. It is also indicated that with an increase in the ratio of the Young's modulus in the circumferential and meridional directions, the larger difference in the DQM and FEM occur. The three sets of orthotropic materials results indicate that the optimum combination of geometric and material properties can produce the higher natural frequencies.

Using the FEM and DQM mode shapes corresponding to the six lowest frequencies were plotted for each of the four cases. Full three-dimensional plots and the projections on the equator of the first six modes for the shells of cases A-D are given in Figs. 3-3 to 3-10, and cross-sectional views of the first six modes for the shell of case C are given in Fig. 3-11. In Fig. 3-11, the circumferential mode numbers for the indicated modes 1-6 are respectively 0, 2, 2, 3, 3, and 4. Full three-dimensional plots of the first six modes for the shell of case A consisting of orthotropic material M1 are given in Fig. 3-12. It is seen that the mode shapes are similar between the isotropic and orthotropic toroidal shells.

Figs. 3-3 to 3-12 indicate that large amplitudes of vibration arise around the intrados of the shell, in a region having negative Gaussian curvature. The amplitudes around the extrados where the Gaussian curvature is positive are relatively low. In the cross-sectional views it is observed that symmetric and antisymmetric modes with regard to the equator arise, similar to the case of curved pipes [Ming, 2002]. In general it is advantageous to have results from two methods to obtain a more detailed picture of the overall shell motion.

In the preceding completely free shells were considered. Shells with immovable circumferential line supports are of practical interest, and can easily be handled with both methods. Two locations for the line support are considered, one at the inner equator (identified by point I in Fig. 3-2), and the other at the bottom crown (point II in Fig. 3-2). For both these two instances the conditions at the line support are taken as $u = v = w = 0$ for each harmonic m (m>0). Implementations of the support conditions in the DQM is effected by replacing the three governing equations at the appropriate meridional sampling point with the three displacement support conditions.

Vibration results for the four shell cases A-D under conditions of circumferential line support are given in Tables 3-9 and 3-10. The results of Table 3-9, corresponding to line support at the inner equator indicate a decrease of the fundamental frequency ω_1 with respect to the completely free shell (Table 3-4). The results of Table 3-10, corresponding to line support at the lower crown, indicate an increase in the fundamental frequency for cases A-C but a decrease for case D. The fundamental frequency for these line supported shells corresponds to an axisymmetric mode except for case D of the bottom crown support shell. The full three-dimensional plots of the first six modes for the shell of case C with inner equator support and bottom crown support are given in Fig. 3-13 and Fig. 3-14. The cross-sectional views for the first six modes for case C of the bottom crown supported shell are given in Fig. 3-15.

As convergence was slower for the line supported shells a total of 120 sampling points was used in the DQM analysis. Two of the eigenvalues for the intrados-supported shell that are predicted by the FEM are not found by the DQM. For all eigenvalues found, the DQM and FEM results agree within less than 1%.

3.8 Conclusion

General equations have been obtained which enable the prediction of the vibration characteristics of orthotropic shells of revolution of arbitrary meridian. Results for natural frequencies and mode shapes for toroidal shells with small *R/r* ratio with 'completely free' support condition are determined. For the specific cases of complete isotropic toroidal shells results are obtained that agree well with previously published results. Two circumferential line support conditions are also considered for the isotropic toroidal shells, and DQM results show good agreement with the FEM results. New results for complete orthotropic toroidal shells with three different orthotropic materials are determined that also show very good agreement with results from the finite element method. This study demonstrates the value of the differential quadrature method for the vibration analysis of a thin shell of revolution.

Chapter 4

Free vibration of a complete orthotropic circular toroidal shell -- large R/r ratio

4.1 Introduction

The capacity of thin-walled shells can be increased by the use of the reinforcement. Such reinforcement may be in the forms of stringers or rings. For toroidal shells it can be in the form of meridional rings. The Rayleigh-Ritz method (RRM) has particular advantage for the study of such reinforced shells. It has been used by a number of researchers, e.g. Ip et al [1996], Singal and Williams [1988], and Kosawada et al [1985], with excellent results, and is thus adopted for the current study. While a number of studies have dealt with isotropic toroidal shells, little work if any is available on the orthotropic shells.

In this chapter the linear free vibration problem of a complete toroidal shell with large *R/r* radius ratios is considered. Theory is developed using the RRM which incorporates the kinematic assumptions of the Sanders-Budiansky first-order linear shell theory. Simplifying assumptions are made that restrict the theory to shells having large bend/cross-section radius ratios. The theory developed enables the determination of the 'stiffness' and 'mass' matrices for the vibration analysis of isotropic and orthotropic toroidal shells. The theory may easily be extended to reinforced shells. Results are given for toroidal shells with large *R/r* ratios using the DQM and FEM, and the effect of using ring stiffeners is determined.

4.2 Shell geometry

The toroidal shell considered has a bend radius R, a cross-sectional radius r, and a thickness h (Fig. 4-1). It is a complete shell, extending through 360° in the circumferential and meridional directions.

A general point P on the shell mid-surface is defined by circumferential and meridional angular coordinates ϕ and θ. The radius vector $\mathbf{r}$ to P is given by Dym [1974] as

$$\mathbf{r} = (R + r\cos\theta)\sin\phi\,\mathbf{i} + (R + r\cos\theta)\cos\phi\,\mathbf{j} + r\sin\theta\,\mathbf{k} \tag{4.1}$$

where **i, j, k** are unit vectors forming a base in the Cartesian x, y, z coordinate system. The first fundamental form of the middle surface is given by

$$ds^2 = A_1^2 d\xi_1^2 + A_2^2 d\xi_2^2$$

where ds is the differential line element, A_1 and A_2 are the Lamé parameters, and ξ_1 and ξ_2 are the base coordinates. The base coordinates are taken as

$$\xi_1 = \theta;\ \xi_2 = \eta = \overline{\rho}\phi \tag{4.2}$$

where $\overline{\rho} = R/r$. The adoption of the second circumferential coordinate η is to allow for extension at a later date of the present theory to incomplete toroidal shells, i.e. curved pipes. The Lamé parameters, and principal radii of curvatures R_1 and R_2, which are used in the shell theory, are given by

$$A_1 = r;\ A_2 = r\zeta;\ R_1 = r;\ R_2 = r\zeta/(\gamma\cos\theta) \tag{4.3}$$

$$\zeta = 1 + \gamma\cos\theta;\ \gamma = r/R = \overline{\rho}^{-1} \tag{4.4}$$

In the development of the theory the inverse of various orders of ζ are required. To facilitate the development of closed form expressions the series for the inverses are truncated as follows

$$\zeta^{-1} = \frac{1}{1+\gamma\cos\theta} = 1-\gamma\cos\theta+\gamma^2\cos^2\theta-\gamma^3\cos^3\theta$$

$$\zeta^{-2} = \frac{1}{(1+\gamma\cos\theta)^2} = 1-2\gamma\cos\theta+3\gamma^2\cos^2\theta-4\gamma^3\cos^3\theta \tag{4.5}$$

$$\zeta^{-3} = \frac{1}{(1+\gamma\cos\theta)^3} = 1-3\gamma\cos\theta+6\gamma^2\cos^2\theta-10\gamma^3\cos^3\theta$$

These truncations for a toroidal shell of radius $R/r \geq 5.0$ lead to a maximum error in the series of 0.44 %. Use of the truncations clearly restricts the theory to toroidal shells with large *R/r* ratios.

4.3 Constitutive relations for an orthotropic shell

The constitutive relations for an orthotropic shell relating the stress and moment resultants to the strain and curvature functions are given as [Raymond et al, 2000]

$$N_\theta = A_{11}(\varepsilon_\theta + \nu_{\eta\theta}\varepsilon_\eta); \quad N_\eta = A_{22}(\varepsilon_\eta + \nu_{\theta\eta}\varepsilon_\theta); \quad \overline{N}_{\theta\eta} = A_{66}\varepsilon_{\theta\eta} \tag{4.6}$$

$$M_\theta = D_{11}(\kappa_\theta + \nu_{\eta\theta}\kappa_\eta); \quad M_\eta = D_{22}(\kappa_\eta + \nu_{\theta\eta}\kappa_\theta); \quad \overline{M}_{\theta\eta} = D_{66}\kappa_{\theta\eta}$$

where $N_\theta, N_\eta, \overline{N}_{\theta\eta}, M_\theta, M_\eta, \overline{M}_{\theta\eta}$ are the meridional, circumferential, and shear stress and moment resultants and $\varepsilon_\theta, \varepsilon_\eta, \varepsilon_{\theta\eta}, \kappa_\theta, \kappa_\eta, \kappa_{\theta\eta}$ are the meridional, circumferential, and shear strains and curvatures. The material constants are given by

$$A_{11} = E_\theta \, h/(1-\nu_{\theta\eta}\nu_{\eta\theta}); \qquad A_{22} = E_\eta \, h/(1-\nu_{\theta\eta}\nu_{\eta\theta})$$

$$A_{66} = G_{\theta\eta} \, h; \qquad A_{12} = A_{11}\nu_{\theta\eta} = A_{22}\nu_{\eta\theta}$$

$$D_{11} = E_\theta \, h/[12(1-\nu_{\theta\eta}\nu_{\eta\theta})]; \quad D_{22} = E_\eta \, h/[12(1-\nu_{\theta\eta}\nu_{\eta\theta})] \tag{4.7}$$

$$D_{66} = G_{\theta\eta} \, h^3/12; \qquad D_{12} = D_{11}\nu_{\theta\eta} = D_{22}\nu_{\eta\theta}$$

where E_θ, E_η are the Young's moduli, $\nu_{\theta\eta}, \nu_{\eta\theta}$ are the Poisson's ratios, and $G_{\theta\eta}$ is the shear modulus.

4.4 Potential energy of the shell

The potential energy due to inplane stretching and bending of the shell is given [Ip et al, 1996] by

$$\begin{aligned}\overline{V} &= \frac{1}{2}\int_0^{2\pi}\int_0^{2\pi}(A_{11}\varepsilon_\theta^2 + 2A_{12}\varepsilon_\theta\varepsilon_\eta + A_{22}\varepsilon_\eta^2 + A_{66}\varepsilon_{\theta\eta}^2)\,dVol \\ &\frac{1}{2}\int_0^{2\pi}\int_0^{2\pi}(D_{11}\kappa_\theta^2 + 2D_{12}\kappa_\theta\kappa_\eta + D_{22}\kappa_\eta^2 + D_{66}\kappa_{\theta\eta}^2)\,dVol\end{aligned} \tag{4.8}$$

where $dVol = A_1 A_2 \, d\theta \, d\eta$ is the volume element. Using the assumptions of the first-order Sanders-Budiansky shell theory [Sanders, 1959] [Budiansky, 1968] the strain and curvatures for a toroidal shell are given by

$$\begin{aligned}\varepsilon_\theta &= a_1 u^\bullet + a_2 w \\ \varepsilon_\eta &= a_3 u + a_4 v' + a_5 w \\ \varepsilon_{\theta\eta} &= a_6 u' + a_7 v + a_8 v^\bullet \\ \kappa_\theta &= a_9 u^\bullet + a_{10} w^{\bullet\bullet} \\ \kappa_\eta &= a_{11} u + a_{12} v' + a_{13} w^\bullet + a_{14} w'' \\ \kappa_{\theta\eta} &= a_{15} u' + a_{16} v^\bullet + a_{17} v + a_{18} w^{\bullet\prime} + a_{19} w'\end{aligned} \tag{4.9}$$

where u, v, w are the displacements in the meridional, circumferential, and radial directions. For convenience the following notations are defined

$$(\ )^{\bullet} = \frac{\partial}{\partial \theta}(\ );\ (\ )' = \frac{\partial}{\partial \eta}(\ )$$

These notations are adopted in chapters 4 and 5; the $a_1 - a_{19}$ are functions of the Lamé parameters and curvatures, which are given in Appendix B1.

4.5 Rayleigh-Ritz procedure

At resonance the mid-surface shell displacements with harmonic variation in time are given as [Soedel, 1993] [Ip et al, 1996]

$$\begin{aligned} u &= U(\theta, \eta)e^{i\omega t} \\ v &= V(\theta, \eta)e^{i\omega t} \\ w &= W(\theta, \eta)e^{i\omega t} \end{aligned} \tag{4.10}$$

where i is the imaginary unity, ω is the natural frequency, and t is the time. Following the Ritz approach the actual displacement functions U, V, W are taken as

$$\begin{aligned} U(\theta, \eta) &= \sum_{1}^{N} u_n \sin n\theta \sin \mu_m \eta \\ V(\theta, \eta) &= \sum_{1}^{N} v_n \cos n\theta \cos \mu_m \eta \\ W(\theta, \eta) &= \sum_{1}^{N} w_n \sin n\theta \sin \mu_m \eta \end{aligned} \tag{4.11}$$

where $\mu_m = m\pi\gamma / \psi$, with $\psi = 2\pi$ for a complete shell, and u_n, v_n, w_n are the unknowns Ritz coefficients. The expressions (4.11) represent a mode of vibration of the shell corresponding to a specified circumferential harmonic *m*.

In the determination of the resonant frequencies ω the Rayleigh-Ritz principle is used. In this method, the stationary values of ω are sought in the Rayleigh quotient

$$\omega^2 = \overline{V}_{\max} / T^*_{\max} \tag{4.12}$$

The maximum potential energy $\overline{V}_{\max}$ for the shell is given by

$$\begin{aligned}
\overline{V}_{\max} = \frac{1}{2}\int_0^{2\pi}\int_0^{2\pi} & (A_{22}[a_{20}(U^\bullet)^2 + a_{21}U^\bullet W + a_{22}W^2] \\
& + 2A_{21}[a_{23}U^\bullet U + a_{24}U^\bullet V' + a_{25}U^\bullet W + a_{26}UW + a_{27}V'W + a_{28}W^2] \\
& + A_{11}[a_{29}U^2 + a_{30}(V')^2 + a_{31}W^2 + a_{32}UV' + a_{33}UW + a_{34}V'W] \\
& + A_{66}[a_{35}(U')^2 + a_{36}V^2 + a_{37}(V^\bullet)^2 + a_{38}U'V + a_{39}U'V^\bullet + a_{40}VV^\bullet] \\
& + D_{22}[a_{41}(U^\bullet)^2 + a_{42}U^\bullet W^{\bullet\bullet} + a_{43}(W^{\bullet\bullet})^2] \\
& + 2D_{12}[a_{44}UU^\bullet + a_{45}U^\bullet V' + a_{46}U^\bullet W^\bullet + a_{47}U^\bullet W'' + a_{48}UW^{\bullet\bullet} \\
& \qquad + a_{49}V'W^{\bullet\bullet} + a_{50}W^{\bullet\bullet}W^\bullet + a_{51}W^{\bullet\bullet}W''] \\
& + D_{11}[a_{52}U^2 + a_{53}UV' + a_{54}(V')^2 + a_{55}(W^\bullet)^2 + a_{56}(W'')^2 + a_{57}UW^\bullet \\
& \qquad + a_{58}V'W^\bullet + a_{59}UW'' + a_{60}V'W'' + a_{61}W^\bullet W''] \\
& + 4D_{66}[a_{62}(U')^2 + a_{63}U'V^\bullet + a_{64}(V^\bullet)^2 + a_{65}V^2 + a_{66}(W^{\bullet\prime})^2 + a_{67}W^{\bullet\prime}W' \\
& \qquad + a_{68}(U')^2 + a_{69}U'V + a_{70}V^\bullet V + a_{71}VW^{\bullet\prime} + a_{72}VW' + a_{73}U'W^{\bullet\prime} \\
& \qquad + a_{74}U'W' + a_{75}V^\bullet W^{\bullet\prime} + a_{76}V^\bullet W'])r^2\zeta\, d\theta\, d\eta
\end{aligned} \tag{4.13}$$

where the constants $a_{20} - a_{76}$ are known functions of the geometry which are given in the Appendix B1. The reduced kinetic energy $T^*_{\max}$ is given in terms of the maximum kinetic energy $T_{\max}$ by $T^*_{\max} = T_{\max} / \omega^2$ where

$$T_{\max} = \frac{1}{2}\rho h \omega^2 \int_0^{2\pi}\int_0^{2\pi} (U^2 + V^2 + W^2) r^2 \zeta\, d\theta\, d\eta \tag{4.14}$$

and ρ is the mass density.

The requirements for the stationarity of the Rayleigh quotient (4.12) are satisfied through the enforcement of the relations

$$\frac{\partial \Pi}{\partial u_j} = 0; \quad \frac{\partial \Pi}{\partial v_j} = 0; \quad \frac{\partial \Pi}{\partial w_j} = 0; \quad for\ j = 1,2,\ldots,N \tag{4.15}$$

where $\Pi = T_{\max} - \overline{V}_{\max}$. The relations (4.15) lead to a set of $3 \times N$ simultaneous linear algebraic equations for each choice of the circumferential harmonic *m*. As the shell is complete no boundary conditions need be specified. The assembly of the domain equations yields for each choice of *m* a matrix equation of the form

$$\left\{ \begin{bmatrix} K_{uu} & K_{uv} & K_{uw} \\ K_{uv}^T & K_{vv} & K_{vw} \\ K_{uw}^T & K_{vw}^T & K_{ww} \end{bmatrix} - \lambda \begin{bmatrix} M_{uu} & 0 & 0 \\ 0 & M_{vv} & 0 \\ 0 & 0 & M_{ww} \end{bmatrix} \right\} \begin{Bmatrix} u \\ v \\ w \end{Bmatrix} = \begin{Bmatrix} 0 \\ 0 \\ 0 \end{Bmatrix} \tag{4.16}$$

where

$$u = \begin{Bmatrix} u_1 \\ u_2 \\ \vdots \\ u_N \end{Bmatrix} \qquad v = \begin{Bmatrix} v_1 \\ v_2 \\ \vdots \\ v_N \end{Bmatrix} \qquad w = \begin{Bmatrix} w_1 \\ w_2 \\ \vdots \\ w_N \end{Bmatrix} \tag{4.17}$$

and $\lambda = \rho r^2 h \omega^2$ is the eigenvalue. The submatrices K_{ij} and M_{ij} are each of size $N \times N$ and the terms are given in Appendix B2.

4.6 Finite element method

The general commercial FEM program ADINA is used as an alternate means to obtain numerical results. Again in this program a nine-node fifty-four degree-of-freedom shear-deformation shell element is available for the free vibration analysis. The entire shell was modeled disregarding the geometric symmetry. Convergence studies were carried out to ensure the validity of the solution.

For the ring-stiffened toroidal shells, the rings are treated as discrete members. In modeling the rings, the nine-node fifty-four degree-of-freedom shear-deformation shell element is also used. Connection of the rings with the shells is automatic in the ADINA program if corresponding nodes coincide.

4.7 Results

Natural frequencies of vibration are determined using the DQM for four cases of isotropic shells with large *R/r* ratio as described in Table 4-1. The shells have the following material parameters

$$\mathrm{E} = 0.207\mathrm{e}12 Pa;\ \mathrm{v} = 0.3;\ \rho = 7800 kg / m^3 \tag{4.18}$$

and are analyzed for completely free support conditions. The DQM convergence study for the first two natural frequencies for the four cases is presented in Table 4-2. The results have rapid convergence with 24 grid points sufficient to give four figure accuracy for these completely free shells. It is noted that for some grid choices the DQM may skip an eigenvalue.

In Table 4-3 are presented the results for the first six natural frequencies for cases 1-4 as obtained using the RKM, DQM and FEM. The RKM results are values obtained previously by Balderes and Armenakas [1973], where the FEM results are the converged values obtained using the nine-node shear-deformation shell element. The results are for an isotropic material as described in equation (4.18). Also presented in the table are the circumferential mode numbers obtained from the DQM solution for each of the frequencies.

For these shells the 2nd circumferential harmonic produces the lowest frequency. The thickness is different between cases 1 and 2, and it is seen that there is an increase in the frequencies for the thicker shell. Cases 2 and 3 have the same wall thickness ratio *r/h* and bend radius *R* but vary in the radius ratio *R/r*. It is noted that as the *R/r* ratio decreases there is an increase in the values of first two frequencies. The agreement between DQM and FEM results is excellent. The agreement with the RKM results is very close, but a maximum difference of 0.7 % in the fifth frequency of case 3 is noted.

The free vibrations of ring-stiffened toroidal shells are considered next. The stiffening rings which are assumed placed at meridional sections, are treated as discrete members (Fig. 4-2). Two different types of equally spaced rings 'light' and 'heavy' are employed for the shells. The rings parameters as defined by Balderes and Armenakas [1973] are given in Table 4-4. As the cross-sectional areas are in the ratio of 2 to 1, the weight of one heavy ring is twice the weight of one light ring.

Table 4-5 gives the frequencies of a validation study involving four 'light' and 'heavy' rings for cases 2 and 3. The effect on frequencies and mode shapes of equally spaced rings is considered. For the 4 'light' rings, cases 2 and 3 have FEM results that agree with the RKM results within 0.7%. For the 4 'heavy' rings, cases 2 and 3 have FEM results that agree with the RKM results within 3%. From the good agreement obtained, it is concluded that the nine-node fifty-four degree-of-freedom isoparametric shear-deformation shell elements is effective for the analysis of the rings attached to the toroidal shells. The effect of a greater number of rings is considered next.

The effect on the frequencies and mode shapes of equally spaced rings involving different number of rings and properties for all cases is considered next. Table 4-6 presents the FEM results for the 'light' rings. The results of this table indicate that the frequencies of the same circumferential harmonic increase when the shells are stiffened and they increase with increasing number of the rings. Cases 1 and 2 are only different in the thickness. It is noted that the frequencies are higher with the thicker stiffened shells. Cases 2 and 3 have the same ratio of r/h and R with different ratio of R/r, the results indicate that the frequencies decrease when the ratio of R/r increases.

In Table 4-7 are given results for stiffening using 'heavy' rings. The results of this table show the trends of frequencies with stiffening arrangements and geometry which are similar to the 'light' rings arrangements. It is seen that for the same number of rings, the frequencies are higher with the heavy rings except for the first frequency of these cases with 4 rings. It is also noted that for eight 'light' rings the shells have the same overall stiffener weight as for four 'heavy' rings. The frequencies for the shells with eight 'light' rings are higher, indicating that a number of 'light' rings are preferable to a few 'heavy' rings if the objective is to stiffen the structure.

In Tables 4-6 and 4-7, it is also seen that for cases 1 and 2, the natural frequencies can be obtained for all numbers of rings; for cases 3 and 4, the natural frequencies are not found when shells have 16 rings because the shell models become unstable in this condition, indicating that for some geometry parameters of the shells involving the particular rings arrangement, the stiffness matrix may not be positive definite, thus causing the numerical models to become unstable.

Shells with orthotropic materials are considered next. The properties of three orthotropic materials are given in Table 3-5. The explanation of this table has been given in chapter 3.

In Tables 4-8 to 4-10 are presented the results for the first six natural frequencies ω_i together with their circumferential mode number *m* for cases 1-4 when the shells consist of an orthotropic material. The three tables are respectively for materials M1, M2 and M3.

Table 4-8 presents the results of material M1 in which the Young's modulus of the circumferential direction is about two times larger than the modulus in the meridional direction ($E_1 = 2.14E_2$). There is generally excellent agreement between the results of the DQM and FEM for cases 1 and 4 with the same *r/h* ratio; the results are mostly within 0.3%, but a maximum difference of 0.9% is noted. For cases 2 and 3 with the same *r/h* ratio there is also close agreement between the DQM and FEM results, with maximum differences less than 2.4%. In case 2, the DQM has skipped the sixth eigenvalue.

Table 4-9 presents the results for material M2 where the Young's modulus of the circumferential direction is about seventeen times larger than the modulus in the meridional direction ($E_1 = 17.6E_2$). It is observed that the results of the DQM and FEM agree well in these four cases, but a few frequency differences of up to 6% are noted. It is also seen that the two sets of results are very close for the axisymmetric circumferential harmonic mode.

In Table 4-10 are given the results for material M3 where the Young's modulus of the circumferential direction is one hundred and five times larger than the meridional direction ($E_1 = 105E_2$). It is indicated that for the results of the DQM and FEM, there is generally good agreement for these shells. In cases 1 and 2 the maximum difference is 7%, while for cases 3 and 4, the maximum difference is 11%. It is also observed that there is excellent agreement of the two results for the axisymmetric circumferential harmonic mode.

The trends observed earlier for isotropic shells with regard to changes in wall thickness and radius ratio are observed again for these orthotropic shells. For the orthotropic shells the 2nd circumferential harmonic contains the lowest frequency. There is generally good agreement of the FEM and DQM results, but for a few frequencies differences of up to 11% are noted. The results show that in all cases the material of M2 produces higher natural frequencies than the materials M1 and M3 due to its greater overall stiffness. It is also indicated that with an increase in the ratio of the Young's modulus in the circumferential and meridional directions, larger differences in the DQM and FEM occur. The results for these three sets of orthotropic materials indicate that a combination of geometric and material properties can be selected to produce the higher natural frequencies.

Using the FEM approach mode shapes corresponding to the six lowest frequencies are plotted for each of the four isotropic cases. The full three-dimensional and the projections on the equator of the first six modes for the unstiffened shells of cases 1-4 are given in Figs. 4-3 to 4-10, respectively. The full three-dimensional and the projections on the equator of the first six modes for the stiffened shells with the 4 'light' and 'heavy' rings of case 2 are given in Figs. 4-11 to 4-14. The full three-dimensional and the projections on the equator of the first six modes for the stiffened shells with 8 'light' and 'heavy' rings of case 3 are given in Figs. 4-15 to 4-18, respectively. The full three-dimensional first six modes of the shell of case 1 with orthotropic material M1 are given in Fig. 4-19.

From the mode shapes of the unstiffened and stiffened shells, it is seen that in the unstiffened shells either the axisymmetric or the 2nd circumferential harmonic produce the lowest frequency while in the stiffened shells the 2nd circumferential harmonic dominates the motion. There is a significant change of the mode shapes between the unstiffened and stiffened shells. For the same number of rings, an obvious change of the mode shapes is observed for the 'light' and 'heavy' rings. It is also observed that the mode shapes are similar between the isotropic and orthotropic toroidal shells.

4.8 Conclusions

The theory for the RRM is developed for the vibration of toroidal shells. The expressions of the stiffness and mass matrices can be derived using this theory. The work can be used for further study. The natural frequencies corresponding to the mode shapes are developed for the toroidal shells with relatively large *R/r* ratio under 'completely free' support condition. For the cases of complete unstiffened and ring-stiffened isotropic toroidal shells, the results are obtained that agree well with previously published results. New results for the ring-stiffened toroidal shells are obtained using the FEM and it is indicated that the shells have higher natural frequencies when they are stiffened and a number of 'light' rings are preferable to a few 'heavy' rings when the two kinds of rings have the same overall stiffener weight. The FEM results presented are useful to indicate trends in shell behavior and can be used as validation results in future studies. The results of three different orthotropic materials determined using DQM show good agreement with results from the FEM. The natural frequencies have higher values when the shells consist of orthotropic material with higher stiffness in both directions. This study further shows the effectiveness and accuracy of the DQM in vibration analysis of toroidal shell structures. It provides useful results indicating that the capacity of toroidal shells can be improved by the use of the reinforcement. It also indicates that the different combinations of geometric and material properties can be selected to influence the size of the natural frequencies.

Chapter 5

Stability of an orthotropic complete circular toroidal shell -- large R/r ratio

5.1 Introduction

Toroidal shells may be stiffened in various ways to achieve greater strength to satisfy the objective of minimum weight of structures. Stability analysis of these shells is important in the design process [Teng, 1996], and may be conducted using a number of methods [Yamaki, 1984]. The Rayleigh-Ritz method (RRM) [Washizu, 1982] has particular advantage for the study of reinforced shells and shells with simple boundary conditions. It has been used by a number of researchers, e.g. Tian, Wang and Swaddiwudhipong [1999], Wang, Tian and Swaddiwudhipong [1994], and Huang [2002], with excellent results, and is thus adopted for the current study.

The classical problem of the stability analysis of an isotropic unreinforced toroidal shell under uniform external pressure has been considered by a number of authors, e.g. Sobel and Flügge [1967], Jordan [1973] and Panagiotopolous [1985]. Analytical results showing good agreement with each other and with limited experimental results have been obtained. With the introduction of orthotropic materials, and with the increased use of light-weight structures employing reinforced thin-walled members, a need has developed for a buckling solution for a toroidal shell going beyond the classical isotropic one.

In this study the linearized buckling problem of an orthotropic complete toroidal shell under external pressure is analyzed using the RRM. Also considered is the buckling of a complete isotropic stiffened toroidal shell. The solution is developed within the context of the Sanders-Budiansky first-order linear shell theory. Numerical results obtained using the FEM are also presented.

5.2 Shell geometry

The toroidal shell considered has a bend radius R, a cross-sectional radius r, and a thickness h (Fig. 4.1). It is a complete shell, extending through 360° in the circumferential and meridional directions.

A general point P on the shell mid-surface is defined by circumferential and meridional angular coordinates ϕ and θ. The radius vector **r** to P is given by Dym [1974] as

$$\mathbf{r} = (R + r\cos\theta)\sin\phi\,\mathbf{i} + (R + r\cos\theta)\cos\phi\,\mathbf{j} + r\sin\theta\,\mathbf{k} \tag{5.1}$$

where **i, j, k** are unit vectors forming a base in the Cartesian x, y, z coordinate system. The first fundamental form of the middle surface is given by

$$ds^2 = A_1^2 d\xi_1^2 + A_2^2 d\xi_2^2$$

where ds is the differential line element, A_1 and A_2 are the Lamé parameters and ξ_1 and ξ_2 are the base coordinates. The base coordinates are taken as

$$\xi_1 = \theta;\ \xi_2 = \eta = \overline{\rho}\phi \tag{5.2}$$

where $\overline{\rho} = R/r$. The adoption of the second circumferential coordinate η is to allow for extension at a later date of the present theory to incomplete toroidal shells, i.e. curved pipes. The Lamé parameters, and principal radii of curvatures R_1 and R_2, which are used in the shell theory, are given by

$$A_1 = r\,; A_2 = r\zeta\,;\; R_1 = r\,;\; R_2 = r\zeta/(\gamma\cos\theta) \tag{5.3}$$

$$\zeta = 1 + \gamma\cos\theta\,;\; \gamma = r/R = \overline{\rho}^{-1} \tag{5.4}$$

In the development of the theory the inverse of various orders of ζ are required. To facilitate the development of closed form expressions the series for the inverses are truncated as follows

$$\zeta^{-1} = \frac{1}{1+\gamma\cos\theta} = 1 - \gamma\cos\theta + \gamma^2\cos^2\theta - \gamma^3\cos^3\theta$$

$$\zeta^{-2} = \frac{1}{(1+\gamma\cos\theta)^2} = 1 - 2\gamma\cos\theta + 3\gamma^2\cos^2\theta - 4\gamma^3\cos^3\theta \tag{5.5}$$

$$\zeta^{-3} = \frac{1}{(1+\gamma\cos\theta)^3} = 1 - 3\gamma\cos\theta + 6\gamma^2\cos^2\theta - 10\gamma^3\cos^3\theta$$

These truncations for a toroidal shell of radius $R/r \geq 5.0$ lead to a maximum error in the series of 0.44%.

5.3 Constitutive relations for an orthotropic shell

The constitutive relations for an orthotropic shell relating the stress and moment resultants to the strain and curvature functions are given as [Raymond et al, 2000]

$$N_\theta = A_{11}(\varepsilon_\theta + \nu_{\eta\theta}\varepsilon_\eta);\quad N_\eta = A_{22}(\varepsilon_\eta + \nu_{\theta\eta}\varepsilon_\theta);\quad \overline{N}_{\theta\eta} = A_{66}\varepsilon_{\theta\eta} \tag{5.6}$$

$$M_\theta = D_{11}(\kappa_\theta + \nu_{\eta\theta}\kappa_\eta);\; M_\eta = D_{22}(\kappa_\eta + \nu_{\theta\eta}\kappa_\theta);\; \overline{M}_{\theta\eta} = D_{66}\kappa_{\theta\eta}$$

where N_θ, N_η, $\overline{N}_{\theta\eta}$, M_θ, M_η, $\overline{M}_{\theta\eta}$ are the meridional, circumferential, and shear stress and moment resultants and ε_θ, ε_η, $\varepsilon_{\theta\eta}$, κ_θ, κ_η, $\kappa_{\theta\eta}$ are the meridional, circumferential, and shear strains and curvatures. The material constants are given by

$$A_{11} = E_\theta\, h/(1-\nu_{\theta\eta}\nu_{\eta\theta});\ \ A_{22} = E_\eta\, h/(1-\nu_{\theta\eta}\nu_{\eta\theta});\ A_{66} = G_{\theta\eta}\, h$$
$$A_{12} = A_{11}\nu_{\theta\eta} = A_{22}\nu_{\eta\theta};\quad D_{11} = E_\theta\, h/[12(1-\nu_{\theta\eta}\nu_{\eta\theta})]; \tag{5.7}$$
$$D_{22} = E_\eta\, h/[12(1-\nu_{\theta\eta}\nu_{\eta\theta})];\ D_{66} = G_{\theta\eta}\, h^3/12;\ D_{12} = D_{11}\nu_{\theta\eta} = D_{22}\nu_{\eta\theta}$$

where E_θ, E_η are the Young's moduli, $\nu_{\theta\eta}$, $\nu_{\eta\theta}$ are the Poisson's ratios, and $G_{\theta\eta}$ is the shear modulus.

5.4 Strain energy of the shell

The strain energy due to inplane stretching and bending of the shell is given [Ip et al, 1996] by

$$\begin{aligned}\overline{U} &= \frac{1}{2}\int_0^{2\pi}\int_0^{2\pi}(A_{11}\varepsilon_\theta^2 + 2A_{12}\varepsilon_\theta\varepsilon_\eta + A_{22}\varepsilon_\eta^2 + A_{66}\varepsilon_{\theta\eta}^2)\,dVol \\ &+ \frac{1}{2}\int_0^{2\pi}\int_0^{2\pi}(D_{11}\kappa_\theta^2 + 2D_{12}\kappa_\theta\kappa_\eta + D_{22}\kappa_\eta^2 + D_{66}\kappa_{\theta\eta}^2)\,dVol\end{aligned} \tag{5.8}$$

where $dVol = A_1 A_2 d\theta\, d\eta$ is the volume element. Using the assumptions of the first-order Sanders-Budiansky shell theory [Sanders, 1959] [Budiansky, 1968] the strain and curvatures for a toroidal shell are given by

$$\begin{aligned}\varepsilon_\theta &= a_1 u^\bullet + a_2 w \\ \varepsilon_\eta &= a_3 u + a_4 v' + a_5 w \\ \varepsilon_{\theta\eta} &= a_6 u' + a_7 v + a_8 v^\bullet \\ \kappa_\theta &= a_9 u^\bullet + a_{10} w^{\bullet\bullet} \\ \kappa_\eta &= a_{11} u + a_{12} v' + a_{13} w^\bullet + a_{14} w'' \\ \kappa_{\theta\eta} &= a_{15} u' + a_{16} v^\bullet + a_{17} v + a_{18} w^{\bullet\prime} + a_{19} w'\end{aligned} \tag{5.9}$$

where *u, v, w* are the displacements in the meridional, circumferential, and radial directions, and the $a_1 - a_{19}$ are functions of the Lamé parameters and curvatures, which are given in Appendix B1.

The displacements of the onset of buckling are taken as

$$
\begin{aligned}
u(\theta,\eta) &= \sum_{n=1}^{N} u_n \sin n\theta \sin \mu_m \eta \\
v(\theta,\eta) &= \sum_{n=1}^{N} v_n \cos n\theta \cos \mu_m \eta \\
w(\theta,\eta) &= \sum_{n=1}^{N} w_n \sin n\theta \sin \mu_m \eta
\end{aligned}
\tag{5.10}
$$

where $\mu_m = m\pi\gamma/\psi$, with $\psi = 2\pi$ for a complete shell, and u_n, v_n, w_n are the unknown Ritz coefficients. The expressions (5.10) represent a buckling mode of the shell corresponding to a specified circumferential harmonic *m*.

The strain energy of the shell is given by

$$
\begin{aligned}
\overline{U} = \frac{1}{2}\int_0^{2\pi}\int_0^{2\pi} & (A_{22}[a_{20}(u^\bullet)^2 + a_{21}u^\bullet w + a_{22}w^2] \\
& + 2A_{21}[a_{23}u^\bullet u + a_{24}u^\bullet v' + a_{25}u^\bullet w + a_{26}uw + a_{27}v'w + a_{28}w^2] \\
& + A_{11}[a_{29}u^2 + a_{30}(v')^2 + a_{31}w^2 + a_{32}uv' + a_{33}uw + a_{34}v'w] \\
& + A_{66}[a_{35}(u')^2 + a_{36}v^2 + a_{37}(v^\bullet)^2 + a_{38}u'v + a_{39}u'v^\bullet + a_{40}vv^\bullet] \\
& + D_{22}[a_{41}(u^\bullet)^2 + a_{42}u^\bullet w^{\bullet\bullet} + a_{43}(w^{\bullet\bullet})^2] \\
& + 2D_{12}[a_{44}uu^\bullet + a_{45}u^\bullet v' + a_{46}u^\bullet w^\bullet + a_{47}u^\bullet w'' + a_{48}uw^{\bullet\bullet} \\
& \qquad + a_{49}v'w^{\bullet\bullet} + a_{50}w^{\bullet\bullet}w^\bullet + a_{51}w^{\bullet\bullet}w''] \\
& + D_{11}[a_{52}u^2 + a_{53}uv' + a_{54}(v')^2 + a_{55}(w^\bullet)^2 + a_{56}(w'')^2 + a_{57}uw^\bullet \\
& \qquad + a_{58}v'w^\bullet + a_{59}uw'' + a_{60}v'w'' + a_{61}w^\bullet w''] \\
& + 4D_{66}[a_{62}(u')^2 + a_{63}u'v^\bullet + a_{64}(v^\bullet)^2 + a_{65}v^2 + a_{66}(w^{\bullet\prime})^2 + a_{67}w^{\bullet\prime}w' \\
& \qquad + a_{68}(u')^2 + a_{69}u'v + a_{70}v^\bullet v + a_{71}vw^{\bullet\prime} + a_{72}vw' + a_{73}u'w^{\bullet\prime} \\
& \qquad + a_{74}u'w' + a_{75}v^\bullet w^{\bullet\prime} + a_{76}v^\bullet w'])r^2\zeta \, d\theta \, d\eta
\end{aligned}
\tag{5.11}
$$

where the constants $a_{20} - a_{76}$ are known functions of the geometry which are given in Appendix B1.

5.5 Strain energy of the stiffeners

The toroidal shell is strengthened by a total of M ring-stiffeners as shown in Fig. 5-1. The stiffeners may be placed externally or internally. The kth ring-stiffener is located at $a_k\pi$ from the yz plane, and has an axial rigidity E_kA_k, torsional rigidity of G_kJ_k, and flexural rigidities of $E_kI_{zk}, E_kI_{\eta k}$ about the z (coordinate normal to middle surface of the shell) and η coordinates respectively. For convenience the following quantities are defined for subsequent use

$$A_1 = \frac{E_kA_k}{r+e_k};\ E_1 = \frac{E_kI_{zk}}{r+e_k};\ E_2 = \frac{E_kI_{zk}}{(r+e_k)^2};\ E_3 = \frac{E_kI_{\eta k}}{(r+e_k)^3} \tag{5.12}$$

$$G_1 = \frac{G_kJ_k}{r+e_k};\ G_2 = \frac{G_kJ_k}{(r+e_k)^2};\ G_3 = \frac{G_kJ_k}{(r+e_k)^3}$$

where e_k is the distance between the centroid of the kth stiffener and the shell mid-surface. A positive value for e_k implies an external stiffener while a negative value an internal one.

The strain energy U_k of the kth ring stiffener is given by Tian [1999]

$$\begin{aligned}\overline{U}_k = \frac{1}{2}\int_0^{2\pi} [&E_1(\frac{\overline{\rho}}{R\zeta} w_k^{s}{}' + \frac{1}{r+e_k} v_k^{s\bullet\bullet})^2 \\ &+ E_3(w_k^s + w_k^{s\bullet\bullet})^2 + A_1(u_k^{s\bullet} - w_k^s)^2 \\ &+ G_1(-\frac{\overline{\rho}}{R\zeta} w_k^{s}{}'^{\bullet} + \frac{1}{r+e_k} v_k^{s\bullet})^2] d\theta\end{aligned} \tag{5.13}$$

From geometrical considerations the relations between the stiffener displacements u_k^s, v_k^s, w_k^s of the kth stiffener and the displacements of the shell u_k, v_k, w_k at the position $\eta = a_k\pi$ of the stiffener are given by

$$
\begin{aligned}
u_k^s &= (1+\frac{e_k}{r})u_k + \frac{e_k}{r} w_k^{\bullet} \\
v_k^s &= v_k + \frac{\bar{\rho} e_k}{R\zeta} w_k^{\bullet} \qquad (5.14) \\
w_k^s &= w_k
\end{aligned}
$$

Substituting eqn. (5.14) into eqn. (5.13) the strain energy of the kth stiffener is obtained as

$$
\begin{aligned}
\overline{U}_k = \int_0^{2\pi} [&(b_1+b_4+b_8)(w_k')^2 + b_2 w_k' v_k^{\bullet\bullet} + b_3 w_k' w_k^{\bullet\bullet\prime} \\
&+ (2b_2+b_{11}) w_k'^{\bullet} w_k' + b_6 (v_k')^2 + b_7 (w_k'^{\bullet})^2 \\
&+ b_9 v_k^{\bullet} w_k'^{\bullet} + b_{10} v_k^{\bullet} w_k' + b_{12} w_k^2 + b_{13} w_k w_k^{\bullet\bullet} \\
&+ b_{14} (w_k^{\bullet\bullet})^2 + b_{15} (u_k^{\bullet})^2 + b_{16} u_k^{\bullet} w_k^{\bullet\bullet} + b_{17} (w_k^{\bullet\bullet})^2 \\
&+ b_{18} (u_k^{\bullet\prime})^2 + b_{19} u_k'^{\bullet} w_k^{\bullet\bullet\prime} + b_{20} (w_k^{\bullet\bullet\prime})^2] d\theta
\end{aligned} \qquad (5.15)
$$

where the $b_1 - b_{20}$ are given in Appendix C1.

5.6 Potential of the pressure

The work done by the uniform external pressure is obtained by taking the product of the pressure and the change in the volume enclosed by the shell mid-surface. From the Sanders-Budiansky theory [Sanders, 1959] [Budiansky, 1968] the work W done by the external pressure p for a toroidal shell is given by

$$
\overline{W} = \frac{p}{2} \int_0^{2\pi} \int_0^{2\pi} [\phi_\theta u + \phi_\eta v + (\varepsilon_\theta + \varepsilon_\eta) w] r^2 \zeta \, d\theta \, d\eta \qquad (5.16)
$$

where the rotations ϕ_θ, ϕ_η of the shell are given by

$$\phi_\theta = -\frac{1}{r}w^\bullet + \frac{u}{r} = a_{77}w^\bullet + a_{78}u \tag{5.17}$$

$$\phi_\eta = -\frac{1}{r\zeta}w' + \frac{v\gamma\cos\theta}{r\zeta} = a_{79}w' + a_{80}v$$

The constants $a_{77} - a_{80}$ are given in the Appendix B1.

5.7 Rayleigh-Ritz procedure

The total potential energy Π of the ring-stiffened shell is given by

$$\Pi = \overline{U} + \sum_{i=1}^{M}\overline{U}_k - \overline{W} \tag{5.18}$$

The requirements for the stationarity of the total potential energy are satisfied through the enforcement of the following relations

$$\frac{\partial\Pi}{\partial u_j} = 0;\ \frac{\partial\Pi}{\partial v_j} = 0;\ \frac{\partial\Pi}{\partial w_j} = 0;\ \text{for } j = 1,2,\ldots,\mathrm{N} \tag{5.19}$$

The equations (5.18) and (5.19) lead to a set of $3\times N$ simultaneous linear algebraic equations for each choice of the circumferential harmonic *m*. As the shell meridian is complete no boundary conditions need be specified. The assembly of the domain equations yields for each choice of *m* a matrix equation of the form

$$\left\{\begin{bmatrix} K_{uu} & K_{uv} & K_{uw} \\ K_{uv}^t & K_{vv} & K_{vw} \\ K_{uw}^t & K_{vw}^t & K_{ww} \end{bmatrix} + \sum_{i=1}^{M}\begin{bmatrix} K_{kuu} & 0 & K_{kuw} \\ 0 & K_{kvv} & K_{kvw} \\ K_{kuw}^t & K_{kvw}^t & K_{kww} \end{bmatrix} - \overline{\lambda}\begin{bmatrix} G_{uu} & 0 & G_{uw} \\ 0 & G_{vv} & G_{vw} \\ G_{uw}^t & G_{vw}^t & G_{ww} \end{bmatrix}\right\}\begin{Bmatrix} u \\ v \\ w \end{Bmatrix} = \begin{Bmatrix} 0 \\ 0 \\ 0 \end{Bmatrix} \tag{5.20}$$

where

$$u = \begin{Bmatrix} u_1 \\ u_2 \\ \vdots \\ u_N \end{Bmatrix} \qquad v = \begin{Bmatrix} v_1 \\ v_2 \\ \vdots \\ v_N \end{Bmatrix} \qquad w = \begin{Bmatrix} w_1 \\ w_2 \\ \vdots \\ w_N \end{Bmatrix} \tag{5.21}$$

and $\overline{\lambda} = p/2$ is the eigenvalue. The submatrices K_{ij}, K_{kij}, G_{ij} are each of size $N \times N$ and formulas for their calculation are given in the Appendix B2.

5.8 Finite element method

The general commercial FEM program ADINA [ADINA, 2003] is used as an alternate means to obtain numerical results. In this program a nine-node fifty-four degree-of-freedom shear-deformation shell element is available. The linearized buckling option was used to obtain results instead of the incremental non-linear analysis used earlier for toroidal shells by Shin and Redekop [2000].

To obtain a buckling solution using ADINA it is necessary to provide supports for the shell. To satisfy this requirement in the analysis either the inner or outer equatorial lines were restrained against displacement or both. The entire shell was modeled disregarding the geometric symmetry. Convergence studies were carried out to ensure the accuracy of the solution.

For the ring-stiffened toroidal shells, the rings placed at meridional sections are treated as discrete members. In the ADINA program, the same nine-node element need for the shell is also used for the rings, and its effectiveness has been discussed in chapter 4.

5.9 Results

The way in which buckling occurs depends on how the shell is loaded and on its geometrical and material properties. Theoretically, the critical buckling loads of toroidal shells under external pressure are dependent on the ratios of bend to cross-section radius (R/r) and the ratio of cross-section to thickness (r/h). Thus, if the sizes of the shells are changed but the ratios of R/r and r/h are kept constant, the buckling loads should remain constant.

In order to set up the proper models using the FEM-ADINA program for buckling analysis, one case was used to check whether the size of the toroidal shells affects the buckling load. The shell for this case has the following geometric and material parameters

$R/r = 10$; $r/h = 100$

$E = 0.207\text{e}12\text{Pa}$; $v = 0.3$

The support condition used in this testing is a fixed line along the inner equator and the loading is the uniform external pressure, $p = 0.1$, 1 and 10 respectively.

In Table 5-1 are given the ADINA buckling results for shells of different size but all having the geometric and material parameters mentioned above. It is seen that the ADINA results for λ decrease as the shell size is increased, i. e. as the thickness is increased. It appears that in the buckling analysis using the ADINA program, for the load used, stable results are obtained for models having a thickness equal to or greater than 0.01. This dependence of λ on shell size in the ADINA results is believed to be due to shear locking, and is accounted for subsequently in this study.

A study of buckling pressures using the FEM of complete toroidal shells is considered next. The buckling pressures are determined for four cases of isotropic toroidal shells (I-IV) as described in Table 5-2. The cases have previously been considered by other researchers. Also presented in Table 5-2 are the descriptions of four further cases (1-4) of toroidal shells for which a parametric study is conducted in the following. All the cases have shell thickness as required for correct FEM results.

Table 5-3 gives the results of a validation study involving the cases I-IV. The values in this table are the critical buckling pressures in *MPa* obtained from the analytical approach of Sobel and Flügge [1967], the formula of Jordan [1973], the FEM approach of Panagiotopolous [1985], and the current FEM approach (FEMA, FEMB, FEMC). The latter results are obtained using a linearized buckling analysis with a nine-node isoparametric shell element available in ADINA.

The three current FEM results are respectively for a fine, medium, and coarse mesh. As an example, for case I the fine mesh (FEMA) has a size of 80×160 elements, the medium mesh (FEMB) a size of 60×120 elements, and the coarse mesh (FEMC) a size of 40×80 elements. This indicates that a very fine mesh has to be used to get accurate results in the FEM analysis. The support condition used in the current analysis is a fixed line along the inner equator, see Fig. 5-2. All results are for an isotropic material with E = 0.21e6 *MPa* and ν = 0.3. The above mentioned investigation predicted that buckling should occur in an axisymmetric mode. Thus it is observed that the buckling modes for these four shells are axisymmetric as seen in the mode shapes given in Fig. 5-3.

These four cases have the same wall thickness *h* and cross-sectional radius *r*, but vary in the bend radius *R*. It is seen that as the bend increases there is a decrease in the value of the critical buckling pressure. The decrease results mainly from the loss of the beneficial effect of double curvature. For cases II and III the present converged FEM results agree with the Sobel and Flügge results to within 0.2%. For cases I and IV larger differences are noted, with a maximum value of 6% arising for case I. From this table, the good agreement indicates that the ADINA models having a thickness equal to or greater than 0.01 is the proper models in linearized buckling analysis and can be applied for the following study.

The critical buckling pressures of four further shells are determined. Analysis for both unstiffened and stiffened conditions was carried out. The shells (labeled 1-4) are described in detail in Table 5-2. These shells have relatively large *R/r* ratios, varying from 5 to 10. The thickness ratio *r/h* of these shells is either 50 or 100. Two different types of rings are employed each with equally spaced reinforcement. The ring parameters are given in Table 4-4 and defined by Balderes and Armenakas [1973].

In Table 5-4 results are given for shells stiffened with 'light' rings. For this stiffening arrangement a nondimensional cross-sectional area of $\overline{A}_k$=0.005 is used per ring. The results of Table 5-4 are for the cases 1-4 under unstiffened conditions and stiffened conditions with 4, 8, 12 or 16 rings. Analyses were carried out assuming a line of support at the inner equator, at the outer equator, or at both equators, see Fig. 5-2. Values given are for the critical buckling pressure in *MPa* determined using the FEM. The material parameters were taken as E = 0.207e6 *MPa* and ν = 0.3. Also presented in the table is the fine mesh size of the shells.

The results of Table 5-4 indicate that for unstiffened shells the buckling pressure is at a minimum when there is support at the inner equator and at a maximum when there is support at both equators. There is a relatively small increase when the support is moved from the inner equator to the outer one. Case 1, 2 and 3 have the same r/h ratio and same bend radius R, but vary in R/r ratio. It is observed that the buckling pressure decreases when the ratio of R/r increases. Cases 3 and 4 differ only in the wall thickness h, the buckling pressure is higher for the thicker shell.

For stiffened shells the minimum buckling pressure occurs when the support is at the inner or outer equator and the maximum when there is support at both equators. Note that generally the buckling pressure increases when the shell is stiffened. There is a significant rise in the buckling pressure with an increase in the number of reinforcement rings. Cases 1, 2 and 3 have the same thickness ratio r/h and bend radius R. For the same ring numbers, the results show that the buckling pressure decreases when the radius ratio of R/r increases. The shell of case 4 has a thickness twice that of shell 3 but is similar in other aspects. It is seen that the buckling pressure of case 4 is approximately four times that of case 3 indicating a quadratic dependence of the buckling pressure on the thickness.

In Table 5-5 results are given for shell stiffening with 'heavy' rings. For this stiffening arrangement a nondimensional cross-sectional area of $\overline{A}_k$=0.01 is used per ring, i.e. twice the area for the 'light' rings. Otherwise, the results given in Table 5-5 are for shells having the same supports, reinforcement arrangements, materials and mesh size as the shells of Table 5-4.

The results of Table 5-5 indicate trends of buckling pressure with supports, stiffening arrangements, and geometry which are similar to those with the 'light' rings. It is seen that for the same number of rings, the buckling pressures are higher with the heavy rings when there is support at the inner or outer equators. It is also observed that for eight 'light' rings the shells have the same overall stiffener weight as for four 'heavy' rings. The buckling pressures for the shells with eight 'light' rings are higher, indicating that a large number of 'light' rings is preferable to a few 'heavy' rings.

In Tables 5-4 and 5-5, it is also observed that for case 1, when the ring number is increased to 12, there is numerical instability in the solutions and their buckling loads are not obtained from FEM, but the buckling loads can be obtained when the shell has 16 rings. In case 2, the buckling loads can be obtained for all numbers of the rings. For cases 3 and 4, the FEM models are unstable and their buckling loads are not found when they have 16 rings. The unstable models with the particular number of rings indicate that for some geometry parameters of the shells involving the arrangement of the rings, the stiffness matrix may not be positive definite, thus the FEM models become unstable in this condition.

Using the FEM, mode shapes corresponding to the lowest buckling pressure are plotted for each of the four cases. Figs. 5-4 to 5-7 present for each of the cases 1-4 the buckling mode shapes of the unstiffened shell and the mode shapes of the shell stiffened with four or eight 'light' or 'heavy' rings with the inner equator support condition. Figs. 5-8 and 5-9 are the three-dimensional view of the buckling mode shapes of the unstiffened shell and mode shapes of the shell stiffened with four or eight 'light' or 'heavy' rings with the outer and both equators support condition for case 1. The predominant mode is $m = 0$ throughout. It is seen that for cases 1-4 the rings have a relatively small effect in modifying the buckling mode. The figures also indicate that there is a relatively small change in the buckling mode shapes when the 'light' rings are replaced with 'heavy' rings for all cases. In case 1, there is obvious change in the buckling mode shapes when the shell has the different boundary conditions.

Shells with orthotropic materials are considered next. In Table 5-6 are presented the results for the critical buckling pressure for cases 1-4 when the shells are unstiffened and consist of three different orthotropic materials. The properties of these materials are given in Table 3-5. The details of this table have been discussed in chapters 3 and 4. The trends observed earlier for isotropic shells with regard to changes in wall thickness and boundary conditions are observed again for these orthotropic shells. It is observed that for material M1, the buckling pressure is at a minimum when there is support at the inner equator, while for material M2, the minimum buckling pressure occurs in the outer equator support condition except for case 4. For material M3, there is a minimum buckling pressure in the outer equator support condition. In all cases, the support at both equators produces the maximum buckling pressure. In case 1 with materials M1, M2 and M3, there is a large increase of buckling pressure when there is support at both equators. It is also seen that for these four cases in material M2, they have higher buckling pressure under the same boundary conditions. It is due to its higher stiffness. It is seen that by selecting different combinations of material and geometric properties higher buckling pressures can be produced.

5.10 Conclusions

Buckling theory based on the RRM has been developed for ring-stiffened toroidal shells. The theory developed is available for further study. Numerical results are presented using the FEM. For the cases of complete isotropic unstiffened toroidal shells, results are obtained that agree well with previously published results. The critical buckling pressures are found for different shell parameters, varying ring properties, various boundary conditions and different material properties. New results for the ring-stiffened toroidal shells with large bend to cross-section radius ratios are obtained using FEM and show that the shells produce higher buckling pressure when they are stiffened and a number of 'light' rings are preferable to a few 'heavy' rings when the two kinds of rings have the same overall stiffener weight. New values for complete unstiffened orthotropic toroidal shells are determined from the FEM with three different orthotropic materials. These three sets of results show that the material with higher stiffness in both directions can produce higher buckling pressures. The results also indicate that different combination of the geometric and material properties can be selected to increase the magnitude of buckling pressures.

Chapter 6

Conclusions

6.1 Free vibration of a complete orthotropic circular toroidal shell -- small R/r ratio

The problem of the free vibration of a thin shell of revolution is studied. The solution of this problem for orthotropic toroidal shells is developed. The effects of the geometric and material properties are also studied for such shells and it is concluded that:

- Good and fast convergence trends of the DQM are observed from the vibration analysis of the toroidal shells with small R/r ratio, indicating that the DQM is a computationally efficient numerical method in applied mechanics area.
- There is generally excellent agreement of the DQM, FEM and RKM results for the complete isotropic toroidal shells with 'completely free' support condition and the good agreement of the DQM and FEM results of such shells with two different line support condition, further indicate the distinctive characteristics of the DQM and its high accuracy in vibration analysis for shell structures with various boundary conditions.
- The fundamental frequency changes with changing geometric parameters, such as the radius, and the ratios *R/r* and *r/h.*
- New values are obtained for complete orthotropic shells with three different orthotropic materials, indicating that the material with higher stiffness in both directions can produce higher fundamental frequency.
- This study confirms the usefulness of the DQM for the vibration analysis of a thin

shell of revolution. By selecting appropriate geometric and material properties desirable values for frequencies of shells can be obtained.

6.2 Free vibration of a complete orthotropic circular toroidal shell -- large R/r ratio

The application of the DQM is furthered through the study of the free vibration problem of toroidal shells with large R/r ratio. The effects of the geometric parameters, ring arrangements, and material properties are studied for such shells, and it is concluded that:

- Good and fast convergence trends of the DQM are observed again from the vibration analysis for shells with large R/r ratio. The results showed excellent agreement between the DQM, FEM and RKM, and further demonstrated that the DQM is a very powerful numerical method in vibration analysis for shell structures.
- The fundamental frequency changes upon changing the geometric parameters, such as the radius, and the ratios R/r and r/h.
- New results are obtained for the ring-stiffened toroidal shells, indicating that the shells have higher fundamental frequency when they are stiffened and when the number of the rings is increased. These new values further indicate that a number of 'light' rings are preferable to a few 'heavy' rings when the two kinds of rings have the same overall stiffener weight.
- The results of three different orthotropic materials for unstiffened toroidal shells determined using the DQM and show good agreement with results from the FEM.

The results indicate that the orthotropic materials with the higher stiffness produce higher fundamental frequency.

6.3 Stability of an orthotropic complete circular toroidal shell -- large R/r ratio

The problem of the buckling analysis of ring-stiffened toroidal shells with large *R/r* ratio was formulated and the critical buckling pressures corresponding to the mode shapes were developed for different shell parameters, various boundary conditions, varying ring properties and different material properties. It is concluded that:

- Good agreement is obtained between the FEM results and previously published results. It is indicated that the appropriate ADINA models having a thickness equal to or greater than 0.01 can be used for buckling analysis.
- The buckling pressure changes upon changing the geometric parameters, such as the ratios of *R/r* or *r/h*.
- New values are obtained for the ring-stiffened toroidal shells with different circumferential boundary conditions, indicating that the shells have higher buckling pressures when they are stiffened and the buckling pressure increases with a increasing number of rings. These new values further indicate that in the case of the same overall stiffener weight, a number of 'light' rings is preferable to a few 'heavy' rings.
- Three sets of results for completely unstiffened orthotropic toroidal shells are determined, indicating that orthotropic material with higher stiffness in both directions can produce higher buckling pressures.

6.4 Suggestions for further research

The current study concerns the vibration and buckling analysis of the perfect complete elastic toroidal shells with circular cross–section. Further research could be conducted on the imperfect circular toroidal shell, perfect and imperfect elliptic toroidal shells.

In the current study, the uniform external pressure is considered for the buckling analysis. Further research could be conducted for more complex types of loadings or support conditions. An example of the latter would be 'point' supports in the nature of those provided in the Stanford Torus.

The stiffening rings are equally spaced around the circumference in the current study. In further research, results could be obtained for the stiffening rings with unequal spacing.

The material adopted for the current study is a one-layered orthotropic material. Further work could be conducted on multi-layer laminated composite materials which have many advantages in engineering practice.

References

Abramovich, H., Singer, J. and Weller, T., Repeated buckling and its influence on the geometrical imperfections of stiffened cylindrical shells under combined loading, International Journal of Non-Linear Mechanics, 37 (2002) 577-588

ADINA Verification Manual, ARD2003-9, ADINA R & D Inc., Watertown, 2003

Araar, M. and Jullien, J.F., Buckling of cylindrical shells under external pressure proposition of a new shape of self-stiffened shell, Structural Engineering and Mechanics, 4,4 (1996) 451-460

Baig, M.I. and Yang, T.Y., Buckling analysis of orthogonally stiffened waffle cylinders, Journal of Spacecraft, 11,12 (1974) 832-837

Baker, E.H., Kovalevsky, L. and Rish, F.L., Structural Analysis of Shells, McGraw Hill, 1972

Baker, W.R., Bello, S.D., Marcuzzi, D., Sonato, P. and Zaccaria, P., Design of a new toroidal shell and support for RFX, Fusion Engineering and Design 63,64 (2002) 461-466

Baker, W.R., Bevilacqua, G., Elio, F., Gneotto, F., Parma, A., Rigadello, D. and Sonato, P., The construction of the RFX vacuum vessel, CH2820-9/89 (1989) IEEE, 974-977

Baker, W.R., Bevilacqua, G., Carretta, R., Elio, F., Fauri, M., Gneotto, F. and Saccrdo, B., Technological aspects in the production of a large aluminium shell, CH2820-9/89, (1989) IEEE, 846-849

Balderes, T. and Armenakas, A.E., Free vibrations of ring-stiffened toroidal shells, AIAA Journal, 11 (1973) 1637-1644

Baruch, M. and Singer, J., Effect of eccentricity of stiffeners on the general instability of stiffened cylindrical shells under hydrostatic pressure, Journal of Mechanical Engineering Science, 5 (1963) 23-27

Bert, C.W., Jang, S.K. and Striz, A.G., Two new approximate methods for analyzing free vibration of structural components, American Institute of Aeronautics and Astronautics Journal 26 (1988) 612-618

Bert, C.W. and Malik, M., Differential quadrature method in computational mechanics: A review, Applied Mechanics Review, 49,1 (1996a) 6-27

Bert, C.W. and Malik, M., Free vibration analysis of thin cylindrical shells by the differential quadrature method, Journal of Pressure Vessel Technology, 118 (1996b) 7-12

Bielski, J., Influence of geometrical imperfections on buckling pressure and post-buckling of elastic toroidal shells, Mechanics of Structures and Machines, 20 (1992) 145-154

Blachut, J. and Jaiswal, O.R., Instabilities in torispheres and toroids under suddenly applied external pressure, International Journal of Impact Engineering, 22 (1999) 511-530

Blachut, J. and Jaiswal, O.R., On buckling of toroidal shells under external pressure, Computers and Structures, 77 (2000) 233-251

Blachut, J., Collapse tests on externally pressurized toroids, Pressure Vessel and Piping Codes and Standards- 2002, ASME (2002) 65-72

Budiansky, B., Notes on nonlinear shell theory, Journal of Applied Mechanics, 40 (1968) 393-401

Bushnell, D., Computerized Buckling Analysis of Shells, Martinus Nijhoff Publishers, Dordrecht, 1985

Bushnell, D., Elastic-plastic bending and buckling of pipes and elbows, Computers and Structures, 13 (1981) 241-248

Chakraverty S., Bhat, R. B. and Stiharu, I., Recent research on vibration of structures using boundary characteristic orthogonal polynomials in the Rayleigh-Ritz method, The Shock and Vibration Digest, 31,3 (1999) 187-194

Choi, S.T. and Chou, Y.T., Vibration analysis of non-circular curved panels by the differential quadrature method, Journal of Sound and Vibration 259,3 (2003) 525-539

Clark, R.A., On the theory of thin elastic toroidal shells, Journal of Mathematics and Physics, 29,3 (1950) 146-178

Das, P.K. Thavalingam, A. and Bai, Y., Buckling and ultimate strength criteria of stiffened shells under combined loading for reliability analysis, Thin-Walled Structures, 41 (2003) 69-88

Dym, C.L., Introduction to the Theory of Shells, Pergamon, Oxford, 1974

Flügge, W., Stresses in Shells, Springer-Verlag, New York, 1967

Galletly, G.D. and Blachut, J., Stability of complete circular and non-circular toroidal shells, Journal of Mechanical Engineering Science, 209 (1995) 245-255

Galletly[a], G.D and Galletly[b], D.A., Buckling of complex toroidal shell structures, Thin-Walled Structures, 26,3 (1996) 195-212

Galletly, G.D., Elastic buckling of complete toroidal shells of elliptical cross-section subjected to uniform internal pressure, Thin-Walled Structures, 30,1,3 (1998a) 23-34

Galletly, G.D., Elastic buckling of imperfect circular toroidal shells under external pressure, Journal of Process Mechanical Engineering, 212 (1998b) 197-209

Galletly, G.D., Buckling of imperfect elastic elliptic toroidal shells subjected to uniform external pressure, Journal of Process Mechanical Engineering, 213 (1999) 199-214

Galletly, G.D., Slankard, R.C. and Wenk, E., General instability of ring-stiffened cylindrical shells subject to external hydrostatic pressure: a comparison of theory and experiment, Journal of Applied Mechanics, 25 (1958) 259-266

Gavelya, S.P. and Kononenko, N.I., Characteristic oscillations and waves on a toroidal shell, Soviet Applied Mechanics, 11 (1975) 31-36

Gnesotto, F., Sonato, P., Bader, W. R., Doria, A., Elio, F., Fauri, M., Fiorentin, P., Marchiori, G. and Zollino, G., The plasma system of RFX, Fusion Engineering and Design, 25 (1995) 335-372

Grigolyuk, E.I. and Lopanitsyn, Y.A., The axisymmetric postbuckling behaviour of shallow spherical domes, Journal of Applied Mathematics and Mechanics, 66,4 (2002) 605-616

Guarracino, F. and Walker, A., Energy Method in Structural Mechanics, Thomas Telfor, 1999

Huang, D.W., Redekop, D. and Xu, B., Natural frequencies and mode shapes of curved pipes, Computers and Structures, 63 (1997) 465-473

Huang, J., Nonlinear buckling of composite shells of revolution, Journal of Aerospace Engineering, 15,2 (2002) 64-71

Hu, X.X., Sakiyama, T., Matsuda, H. and Morita, C., Vibration of twisted laminated composite conical shells, International Journal of Mechanical Sciences, 44 (2002) 1521-1541

Hu, X. X., Sakiyama, T., Lim, C.W., Xiong, Y., Matsuda, H. and Morita, C., Vibration of angle-ply laminated plates with twist by Rayleigh-Ritz procedure, Computer Methods in Applied Mechanics and Engineering, 193 (2004) 805-823

Ip, D.H., Chan, W.K., Tse, P.C. and Lai, T.C., Vibration analysis of orthotropic thin cylindrical shells with free ends by the Rayleigh-Ritz method, Journal of Sound and Vibration, 195 (1996) 117-135

Jiang, W. and Redekop, D., Polar axisymmetric vibration of a hollow toridal using the differential quadrdture method, Journal of Sound and Vibration 251,4 (2002) 761-765

Jiang, W. and Redekop, D., Static and vibration analysis of orthotropic toroidal shells of variable thickness by differential quadrature, Thin-Walled Structures, 41,5 (2003) 461-478

Jha, A.K. and Inman, D.J., Piezoelectric actuator and sensor models for an inflated toroidal shell, Mechanical Systems and Signal Processing, 16,1 (2002) 97-122

Jha, A.K. and Inman, D.J., and Plaut, R.H., Free vibration analysis of an inflated toroidal shell, Journal of Vibration and Acoustics, 124 (2002) 387-396

Jones, R.M., Mechanics of Composite Materials, McGraw-Hill, 1975

Jordan, P.F., Buckling of toroidal shells under hydrostatic pressure, AIAA Journal, 11 (1973) 1439-1441

Kendrick, S., The buckling under external pressure of circular shell with evenly spaced equal strength circular ring frames, Part I, Naval Construction Research Establishment Report, R211, 1953

Kosawada, T., Suzuki, K. and Takahashi, S., Free vibrations of thin toroidal shells, Bulletin of JSME, 28,243 (1985) 2041-2047

Kosheleva, T.I. and Myachenkov, V.I., Stability of toroidal shells with localized loadings, Soviet Applied Mechanics, 7,4 (1971) 370-373

Kraus, H., Thin Elastic Shell, John Wiley, New York, 1967

Kwon, Y.W. and Cunningham, R.E., Comparison of USA-DYNA finite element models for a stiffened shell subject to underwater shock, Computers and Structures, 66,1 (1998) 127-144

Lahtinen, H. and Pramila A., Accuracy of composite shell elements in transient analysis involving multiple impacts, Computers and Structures, 59,4 (1996) 593-600

Lee, Y.S., Yang, M.S., Kim, H.S. and Kim, J.H., A study on the free vibration of the joined cylindrical-spherical shell structures, Computers and Structures, 80 (2002) 2405-2414

Leissa, A.W., Vibration of Shells, NASA, SP-288, 1973

Leissa, A.W. and Kang, J.H., Three-dimensional vibration analysis of thick shells of revolution, ASCE Journal of Engineering Mechanics, 125 (1999) 1365-1371

Leung, A.Y.T. and Kwok, N.T.C., Dynamic stiffness analysis of toroidal shells, Thin-Walled Structures, 20 (1995) 43-64

Leung, A.Y.T. and Kwok, N.T.C., Free vibration analysis of a toroidal shell, Thin-Walled Structures, 18 (1994) 317-332

Lewis, J.A., and Inman, D.J., Finite element modeling and active control of an inflated torus using piezoelectric devices, Journal of Intelligent Material Systems and Structures, 12 (2001) 819-833

Lewis, G.D. and Chao, Y.J., Flexibility of trunnion piping elbows, Journal of Pressure Vessel Technology, 112 (1990) 184-189

Li, S. and Cook, J., An analysis of filament overwound toroidal pressure vessels and optimum design of such structures, Journal of Pressure Vessel Technology, 124 (2002) 215-222

Liepins, A.A., Free vibration of prestressed toroidal membrane, AIAA Journal, 3,10 (1965) 1924-1933

Ming, R.S., Pan, J. and Norton, M.P., Free vibration of elastic circular toroidal shells, Applied Acoustics, 63 (2002) 513-528

Naboulsi, S.K., Palazotto, A.N. and GREER J.M. JR., Static-dynamic analyses of toroidal shells, Journal of Aerospace Engineering, (2000) 110-121

Niordson, F.I., Shell Theory, North-Holland Series in Applied Mathematics and Mechanics, 9 (1985)

Nordell, W.J. and Crawford, J.E., Analysis of behavior of unstiffened toroidal shells, IASS Pacific Symposium on Hydromechanically Loaded Shells, Honolulu, (1971) 304-314.

Novozhilov, V.V., The Theory of Thin Shells, Noordhoff, the Netherlands, 1959

Omurtag, M.H. and Aköz, A.Y., A compatible cylindrical shell element for stiffened cylindrical shells in a mixed finite element formulation, Computers and Structures, 49,2 (1993) 363-370

Panagiotopoulos, G.D., Stress and stability analysis of toroidal shells, International Journal of Pressure Vessel and Piping, 20 (1985) 87-100

Park, G., Kim, M. and Inman, D.J., Integration of smart materials into dynamics and control of inflatable space structures, Journal of Intelligent Material Systems and Structures, 12 (2001) 423-433

Pomares, R.J. and Durlofsky, H., Collapse analysis of totoidal shell, International Journal of Pressure Vessel and Piping, 199 (1998) 23-33

Prusty, B.G. and Satsangi, S.K., Analysis of stiffened shell for ships and ocean structures by finite element method, Ocean Engineering, 28 (2001) 621-638

Raj, D.M., Narayanan, R. and Khadakkar, A.G., Effect of ring stiffeners on vibration of cylindrical and conical shell models, Journal of Sound and Vibration, 179,3 (1995) 413-426

Raymond, H.P., Goh, J.K.S., Kigudde, M. and Hammerand, D.C., Shell analysis of an inflatable arch subjected to snow and wind loading, International Journal of Solids and Structures 37 (2000) 4275-4288

Redekop, D., Natural frequencies of a short curved pipe, Transactions of the CSME, 18,1 (1994) 35-45

Redekop, D. and Xu, B., Vibration analysis of toroidal panels using the differential quadrature method, Thin-Walled Structures, 34 (1999) 217-231

Redekop, D., Instability of a curved pipe under three-point bending, International Journal of Pressure Vessel and Piping, 70 (1997) 209-210

Redekop, D., Free vibration of hollow bodies of revolution, Journal of Sound and Vibration, 273 (2004) 415-420

Redekop, D., Vibration analysis of a torus-cylinder shell assembly, Journal of Sound and Vibration, in press

Rikards, R., Chate, A. and Ozolinsh, O., Analysis for buckling and vibrations of composite stiffened shells and plates, Composite Structures, 51 (2001) 361-370

Rossetto, J.N. and Sanders, J.N., Toroidal shell under internal pressure in the transition range, AIAA Journal, 3,10 (1965)1901-1909

Ross, C.T.F. and Etheridge, J., The buckling and vibration of tube-stiffened axisymmetric shells under external hydrostatic pressure, Ocean Engineering, 27 (2000) 1373-1390

Ross, C.T.F. and Lane, G.L., A conceptual design of an underwater drilling rig, Marine Technology, 35,2 (1998) 99-113

Ruzzene, M., Dynamic buckling of periodically stiffened shells: application to supervavitating vehicles, International Journal of Solids and Structures, 41 (2004) 1039-1059

Salley, L. and Pan, J., A study of the modal characteristics of curved pipes, Applied Acoustics, 63 (2002) 189-202

Samanta, A. and Mukhopadhyay, M., Finite element large deflection static analysis of shallow and deep stiffened shells, Finite Element in Analysis and Design, 33 (1999) 187-208

Samanta, A. and Mukhopadhyay, M., Free vibration analysis of stiffened shells by the finite element technique, European Journal of Mechanics A/Solids, 23 (2004) 159-179

Samuelson, L.A. and Eggwertz, S., Shell Stability Handbook, Elsevier Applied Science, 1992

Sanders, J.L., An improved first-approximation theory for thin shells Langley Research Center, TR R-24 (1959)

Sanders, J.L. and Liepins, A.A., Toroidal membrane under internal pressure, AIAA Journal, 1,9 (1963) 2105-2110

Shin, H. S. and Redekop, D., Nonlinear analysis of axisymmetric toroidal shells using the DQM, CSME Forum 2000, Montreal, 2000, 10 pages

Shu, C., Differential Quadrature and Its Application in Engineering, Springer, 2000

Singal, R.K. and Williams, K.A., A theoretical and experimental study of vibration of thick circular cylindrical shells and rings, Journal of Vibration, Acoustics, Stress and Reliability in Design, 110 (1988) 533-537

Skrzypek, J. and Bielski, J., Unimodal and bimodal optimal design of elastic toroidal shells subject to buckling under external pressure, Mechanics of Structures and Machines, 16,3 (1988) 359-386

Soedel, W., Vibration of Shells and Plates, 2nd Ed., Marcell Dekker, New York, 1993

Sobel, L.H. and Flügge, W., Stability of toroidal shells under uniform external pressure, AIAA Journal, 5 (1967) 425-431

Spagnoli, A., Different buckling modes in axially stiffened conical shells, Engineering Structures, 23 (2001) 957-965

Stangeby, P.C., Pitcher, P.C., Elder, J.D., Fundamenski, W. and Llsgo, S., Studies on tokamaks, Enginnering Physics, (1994-1995) 49-51

Tan, D.Y., Free vibration analysis of shells of revolution, Journal of Sound and Vibration, 213 (1998) 15-33

Teng, J.G., Buckling of thin shells: Recent advances and trends, Applied Mechanics Review, 49,4 (1996) 263-274

Thomson, G. and Spence, J., Maximum stresses and flexibility factors of smooth pipe bends with tangent pipe terminations under in-plane bending, Journal of Pressure Vessel Technology, 105 (1983a) 329-336

Thomson, G. and Spence, J., The influence of flanged end constraints on smooth curved tubes under in-plane bending, International Journal of Pressure Vessel and Piping, 13 (1983b) 65-83

Tian, J., Wang, C.M. and Swaddiwudhipong, S., Elastic buckling analysis of ring-stiffened cylindrical shells under general pressure loading via the Ritz method, Thin-Walled Structures, 35 (1999) 1-24

Tzou, H.S. and Wang, D.W., Vibration control of toroidal shells with parallel and diagonal piezoelectric actuators, Journal of Pressure Vessel Technology, 125 (2003) 171-176

Tzou, H.S. and Wang, D.W., Micro-Sensing characteristics and modal voltages of linear/non-linear toroidal shells, Journal of Sound and Vibration, 254,2 (2002) 203-218

Wang, A. and Zhang, W., Asymptotic solution for buckling of toroidal shells, International Journal of Pressure Vessel and Piping, 45 (1991) 61-72

Wang, C.M., Tian, J. and Swaddiwudhipong, S. Buckling of cylindrical shells with internal ring supports, Structural Engineering and Mechanics, 2,4 (1994) 369-381

Wang, X.D., Numerical analysis of moving orthotropic thin plates, Computers and Structures 70 (1999) 467-486

Washizu, K., Variational Methods in Elasticity and Plasticity, 3rd. Ed., Pergamon, Oxford, 1982

Whatham, J.F., Pipe bend analysis by thin shell theory, Journal of Applied Mechanics, 53 (1986) 173-180

Whatham, J.F., Thin shell equations for circular pipe bends, Nuclear Engineering and Design, 65 (1981) 77-89

Wu, C.P. and Lee, C.Y., Differential quadrature solution for the free vibration analysis of laminated conical shells with variable stiffness, International Journal of Mechanical Sciences 43 (2001) 1853-1869

Wu, T.Y. and Liu, G.R., Axisymmetric bending solution of shells of revolution by the generalized differential quadrature rule, International Journal of Pressure Vessels and Piping 77 (2000) 149-157

Wu, T.Y., Wang, Y.Y. and Liu, G.R., A generalized differential quadrature rule for bending analysis of cylindrical barrel shells, Computer Methods in Applied Mechanics and Engineering, 192 (2003) 1629-1647

Yaffe, R. and Abramovich, H., Dynamic buckling of cylindrical stringer stiffened shells, Computers and Structures, 81 (2003) 1031-1039

Yamada, G., Kobayashi, Y., Ohta, Y. and Yokota, S., Free vibration of a toroidal shell with elliptical cross-section, Journal of Sound and Vibration, 135,3 (1989) 411-425

Yamaki, N., Elastic Stability of Circular Cylindrical Shells, North-Holland, 1984

Yamazaki, K. and Tsubosaka, N., A stress analysis technique for plate and shell built-up structures with junctions and its application to minimum weight design of stiffened structures, Structural Optimization, 14 (1997) 173-183

Young, P.G., Application of a three-dimensional shell theory to the free vibration of shells arbitrarily deep in one direction, Journal of Sound and Vibration, 238,2 (2000) 257-269

Yuan, J. and Dickinson, M., The free vibration of circularly cylindrical shell and plate system, Journal of Sound and Vibration, 175,2 (1994) 241-263

Zhang, F. and Redekop, D., Surface loading of a thin-walled toroidal shell, Computers and Structures, 43,6 (1992) 1019-1028

Zheng, X.J., Zhou, Y.H., and Lee, J.S., Instability of superconducting partial torus with two pin supports, Journal of Engineering Mechanics, (1999) 174-179

Table 1-1: Applications of toroidal shells with the shell geometries and the material properties

Application	R(m)	r(m)	h(m)	R/r	r/h	Material	Reference
Fusion Reactor Vessel	2	0.6	0.047	3.33	12.77	Stainless Steel	Baker et al (2002)
	2.003	0.475	0.03	4.22	15.83	Inconel 625	Baker et al (1989)
	2	0.535				Aluminium Alloy 6061	Baker et al (1989)
	0.09		0.0006			Steel	Zhang (1999)
	1.6	0.56	0.0056	3	100	Steel	Stangeby et al (1995)
	2	0.535	0.056	3.74	9.55	Al Alloy 6061	Gnesotto et al (1995)
Satellite Antennas Support	3.2	0.56	0.0056	5.7	100	Smart Material (PVDF)	Tzou & Wang (2003)
	7.62	1.22	76.2e-6	6.25		Kapton E=2.55e9(Pa)	Jha & Inman (2002)
	15.2	0.61	76.2e-6			Neoprene Rubber	Jackson (2001)
			1.43e-3	3.7		Smart Material (PVDF)	Gyuhae (2001)
				4		Smart Material (PVDF)	Tzou et al (2002)
Stiffeners for Submarine				2.63	20.6	Steel	Galletly[a] & Galletly[b] (1996)
Underwater Drilling Rig	40	5	0.97			Aluminium Alloys	Ross & Etheridge (1998)
			0.522			Titanium Alloys	
			0.35			Composites	
Transportation Packaging	1.8288	0.6096		3		Stainless Steel 304	Pomares & Durlofsky (1988)

Table 1-1 (continued)

Application	R(m)	r(m)	h(m)	R/r	r/h	Material	Reference
Diver's Tank	0.13	0.06	5.299e-3	2.17	11.32	Armid Fibers	Li & Cook (2002)
Short Elbows	2.5465	1	0.01	2.5465	100	Steel	Leung & Kwok (1994)
				3	42.86	Steel	Thomson & Spence (1983a)
				2	28.57		
				2.77	25.2		
		0.8415	0.0071	1.5		Steel	Lewis & Chao (1990)
		0.162	0.0095				
				2	20	Steel	Whatham (1986)
	0.375	0.1312	0.0125				
				2	20	Steel	Whatham (1981)
					10		
					5		
					3.33		
	0.252	0.0842	7.1e-3			Steel	Zhang et al (1999)
Long Elbows				10	142.9	Steel	Thomson & Spence (1983b)
				5	20	Steel	Whatham (1981)
					10		
					5		
					3.33		
	0.6	0.1	0.005			Steel	Salley & Pan (2002)
				10	33.33	Steel	Ming et al (2002)
	4	1	0.01			Steel	Leung & Kwok (1995)
Stanford Torus	900	65					Kokh (1996)

Table 3-1: Validation of method-comparison of ω (Hz) with FEM and RKM

Method	ω_1	ω_2	ω_3	ω_4	ω_5	ω_6
m	2	2	0	3	3	4
DQM1	475.4	519.7	653.0	1053.3	1077.9	1510.3
DQM2	487.3	491.6	631.1	985.0	996.9	1400.4
DQM3	487.3	491.6	631.1	985.0	996.9	1400.4
DQM4	487.3	491.6	631.1	985.0	996.9	1400.4
FEM	488.0	492.0	631.7	986.2	998.2	1402.6
RKM	489.0	493.0	630.9	989.6	991.0	1408.4

Table 3-2: Description of circular toroidal shell cases

Case	*R(m)*	*r(m)*	*h(m)*	*R/r*	*r/h*
A	1.0	0.25	0.0025	4.0	100
B	1.0	0.25	0.0050	4.0	200
C	1.0	0.5	0.0050	2.0	100
D	1.0	0.75	0.0075	1.3	100

Table 3-3: DQM convergence study- $\omega_1, \omega_2\,(Hz)$ for isotropic toroidal shells

	Case A		*Case B*		*Case C*		*Case D*	
Grid	ω_1	ω_2	ω_1	ω_2	ω_1	ω_2	ω_1	ω_2
10	403.1	500.2	525.2	578.7	-	-	-	-
20	363.9	373.5	521.6	536.0	284.9	447.1	265.2	563.2
30	363.9	373.3	521.6	536.0	279.4	442.5	247.3	546.3
40	363.9	373.3	521.6	536.0	279.4	442.5	247.2	546.4
m	2	2	2	2	0	2	0	2

Table 3- 4: Comparison of ω (Hz) for isotropic toroidal shells with FEM

Case	*Method*	ω_1	ω_2	ω_3	ω_4	ω_5	ω_6
A	m	2	2	0	3	3	4
	FEM	364.1	373.7	383.4	663.0	671.0	912.1
	DQM	363.9	373.3	383.1	662.4	670.4	911.1
B	m	2	2	0	3	3	4
	FEM	521.6	536.5	553.4	991.2	1004.8	1417.9
	DQM	521.6	536.1	553.3	990.9	1004.3	1414.9
C	m	0	2	2	3	3	4
	FEM	279.2	442.4	477.6	759.6	761.7	1098.3
	DQM	279.4	442.5	477.2	759.5	761.1	1092.7
D	m	0	2	2	3	3	2
	FEM	245.9	546.8	575.4	1043.2	1043.4	1236.9
	DQM	247.3	546.3	576.4	1040.6	1094.1	1236.9

Table 3-5: Orthotropic material properties- M1, M2 and M3

Material properties	*M1*	*M2*	*M3*
$E_1 (Pa)$	7.44e9	181.81e9	0.88157e9
$E_2 (Pa)$	3.47e9	10.35e9	0.0084e9
E_1 / E_2	2.14	17.6	105
ν_{12}	0.319	0.28	0.551
ν_{21}	0.149	0.0159	0.00525
$G_{12} (Pa)$	2.04e9	7.17e9	0.00785e9
$G_{13} (Pa)$	0.099e9	7.17e9	0.00785e9
$G_{23} (Pa)$	0.137e9	4e9	0.00471
$\rho (Kg/m^3)$	700	1579	1190
Reference	[Wang, 1999]	[Lahtinen, Pramila, 1996]	[Jiang, Redekop, 2003]

Table 3-6: Comparison of ω (Hz) for orthotropic toroidal shells for material M1

Case	*Method*	ω_1	ω_2	ω_3	ω_4	ω_5	ω_6
A	m	2	2	0	3	3	4
	FEM	187.4	192.0	197.6	335.2	339.1	453.0
	DQM	186.2	191.2	199.7	330.4	334.3	442.4
B	m	2	2	0	3	3	4
	FEM	267.0	274.3	283.6	495.4	501.8	693.4
	DQM	263.4	271.3	287.5	485.1	491.7	670.7
C	m	0	2	2	3	3	1
	FEM	144.2	225.1	242.6	379.2	380.1	541.0
	DQM	146.0	220.4	238.0	364.0	364.8	-
D	m	0	2	2	2	1	2
	FEM	126.8	278.7	292.5	525.7	525.9	596.4
	DQM	129.1	269.6	284.2	529.4	542.8	546.1

Table 3-7: Comparison of ω (Hz) for orthotropic toroidal shells for material M2

Case	*Method*	ω_1	ω_2	ω_3	ω_4	ω_5	ω_6
A	m	2	2	0	3	3	4
	FEM	345.2	354.1	378.0	587.0	593.6	755.9
	DQM	329.2	338.7	378.2	549.4	556.0	694.5
B	m	2	2	0	3	3	4
	FEM	482.2	495.9	541.3	842.1	852.8	1116.0
	DQM	450.1	465.7	541.6	775.5	786.3	1015.7
C	m	0	2	2	3	3	3
	FEM	277.4	399.4	430.9	646.1	647.5	921.5
	DQM	277.8	370.8	401.9	594.3	595.6	-
D	m	0	2	2	1	2	2
	FEM	245.1	524.8	552.5	776.3	799.0	836.0
	DQM	246.0	491.5	521.2	685.2	706.4	743.5

Table 3-8: Comparison of ω (Hz) for orthotropic toroidal shells for material M3

Case	*Method*	ω_1	ω_2	ω_3	ω_4	ω_5	ω_6
A	m	2	2	0	3	3	4
	FEM	16.50	17.03	19.28	27.20	27.54	34.40
	DQM	15.19	15.67	19.29	24.43	24.73	30.72
B	m	2	2	0	3	3	4
	FEM	22.70	23.40	27.61	38.80	39.31	51.71
	DQM	20.3	21.10	27.63	34.66	35.18	46.94
C	m	0	2	2	3	3	4
	FEM	14.24	19.20	20.01	33.49	33.58	51.19
	DQM	14.26	17.55	19.17	31.35	31.46	52.44
D	m	0	1	2	2	2	2
	FEM	12.64	28.44	28.76	31.25	33.06	35.95
	DQM	12.70	25.95	26.46	29.42	29.71	32.35

Table 3-9: Comparison of ω (Hz) for shell with inner equator support

Case	*Method*	ω_1	ω_2	ω_3	ω_4	ω_5	ω_6
A	m	0	1	2	1	2	3
	FEM	239.8	997.4	2408.3	2518.8	2550.3	2581.5
	DQM	239.6	997.4	2407.8	2517.7	2547.8	2578.1
B	m	0	1	2	1	2	0
	FEM	342.3	1020.2	2463.3	2698.9	2851.5	2940.7
	DQM	342.2	1020.3	2463.5	2700.7	2851.8	2940.3
C	m	0	1	0	1	3	3
	FEM	157.5	667.8	1176.1	1293.8	1848.0	1852.0
	DQM	157.4	668.3	-	1296.8	1847.8	1850.5
D	m	0	0	1	1	2	2
	FEM	120.9	310.4	336.7	518.0	1217.4	1220.8
	DQM	120.6	-	338.7	518.9	1220.9	1222.3

Table 3-10: Comparison of ω (Hz) for shell with bottom crown support

Case	*Method*	ω_1	ω_2	ω_3	ω_4	ω_5	ω_6
A	m	0	1	0	2	3	4
	FEM	486.3	611.0	733.2	774.2	998.5	1170.1
	DQM	486.6	611.0	733.3	774.9	1000.1	1171.9
B	m	0	1	0	2	3	4
	FEM	683.0	832.8	1014.7	1042.8	1392.8	1717.2
	DQM	684.1	834.6	1017.4	1045.1	1396.0	1720.6
C	m	0	1	0	2	3	3
	FEM	324.3	325.7	573.1	741.2	952.3	1188.5
	DQM	325.3	326.2	574.8	743.0	954.4	1191.3
D	m	1	0	0	2	2	3
	FEM	189.0	248.7	530.2	764.4	902.2	1137.8
	DQM	189.5	250.0	533.8	766.7	902.7	1138.7

Table 4-1: Description of circular toroidal shells

Case	*R(m)*	*r(m)*	*h(m)*	*R/r*	*r/h*
1	1.0	0.10	0.0010	10.0	100
2	1.0	0.10	0.0020	10.0	50
3	1.0	0.20	0.0040	5.0	50
4	20.	3.00	0.0300	6.7	100

Table 4-2: Convergence study of DQM- ω_1, ω_2 (Hz) for isotropic toroidal shells-cases 1-4

	Case 1		*Case 2*		*Case 3*		*Case 4*	
Grid	ω_1	ω_2	ω_1	ω_2	ω_1	ω_2	ω_1	ω_2
12	245.7	263.8	341.8	365.4	-	-	15.77	16.26
16	241.3	260.1	341.6	365.3	487.4	491.6	14.82	15.51
20	241.3	260.1	341.6	365.3	487.3	491.6	14.80	15.50
24	241.3	260.1	341.6	365.3	487.3	491.6	14.79	15.50
28	241.3	260.1	341.6	365.3	487.4	491.6	14.79	15.50
32	241.3	260.1	341.6	365.3	487.3	491.6	14.79	15.50
36	241.3	260.1	341.6	365.3	487.3	491.6	14.79	15.50
m	2	2	2	2	2	2	2	2

Table 4-3: Comparison of ω (Hz) for isotropic toroidal shells

Case	*Method*	ω_1	ω_2	ω_3	ω_4	ω_5	ω_6
	m	2	2	3	3	0	4
1	RKM	241.6	260.7	600.8	611.7	626.7	904.1
	DQM	241.3	260.1	600.7	609.7	626.5	902.0
	FEM	241.6	260.3	601.4	610.4	627.1	903.1
	m	2	2	3	3	0	4
2	RKM	342.5	366.4	874.2	886.3	914.3	1359.1
	DQM	341.6	365.3	871.3	883.3	914.9	1355.4
	FEM	341.8	365.3	871.8	883.8	915.4	1355.7
	m	2	2	0	3	3	4
3	RKM	489.0	493.0	630.9	989.6	991.0	1408.0
	DQM	487.3	491.6	631.1	985.0	996.9	1400.4
	FEM	488.0	492.0	631.7	986.2	998.2	1402.6
	m	2	2	0	3	3	4
4	RKM	-	-	-	-	-	-
	DQM	14.8	15.5	25.3	32.5	32.6	45.3
	FEM	14.8	15.5	25.3	32.5	32.6	45.3

Table 4-4: Parameters of the *k*th stiffener

Ring	$\overline{A}_k$	$\overline{I}_{\eta k}$	$\overline{I}_{zk}$	$\overline{J}_k$	$\overline{\rho}_k$	$\overline{E}_k$	$\overline{G}_k$
Light	0.005	5e-6	2e-6	5e-6	1	1	1/3
Heavy	0.01	1e-6	2e-6	5e-6	1	1	1/3

Table 4-5: Validation study of ω (Hz) for cases 2 and 3

Case	*Rings*	*Method*	ω_1	ω_2	ω_3	ω_4	ω_5	ω_6
2	4 light rings	RKM	342.5	366.4	386.2	410.5	928.7	940.1
		FEM	341.6	365.3	397.0	420.0	935.1	944.1
	4 heavy rings	RKM	340.2	366.5	412.1	435.0	958.2	967.9
		FEM	340.6	365.4	447.2	468.2	990.9	997.4
3	4 light rings	RKM	487.1	493.3	587.3	589.4	696.9	1102.5
		FEM	485.2	491.7	603.5	603.8	715.2	1104.0
	4 heavy rings	RKM	484.1	492.5	635.1	635.2	737.6	1149.6
		FEM	483.0	492.0	694.9	701.0	796.6	1191.0

Table 4-6: The frequencies ω (Hz) of cases 1-4 with the light rings (FEM)

Case	*Rings*	ω_1	ω_2	ω_3	ω_4	ω_5	ω_6
	0	241.6	260.3	601.4	610.4	627.1	903.1
1	4	240.0	260.4	344.5	365.1	709.8	716.6
	8	337.1	343.0	360.7	365.4	768.1	774.7
	16	424.4	429.2	448.8	452.2	1093.0	1105.0
	0	341.8	365.3	871.8	883.8	915.4	1355.7
2	4	341.6	365.3	397.0	420.0	935.1	944.1
	8	391.9	396.0	416.7	420.8	983.7	990.6
	16	441.0	444.6	465.8	468.6	1140.0	1149.0
	0	488.0	492.0	631.7	986.2	998.2	1402.6
3	4	485.2	491.7	603.5	603.8	715.2	1104.0
	8	601.9	603.6	604.8	792.9	1204.7	1213.9
	16	-	-	-	-	-	-
	0	14.8	15.5	25.3	32.5	32.6	45.7
4	4	14.7	15.5	25.6	26.5	34.6	42.4
	8	25.4	25.7	26.5	46.6	46.8	47.2
	16	-	-	-	-	-	-

Table 4-7: The frequencies ω (Hz) of cases 1-4 with the heavy rings (FEM)

Case	*Rings*	ω_1	ω_2	ω_3	ω_4	ω_5	ω_6
	0	241.6	260.3	601.4	610.4	627.1	903.1
1	4	238.4	260.7	405.1	423.3	751.1	767.2
	8	396.2	402.0	421.1	424.0	837.7	842.3
	16	522.0	526.2	541.6	542.5	1369.0	1378.0
	0	341.8	365.3	871.8	883.8	915.4	1355.7
2	4	340.6	365.4	447.2	468.2	990.9	997.4
	8	439.6	445.0	464.7	468.4	1066.0	1073.0
	16	527.0	531.2	548.4	550.6	1376.0	1387.0
	0	488.0	492.0	631.7	986.2	998.2	1402.6
3	4	483.0	492.0	694.9	701.0	796.6	1191.0
	8	695.7	696.0	699.8	703.5	951.7	1343.9
	16	-	-	-	-	-	-
	0	14.8	15.5	25.3	32.5	32.6	45.7
4	4	14.6	15.6	27.8	28.2	36.1	43.9
	8	27.4	27.7	28.3	28.7	47.7	47.8
	16	-	-	-	-	-	-

Table 4-8: Comparison of ω (Hz) for orthotropic toroidal shells for material M1

Case	*Method*	ω_1	ω_2	ω_3	ω_4	ω_5	ω_6
1	m	2	2	3	3	0	4
	DQM	123.7	132.3	303.4	307.4	319.3	447.8
	FEM	123.3	132.8	303.5	307.6	316.3	448.8
2	m	2	2	3	3	0	4
	DQM	174.5	184.0	435.8	440.3	463.6	-
	FEM	174.2	186.2	436.8	442.9	457.7	664.5
3	m	2	2	0	3	3	4
	DQM	244.5	245.5	321.8	479.6	485.3	661.8
	FEM	246.2	248.4	317.5	486.3	491.1	678.0
4	m	2	2	0	3	3	4
	DQM	7.54	7.87	12.92	16.23	16.28	22.17
	FEM	7.53	7.89	12.78	16.30	16.34	22.39

Table 4-9: Comparison of ω (Hz) for orthotropic toroidal shells for material M2

Case	*Method*	ω_1	ω_2	ω_3	ω_4	ω_5	ω_6
1	m	2	2	3	3	0	4
	DQM	231.3	242.5	545.7	550.8	598.7	773.0
	FEM	234.8	250.5	559.3	566.5	598.6	797.2
2	m	2	2	3	3	0	4
	DQM	321.8	327.1	762.5	764.7	860.7	1095.1
	FEM	329.0	345.2	788.4	796.2	860.2	1137.0
3	m	2	2	0	3	3	4
	DQM	426.1	428.5	604.4	784.1	793.8	1017.8
	FEM	451.8	453.6	604.0	842.1	851.4	1110.0
4	m	2	2	0	3	3	4
	DQM	13.80	14.30	24.30	28.30	28.40	36.80
	FEM	14.18	14.77	24.28	29.48	29.56	38.91

Table 4-10: Comparison of ω (Hz) for orthotropic toroidal shells for material M3

Case	*Method*	ω_1	ω_2	ω_3	ω_4	ω_5	ω_6
1	m	2	2	3	3	0	4
	DQM	11.32	11.62	25.64	25.79	30.32	34.94
	FEM	11.81	12.36	27.17	27.51	30.30	37.40
2	m	2	2	3	3	0	4
	DQM	15.13	15.34	34.67	34.79	43.42	47.92
	FEM	16.19	16.61	37.26	37.50	43.49	51.63
3	m	2	2	0	3	3	4
	DQM	19.32	19.60	30.74	34.54	35.00	44.66
	FEM	21.50	21.51	30.73	38.69	39.13	50.01
4	m	2	2	0	3	3	1
	DQM	1.240	1.290	1.295	1.613	1.617	2.299
	FEM	1.240	1.406	1.413	1.795	1.800	2.109

Table 5-1: Variation of buckling pressure λ (MPa) with shell size in FEM analysis

Model No.	*R (m)*	*r (m)*	*h (m)*	*R/r*	*r/h*	*Support equator*	*Buckling loading λ (p=0.1)*	*Buckling loading λ (p=1)*	*Buckling loading λ (p=10)*
1	1	0.1	0.001	10	100	inner	7.187	-	0.07186
2	2	0.2	0.002	10	100	inner	3.877	0.3877	0.03877
3	4	0.4	0.004	10	100	inner	2.440	0.2440	0.02440
4	8	0.8	0.008	10	100	inner	2.021	0.2021	0.02021
5	10	1	0.01	10	100	inner	1.971	0.1971	0.01971
6	20	2	0.02	10	100	inner	1.898	0.1898	0.01898
7	40	4	0.04	10	100	inner	1.896	0.1896	0.01896
8	80	8	0.08	10	100	inner	1.895	0.1895	0.01895
9	100	10	0.1	10	100	inner	1.895	0.1895	0.01895
10	200	20	0.2	10	100	inner	1.895	0.1895	0.01895

Table 5-2: Description of toroidal shells

Case	*R(m)*	*r(m)*	*h(m)*	*R/r*	*r/h*
I	2.0	1.0	0.01	2.0	100
II	4.0	1.0	0.01	4.0	100
III	8.0	1.0	0.01	8.0	100
IV	20.	1.0	0.01	20.	100
1	20.	4.0	0.04	5.0	100
2	20.	2.67	0.0267	7.5	100
3	20.	2.0	0.02	10.	100
4	20.	2.0	0.04	10.	50

Table 5-3: Validation of critical pressure (MPa) for isotropic toroidal shells (cases I-IV)

Study	*Case I*	*Case II*	*Case III*	*Case IV*
Sobel and Flügge (1967)	0.5628	0.3633	0.2394	0.1428
Jordan (1973)	0.5273	0.3322	0.2092	0.1136
Panagiotopolous (1985)	0.5294	0.3297	0.2066	0.1110
FEMA	0.5969	0.3633	0.2399	0.1153
FEMB	0.6247	0.3645	0.2663	0.1163
FEMC	0.6543	0.3705	0.3915	0.1179

Table 5-4: Comparison of λ_1 (MPa) for isotropic toroidal shells with light stiffeners

Rings	*Support equator*	*Case 1* (40×200)	*Case 2* (30×240)	*Case 3* (30×300)	*Case 4* (30×300)
0	Inner	0.3052	0.2321	0.1908	0.9391
	Outer	0.3080	0.2341	0.1923	0.9532
	Both	6.5484	3.6317	2.4483	16.077
4	Inner	0.6688	0.4555	0.3524	1.1972
	Outer	0.6469	0.3815	0.2896	1.1528
	Both	7.9726	3.9976	2.7345	17.558
8	Inner	1.1220	0.7056	0.5343	1.4562
	Outer	1.0444	0.6805	0.5356	1.4786
	Both	9.7923	4.8109	3.0783	19.071
12	Inner	-	1.0099	0.7252	1.7087
	Outer	-	0.9727	0.7033	1.7325
	Both	-	5.9815	3.6369	20.919
16	Inner	2.2168	1.3069	-	-
	Outer	2.2459	1.3024	-	-
	Both	16.448	7.5797	-	-

Table 5-5: Comparison of λ_1 (*MPa*) for isotropic toroidal shells with heavy stiffeners

Rings	*Support equator*	*Case 1* (40×200)	*Case 2* (30×240)	*Case 3* (30×300)	*Case 4* (30×300)
0	Inner	0.3052	0.2321	0.1908	0.9391
	Outer	0.3080	0.2341	0.1923	0.9532
	Both	6.5484	3.6317	2.4483	16.077
4	Inner	1.0929	0.7403	0.5636	1.5591
	Outer	0.9588	0.4666	0.3340	1.3057
	Both	7.7178	3.8426	2.6360	17.669
8	Inner	2.1592	1.3573	1.0122	2.2288
	Outer	2.0373	1.3456	0.9833	2.2210
	Both	9.3072	4.4809	2.9047	19.416
12	Inner	-	2.1110	1.5085	2.8883
	Outer	-	2.0458	1.4783	2.9343
	Both	-	5.5128	3.2390	21.528
16	Inner	4.8309	2.8561	-	-
	Outer	4.8387	2.8340	-	-
	Both	16.598	7.0489	-	-

Table 5-6: Comparison of λ_1 (*MPa*) for orthotropic toroidal shells for materials - M1, M2 and M3

Material	*Support equator*	*Case 1* (40×200)	*Case 2* (30×240)	*Case 3* (30×300)	*Case 4* (30×300)
M1	Inner	0.6256×10^{-2}	0.4773×10^{-2}	0.3940×10^{-2}	0.1958×10^{-1}
	Outer	0.6289×10^{-2}	0.4804×10^{-2}	0.3966×10^{-2}	0.1973×10^{-1}
	Both	0.1402	0.7761×10^{-1}	0.5074×10^{-1}	0.3532
M2	Inner	0.3941×10^{-1}	0.2964×10^{-1}	0.2429×10^{-1}	0.1235
	Outer	0.3924×10^{-1}	0.2963×10^{-1}	0.2432×10^{-1}	0.1237
	Both	0.7865	0.3969	0.2637	1.4605
M3	Inner	0.6469×10^{-4}	0.4739×10^{-4}	0.3805×10^{-4}	0.1974×10^{-3}
	Outer	0.6395×10^{-4}	0.4717×10^{-4}	0.3798×10^{-4}	0.1966×10^{-3}
	Both	0.1861×10^{-1}	0.7004×10^{-3}	0.4633×10^{-3}	0.2517×10^{-2}

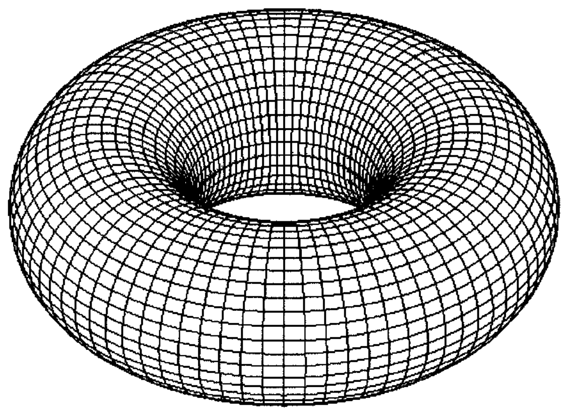

Fig. 3-1 Complete circular toroidal shell

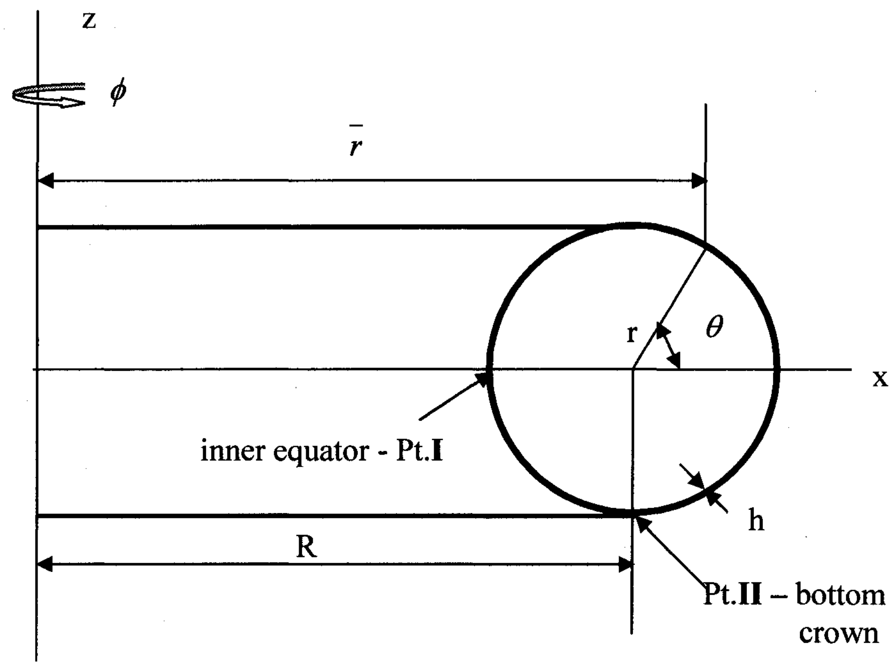

Fig. 3-2 Geometry of toroidal shell

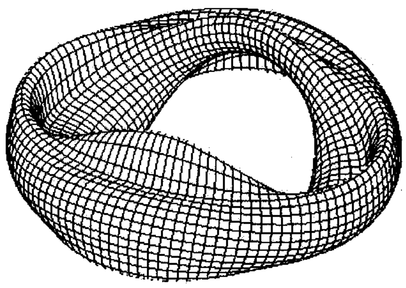

(a) Mode 1 - ω_1

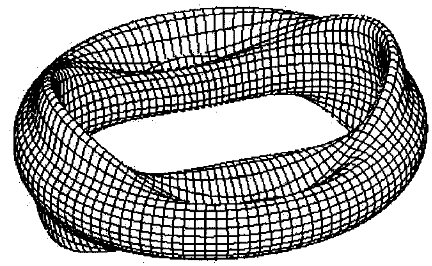

(b) Mode 2 - ω_2

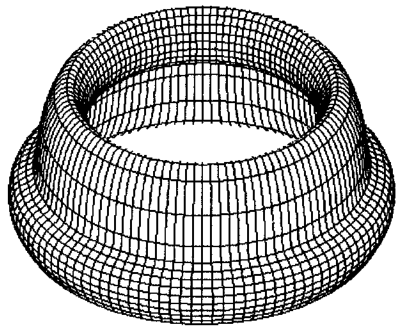

(c) Mode 3 - ω_3

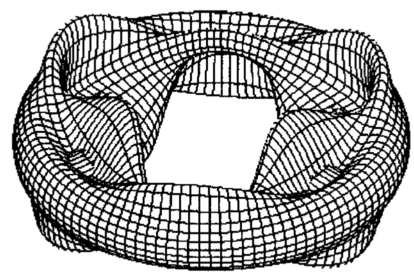

(d) Mode 4 - ω_4

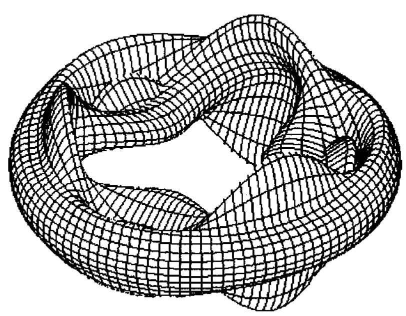

(e) Mode 5 - ω_5

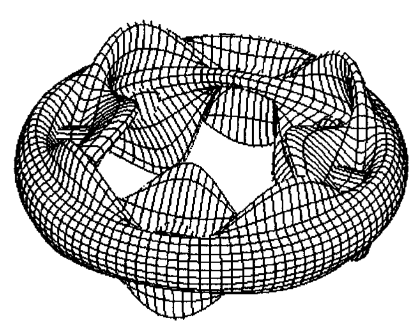

(f) Mode 6 - ω_6

Fig. 3-3 Three-dimensional views of mode shapes 1-6 of case A from FEM

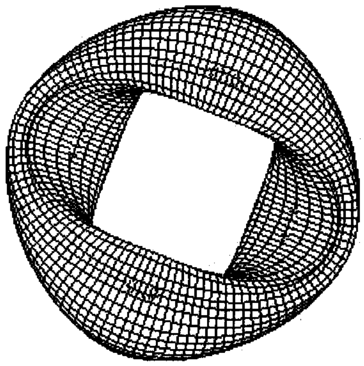

(a) Mode 1 - ω_1

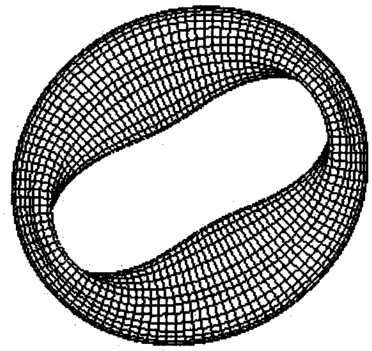

(b) Mode 2 - ω_2

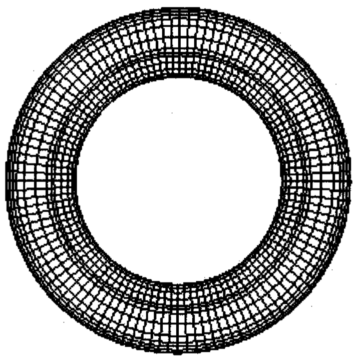

(c) Mode 3 - ω_3

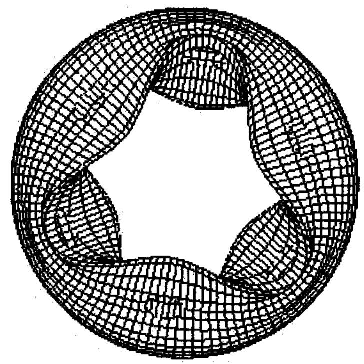

(d) Mode 4 - ω_4

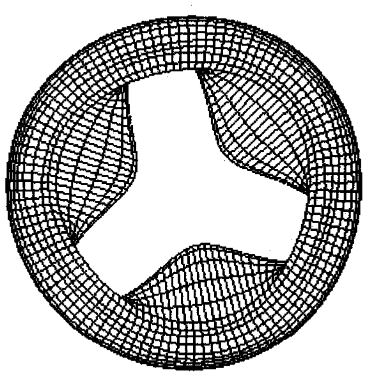

(e) Mode 5 - ω_5

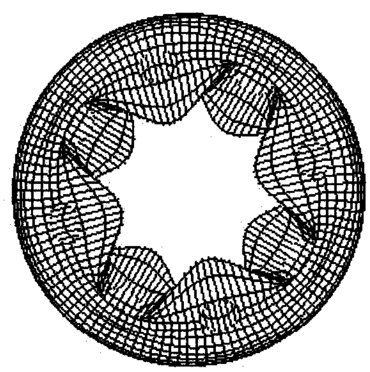

(f) Mode 6 - ω_6

Fig. 3-4 Projections on equator of mode shapes 1-6 of case A from FEM

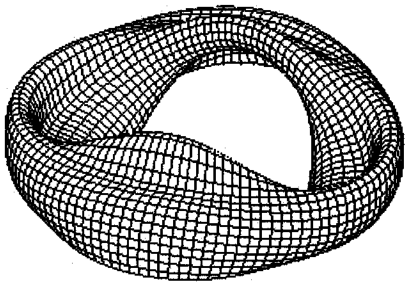

(a) Mode 1 - ω_1

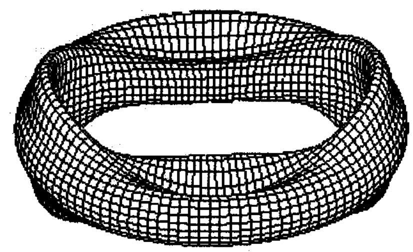

(b) Mode 2 - ω_2

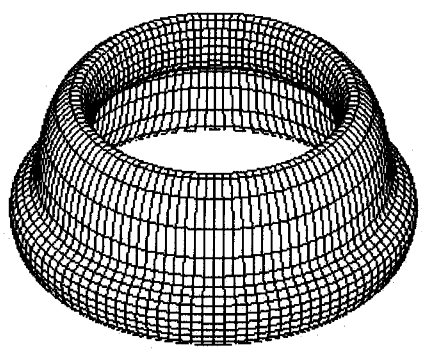

(c) Mode 3 - ω_3

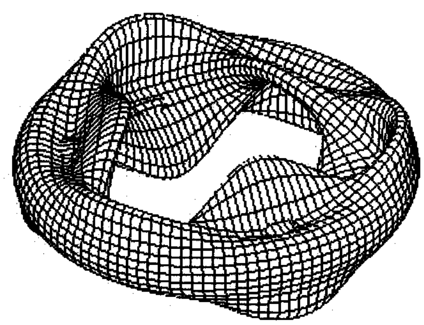

(d) Mode 4 - ω_4

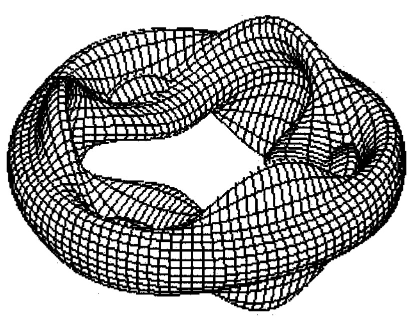

(e) Mode 5 - ω_5

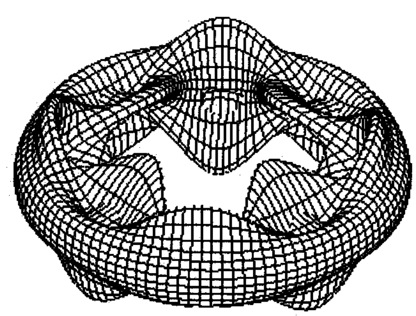

(f) Mode 6 - ω_6

Fig. 3-5 Three-dimensional views of mode shapes 1-6 of case B from FEM

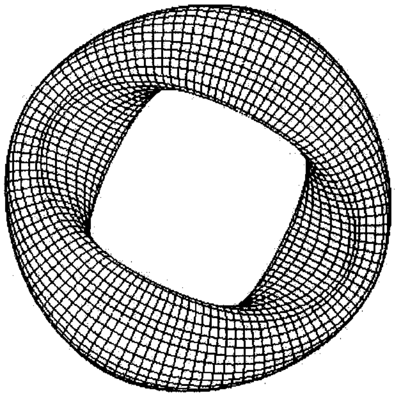

(a) Mode 1 - ω_1

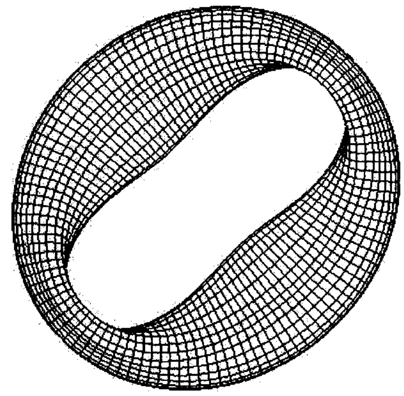

(b) Mode 2 - ω_2

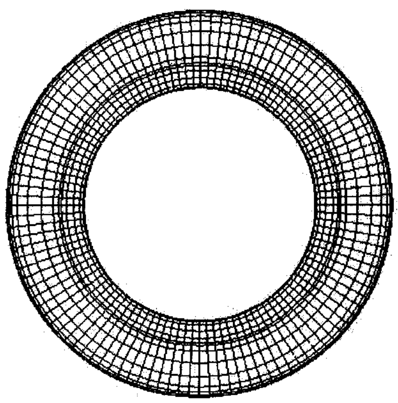

(c) Mode 3 - ω_3

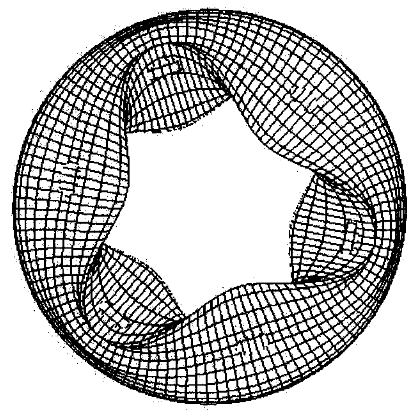

(d) Mode 4 - ω_4

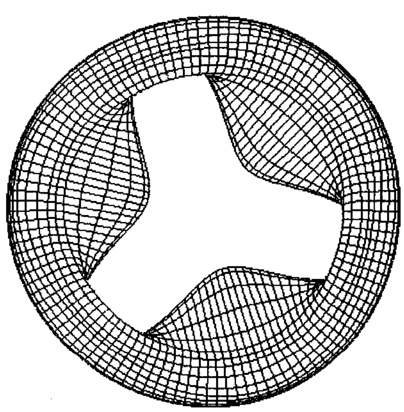

(e) Mode 5 - ω_5

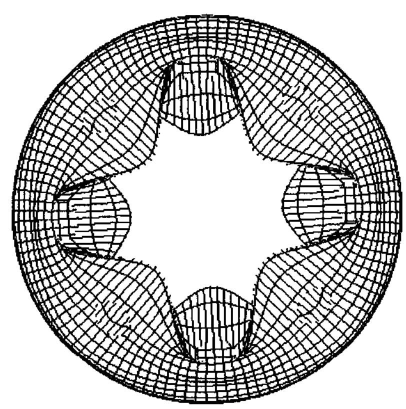

(f) Mode 6 - ω_6

Fig. 3-6 Projections on equator of mode shapes 1-6 of case B from FEM

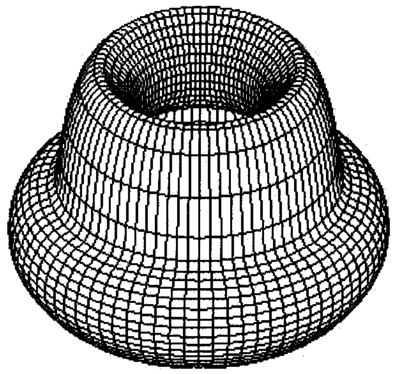

(a) Mode 1 - ω_1

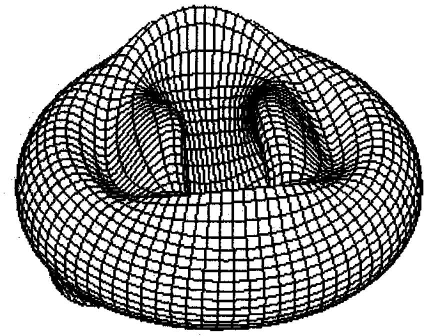

(b) Mode 2 - ω_2

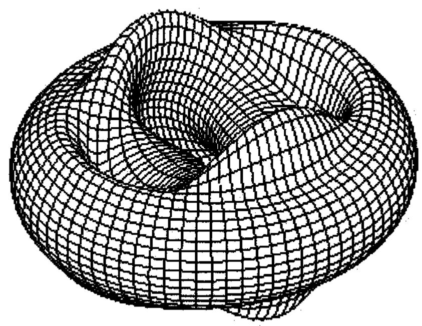

(c) Mode 3 - ω_3

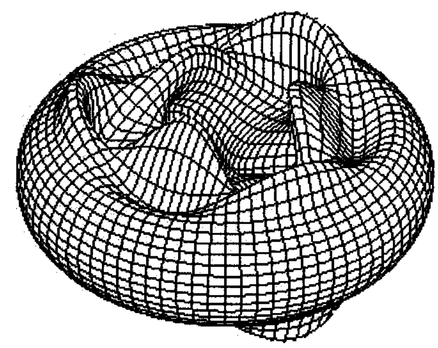

(d) Mode 4 - ω_4

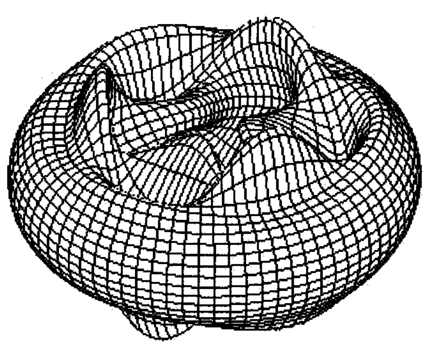

(e) Mode 5 - ω_5

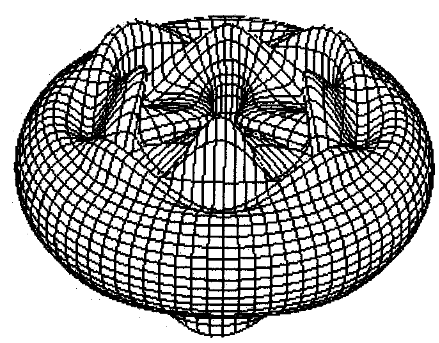

(f) Mode 6 - ω_6

Fig. 3-7 Three-dimensional views of mode shapes 1-6 of case C from FEM

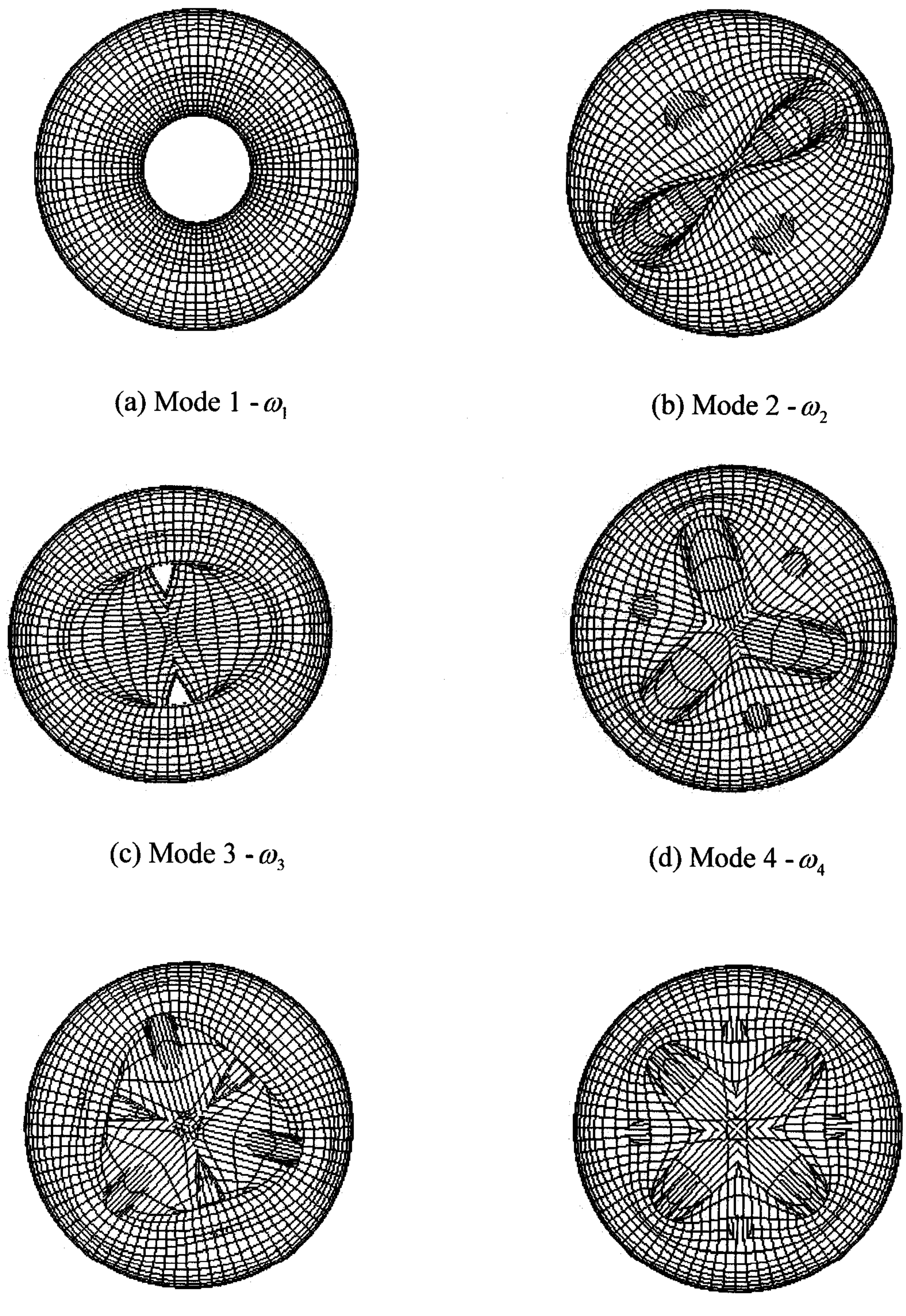

Fig. 3-8 Projections on equator of mode shapes 1-6 of case C from FEM

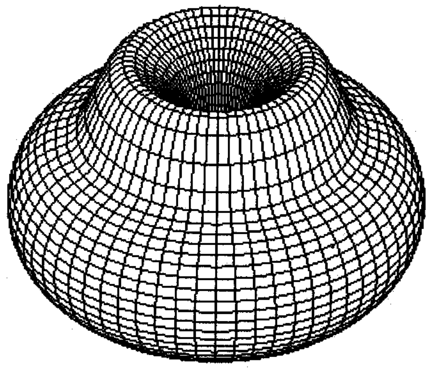

(a) Mode 1 - ω_1

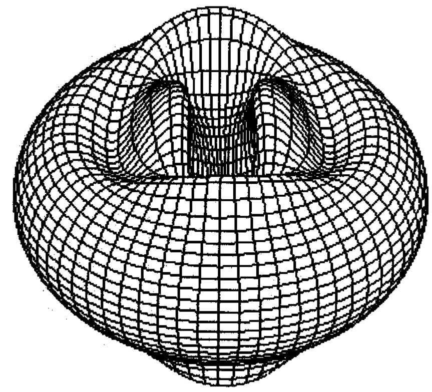

(b) Mode 2 - ω_2

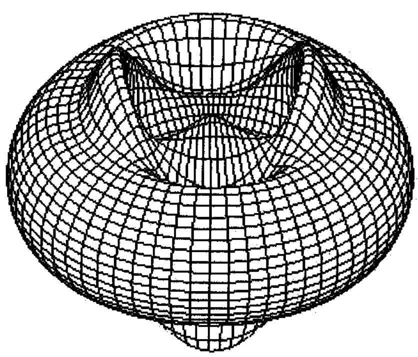

(c) Mode 3 - ω_3

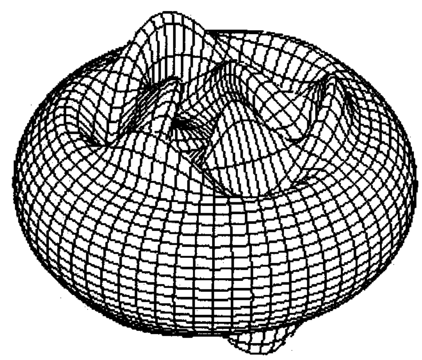

(d) Mode 4 - ω_4

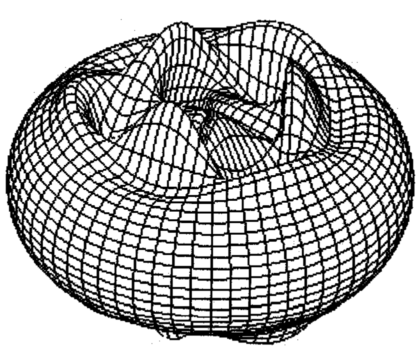

(e) Mode 5 - ω_5

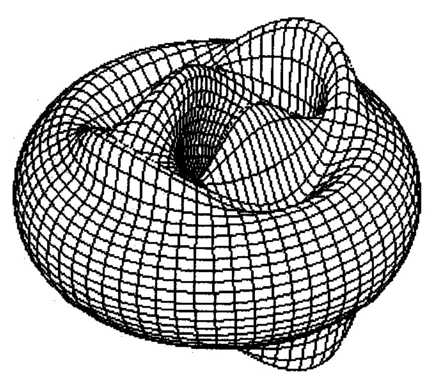

(f) Mode 6 - ω_6

Fig. 3-9 Three-dimensional views of mode shapes 1-6 of case D from FEM

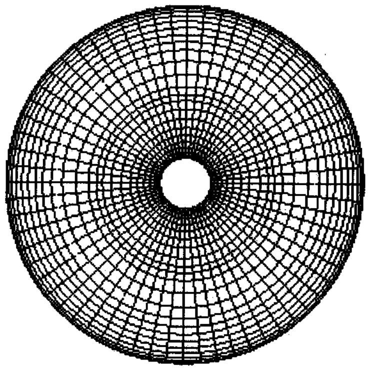

(a) Mode 1 - ω_1

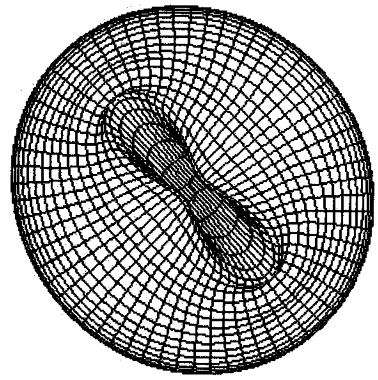

(b) Mode 2 - ω_2

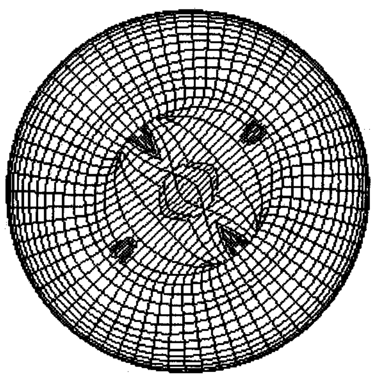

(c) Mode 3 - ω_3

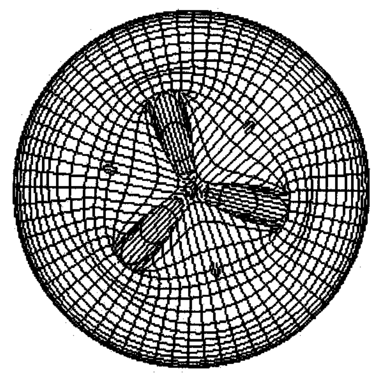

(d) Mode 4 - ω_4

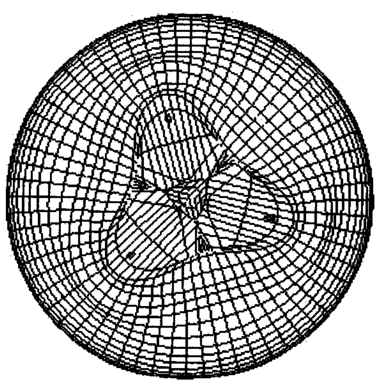

(e) Mode 5 - ω_5

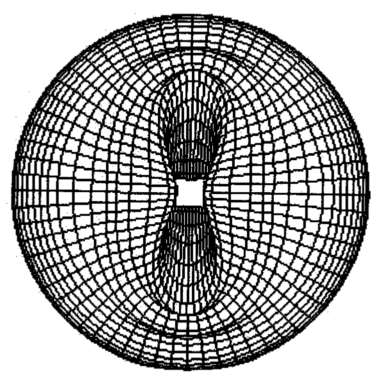

(f) Mode 6 - ω_6

Fig. 3-10 Projections on equator of mode shapes 1-6 of case D from FEM

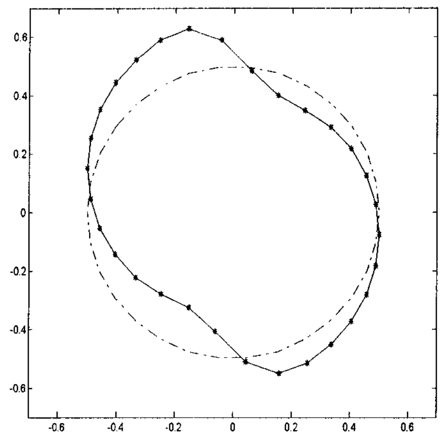

(a) Mode 1- ω_1

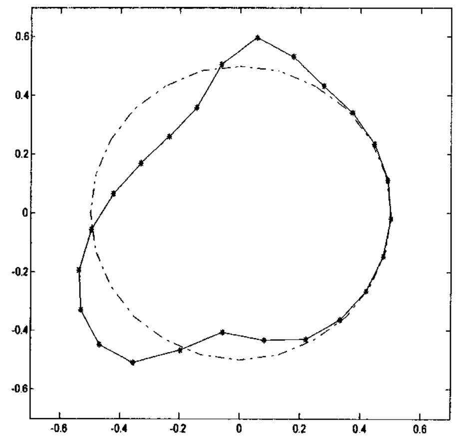

(b) Mode 2- ω_2

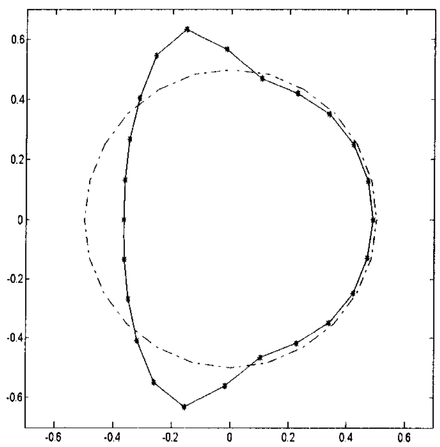

(c) Mode 3- ω_3

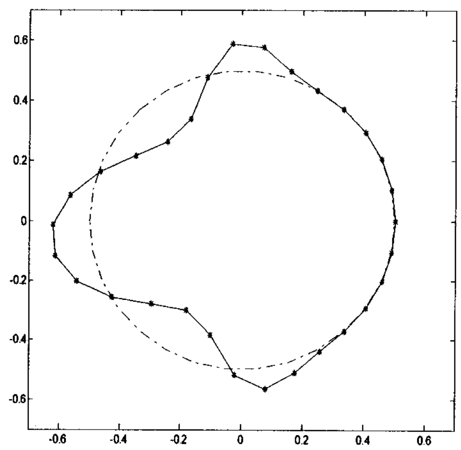

(d) Mode 4- ω_4

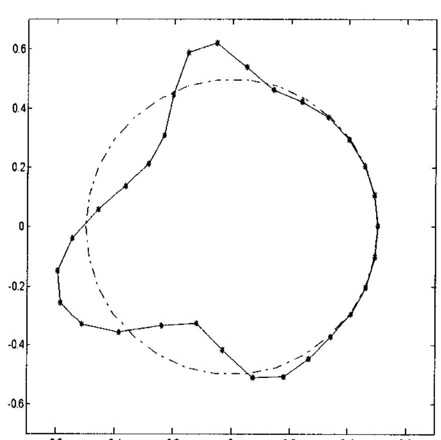

(e) Mode 5- ω_5

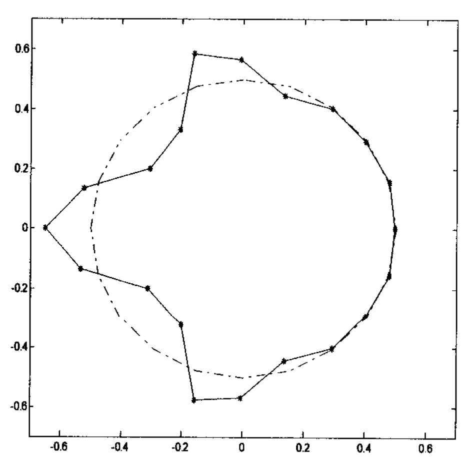

(f) Mode 6 - ω_6

Fig. 3-11 Cross-sectional views of mode shapes 1-6 of case C from DQM

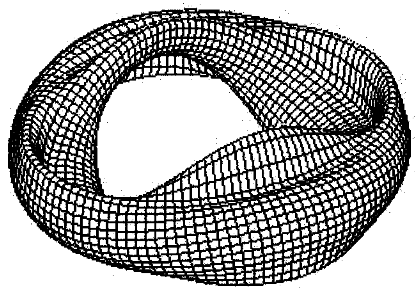

(a) Mode 1 - ω_1

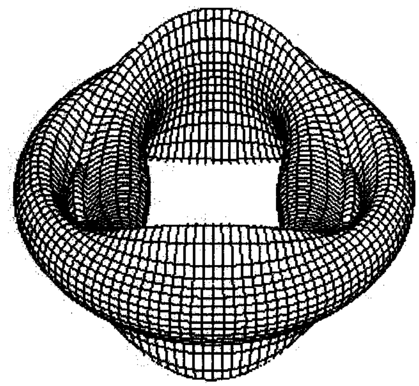

(b) Mode 2 - ω_2

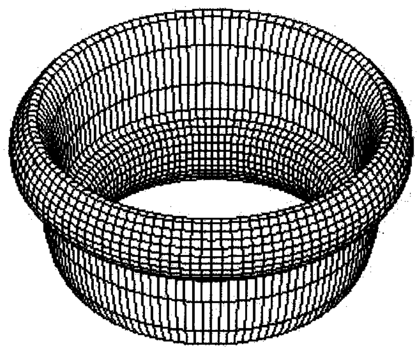

(c) Mode 3 - ω_3

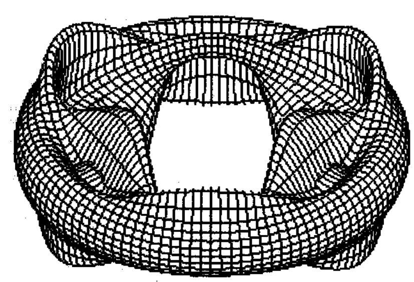

(d) Mode 4 - ω_4

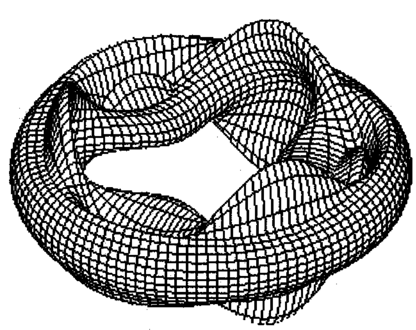

(e) Mode 5 - ω_5

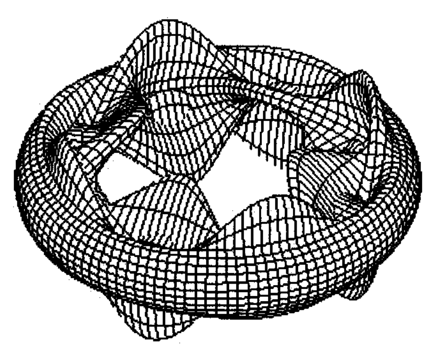

(f) Mode 6 - ω_6

Fig. 3-12 Three-dimensional views of mode shapes 1-6 of case A with orthotropic material M1

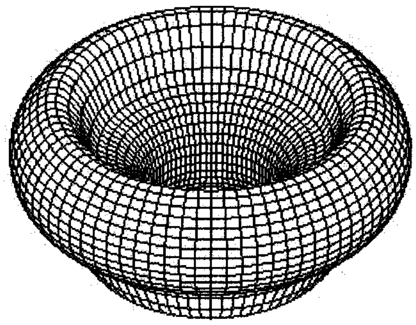

(a) Mode 1 - ω_1

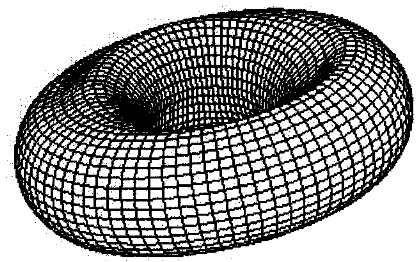

(b) Mode 2 - ω_2

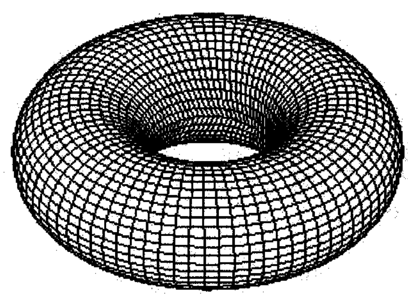

(c) Mode 3 - ω_3

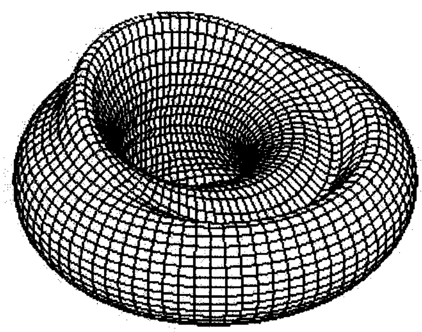

(d) Mode 4 - ω_4

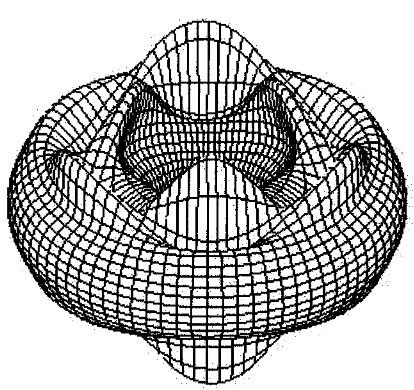

(e) Mode 5 - ω_5

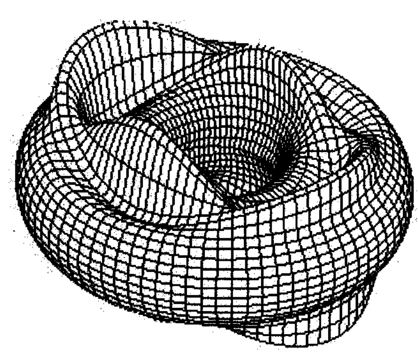

(f) Mode 6 - ω_6

Fig. 3-13 Three-dimensional views of mode shapes 1-6 of case C with inner equator support

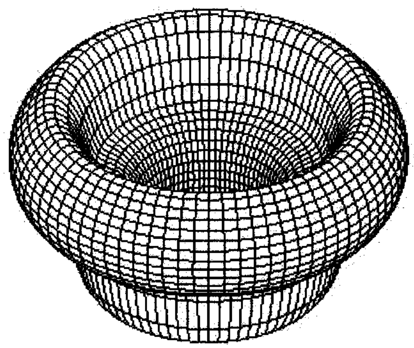

(a) Mode 1 - ω_1

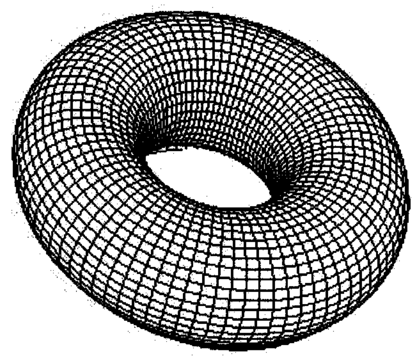

(b) Mode 2 - ω_2

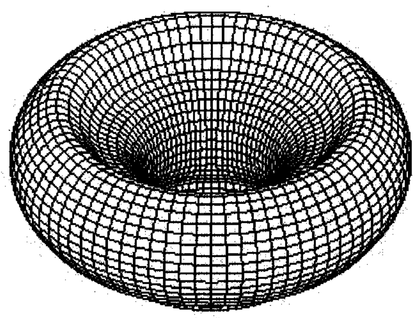

(c) Mode 3 - ω_3

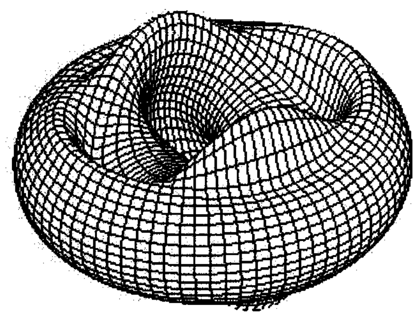

(d) Mode 4 - ω_4

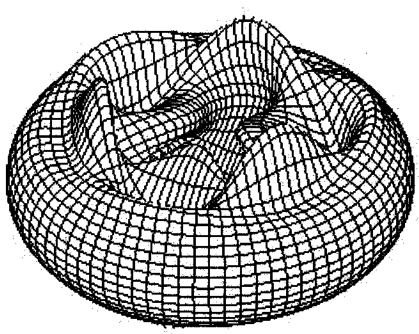

(e) Mode 5 - ω_5

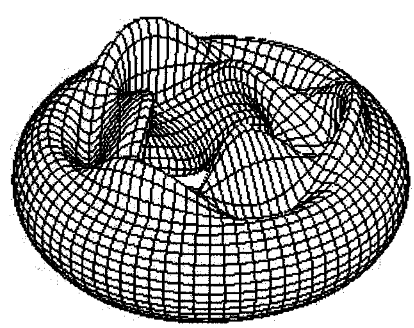

(f) Mode 6 - ω_6

Fig. 3-14 Three-dimensional views of mode shapes 1-6 of case C with bottom crown support

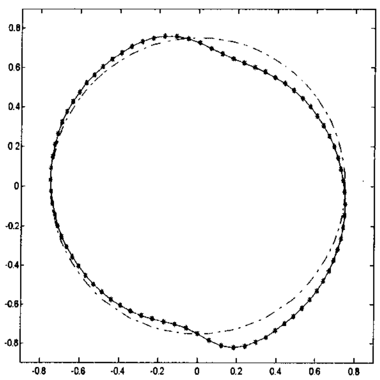

(a) Mode 1- ω_1

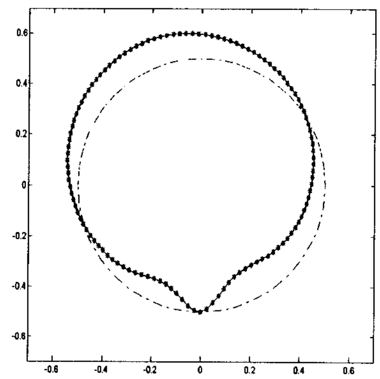

(b) Mode 2 - ω_2

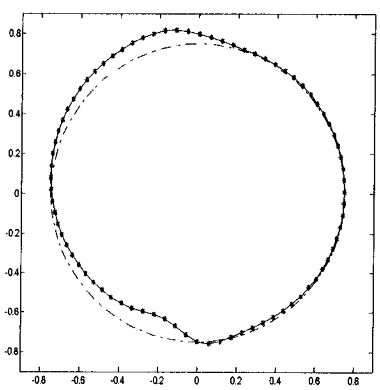

(c) Mode 3 - ω_3

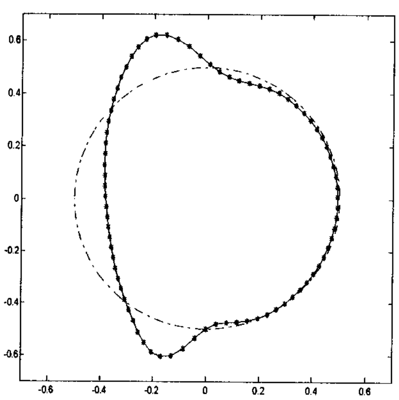

(d) Mode 4 - ω_4

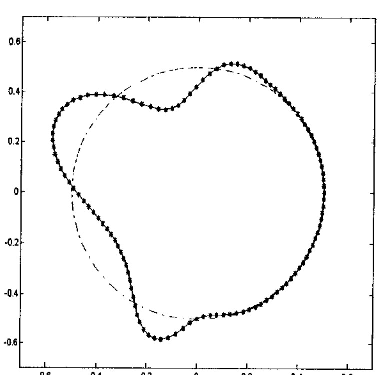

(e) Mode 5 - ω_5

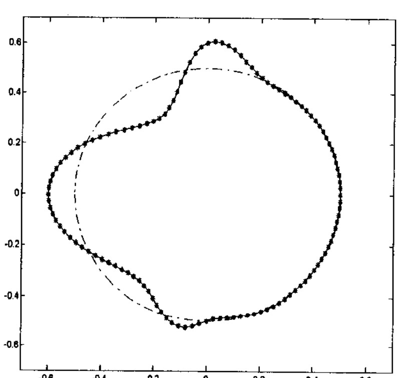

(f) Mode 6 - ω_6

Fig. 3-15 Cross-sectional views of mode shapes 1-6 of case C with bottom crown support

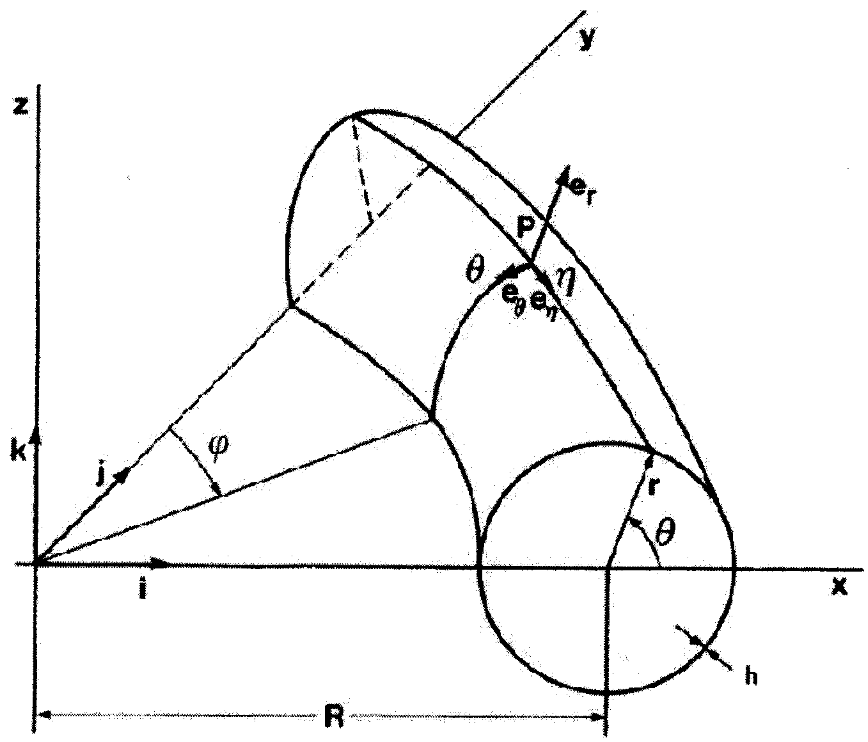

Fig. 4-1 Toroidal coordinate system

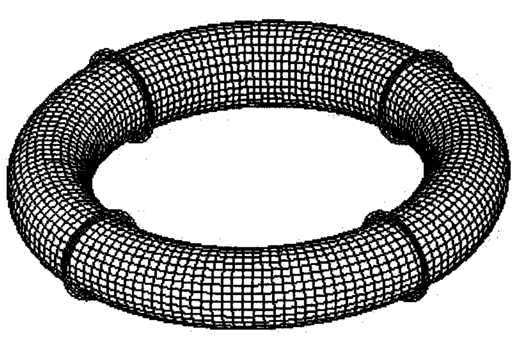

Fig. 4-2 Ring-stiffened toroidal shell

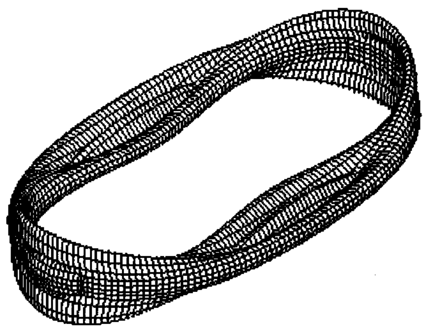

(a) Mode 1 - ω_1

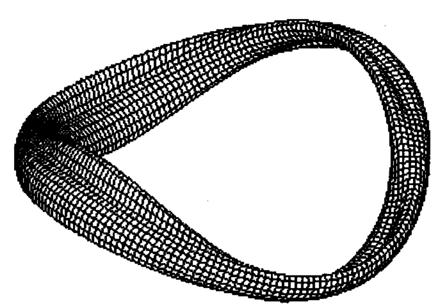

(b) Mode 2 - ω_2

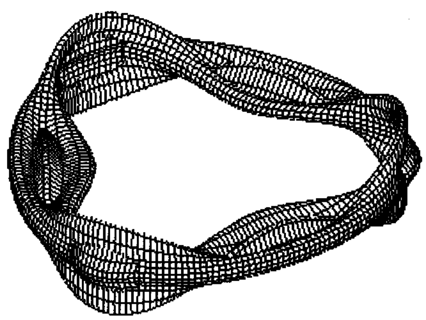

(c) Mode 3 - ω_3

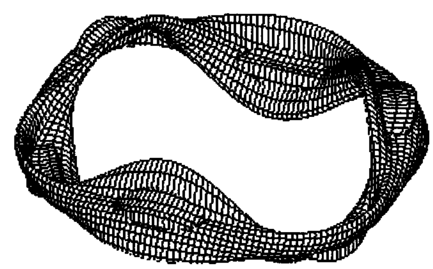

(d) Mode 4 - ω_4

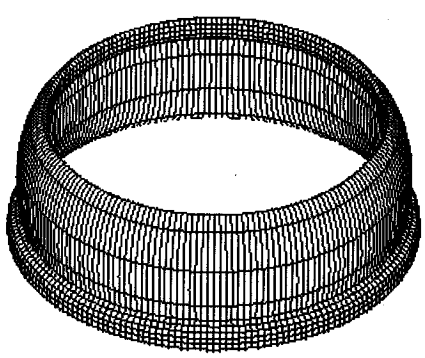

(e) Mode 5 - ω_5

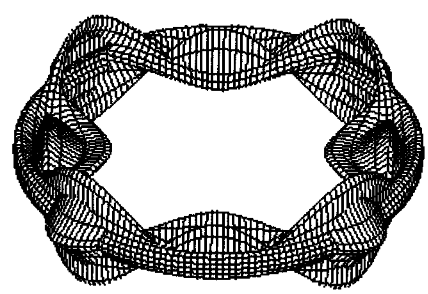

(f) Mode 6 - ω_6

Fig. 4-3 Three-dimensional views of mode shapes 1-6 of case 1 (FEM)

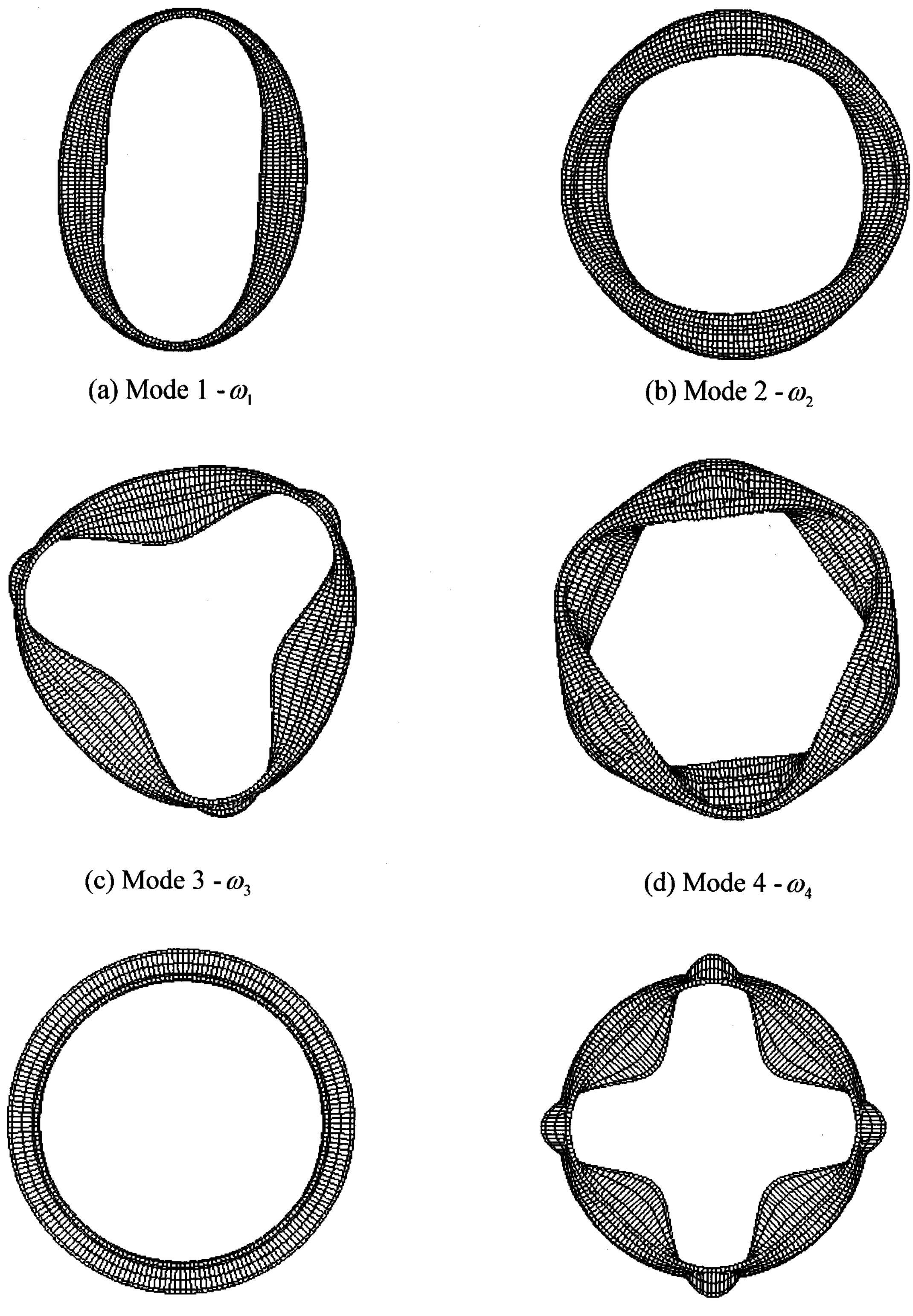

(a) Mode 1 - ω_1

(b) Mode 2 - ω_2

(c) Mode 3 - ω_3

(d) Mode 4 - ω_4

(e) Mode 5 - ω_5

(f) Mode 6 - ω_6

Fig. 4-4 Projections on equator of mode shapes 1-6 of case 1(FEM)

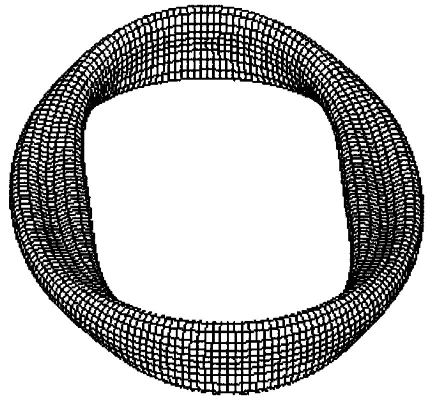

(a) Mode 1 - ω_1

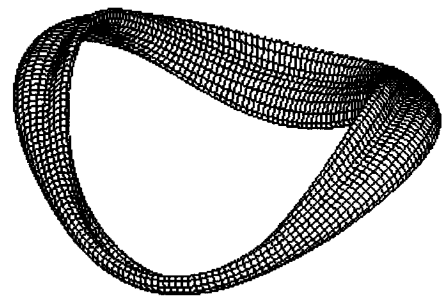

(b) Mode 2 - ω_2

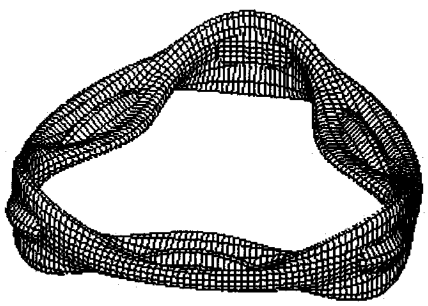

(c) Mode 3 - ω_3

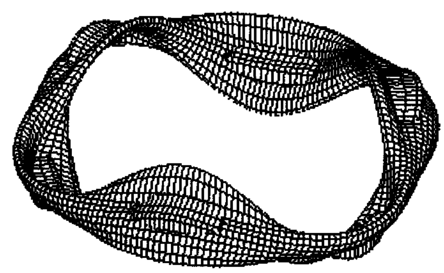

(d) Mode 4 - ω_4

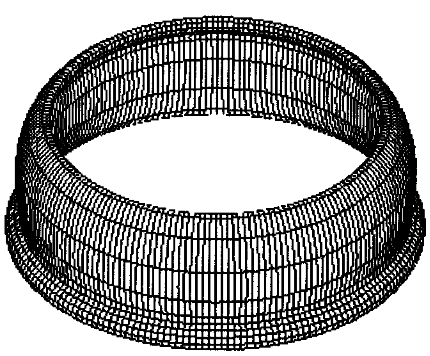

(e) Mode 5 - ω_5

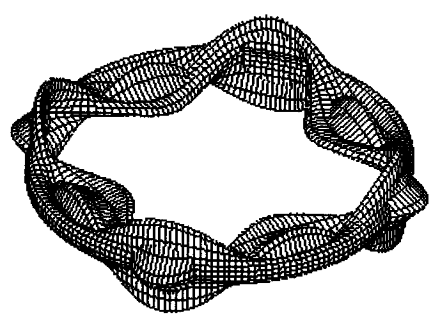

(f) Mode 6 - ω_6

Fig. 4-5 Three-dimensional views of mode shapes 1-6 of case 2 (FEM)

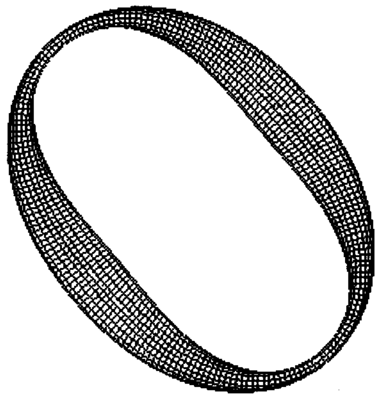

(a) Mode 1 - ω_1

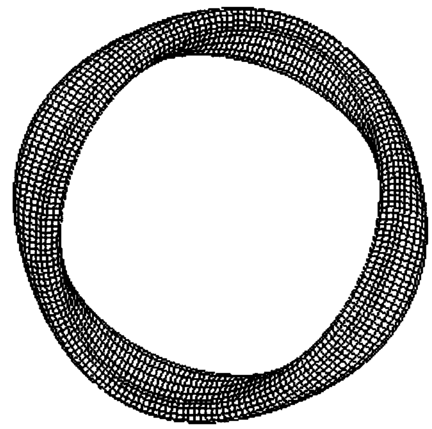

(b) Mode 2 - ω_2

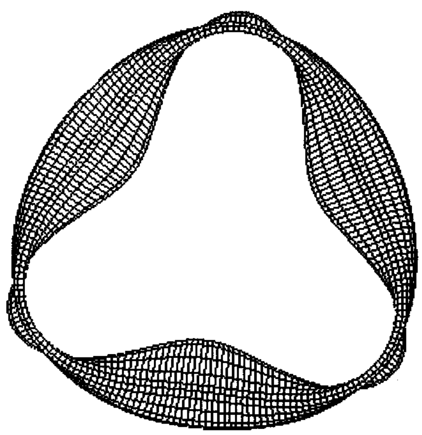

(c) Mode 3 - ω_3

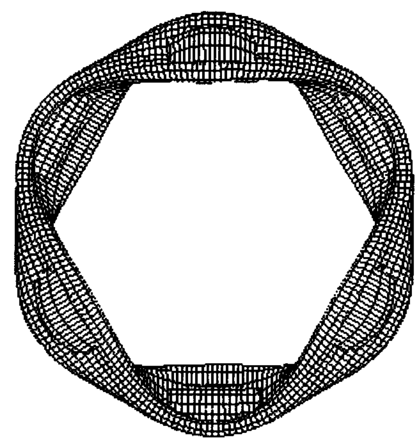

(d) Mode 4 - ω_4

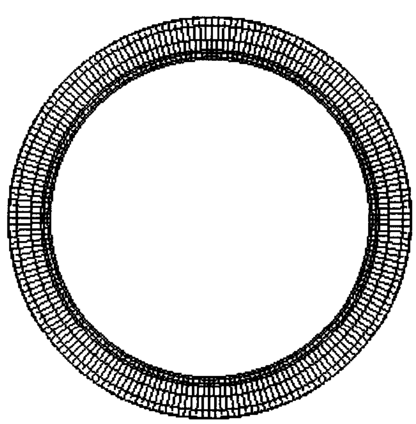

(e) Mode 5 - ω_5

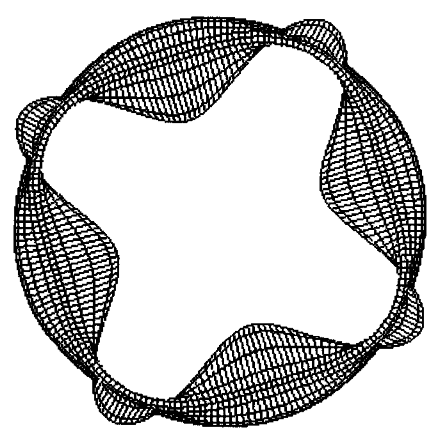

(f) Mode 6 - ω_6

Fig. 4-6 Projections on equator of mode shapes 1-6 of case 2 (FEM)

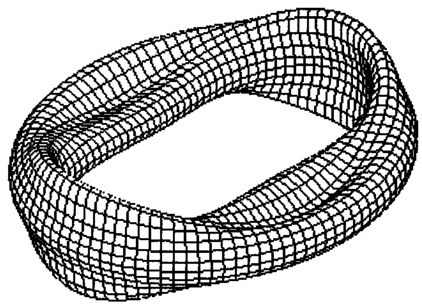

(a) Mode 1 - ω_1

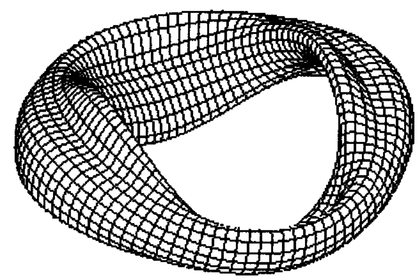

(b) Mode 2 - ω_2

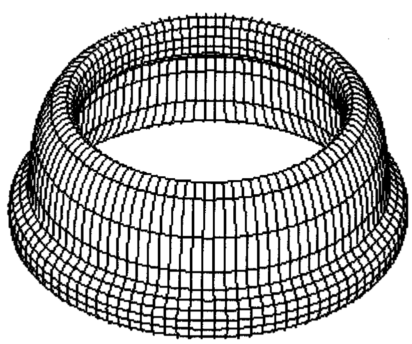

(c) Mode 3 - ω_3

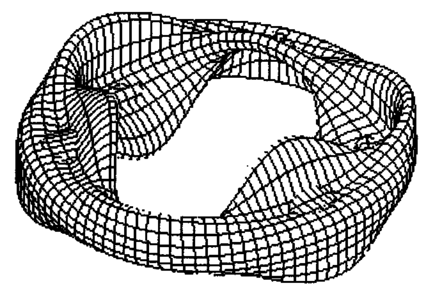

(d) Mode 4 - ω_4

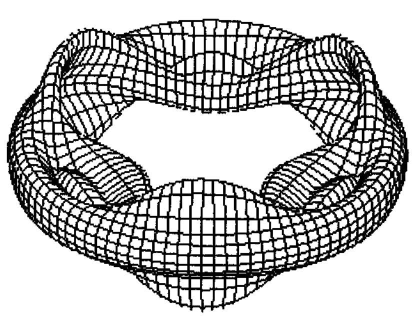

(e) Mode 5 - ω_5

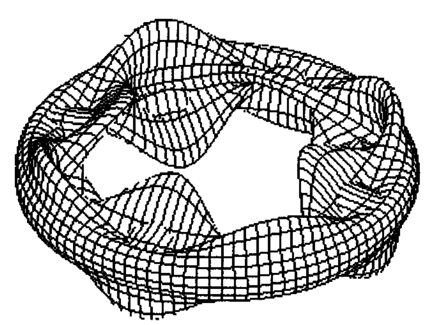

(f) Mode 6 - ω_6

Fig. 4-7 Three-dimensional views of mode shapes 1-6 of case 3 (FEM)

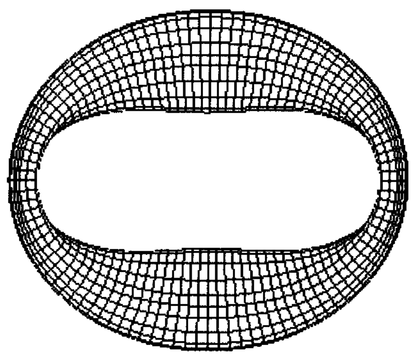

(a) Mode 1 - ω_1

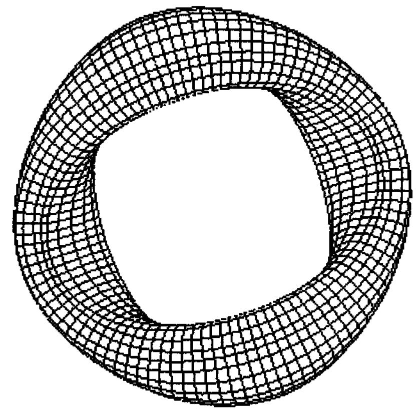

(b) Mode 2 - ω_2

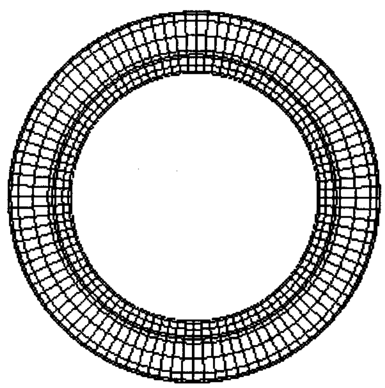

(c) Mode 3 - ω_3

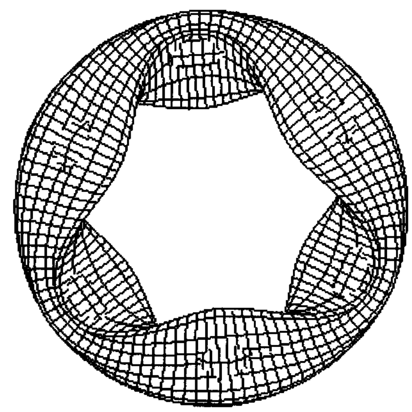

(d) Mode 4 - ω_4

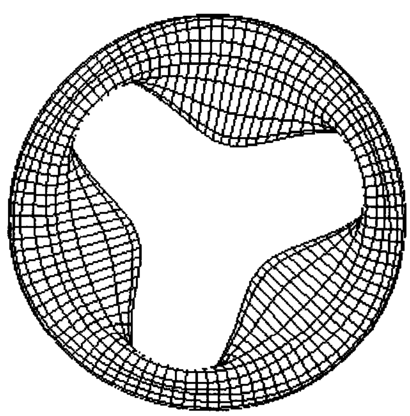

(e) Mode 5 - ω_5

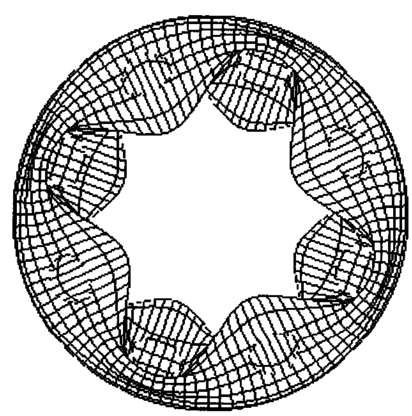

(f) Mode 6 - ω_6

Fig. 4-8 Projections on equator of mode shapes 1-6 of case 3 (FEM)

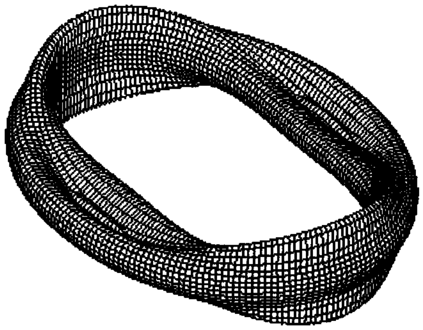

(a) Mode 1 - ω_1

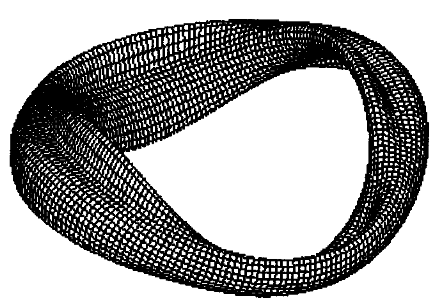

(b) Mode 2 - ω_2

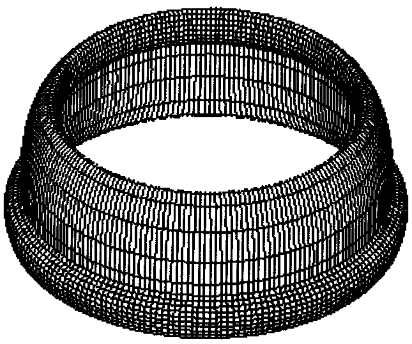

(c) Mode 3 - ω_3

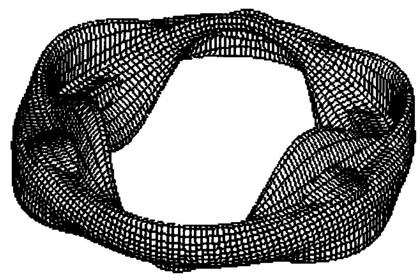

(d) Mode 4 - ω_4

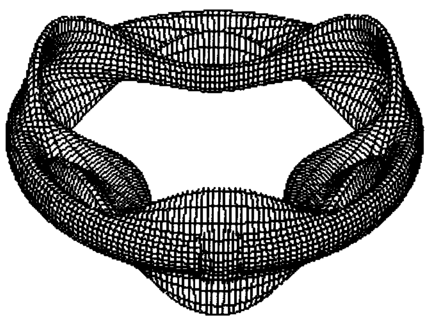

(e) Mode 5 - ω_5

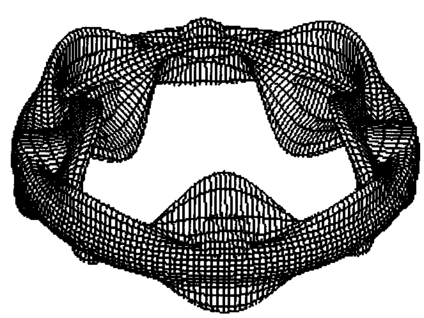

(f) Mode 6 - ω_6

Fig. 4-9 Three-dimensional views of mode shapes 1-6 of case 4 (FEM)

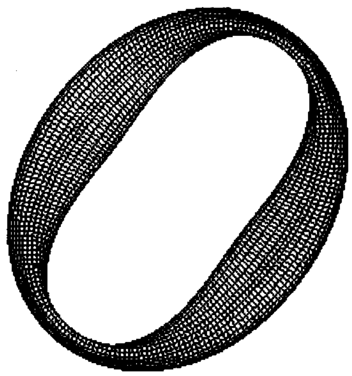

(a) Mode 1 - ω_1

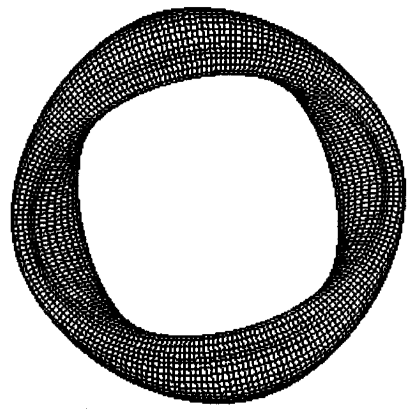

(b) Mode 2 - ω_2

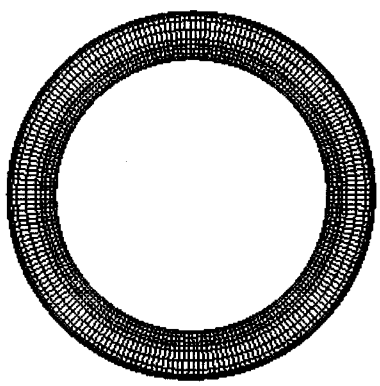

(c) Mode 3 - ω_3

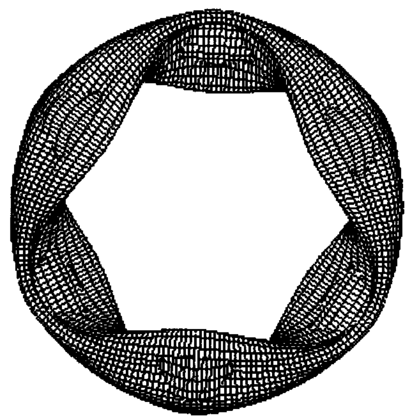

(d) Mode 4 - ω_4

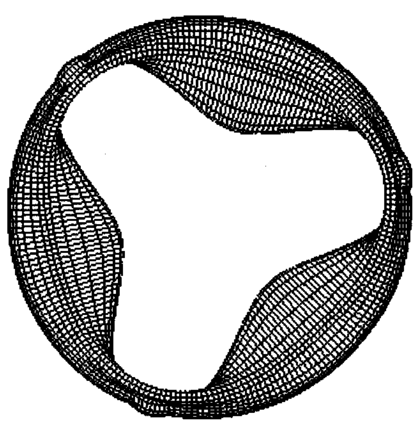

(e) Mode 5 - ω_5

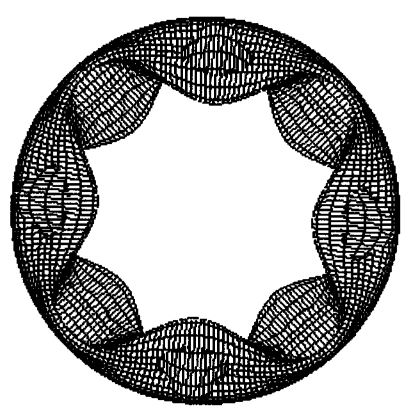

(f) Mode 6 - ω_6

Fig. 4-10 Projections on equator of mode shapes 1-6 of case 4 (FEM)

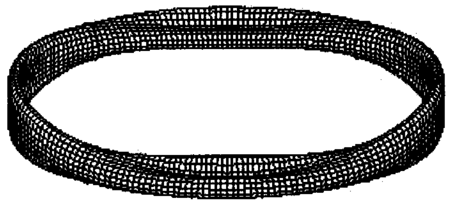

(a) Mode 1 - ω_1

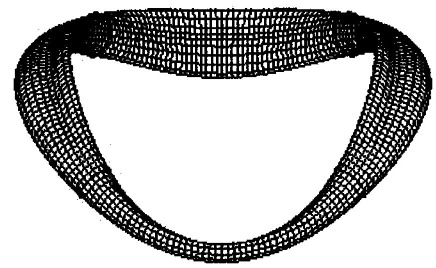

(b) Mode 2 - ω_2

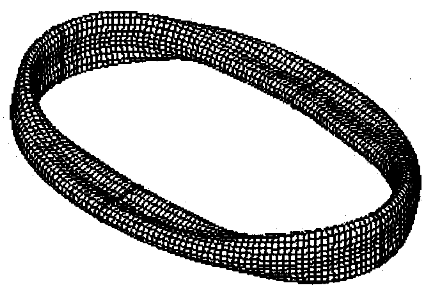

(c) Mode 3 - ω_3

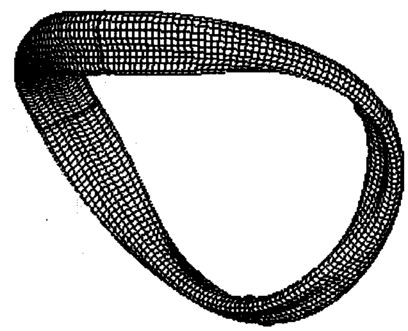

(d) Mode 4 - ω_4

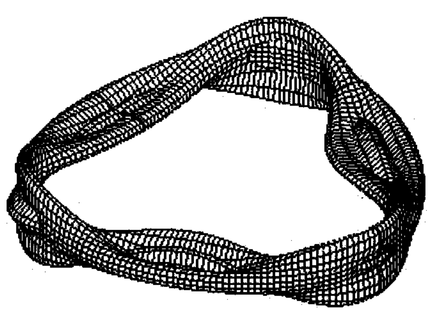

(e) Mode 5 - ω_5

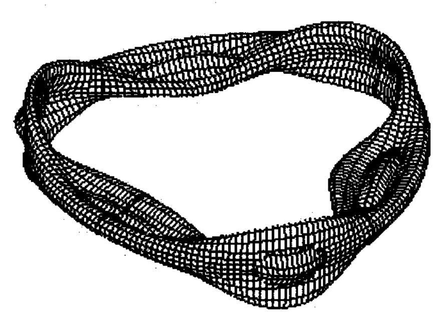

(f) Mode 6 - ω_6

Fig. 4-11 Three-dimensional views of mode shapes 1-6 of case 2 with 4 light rings

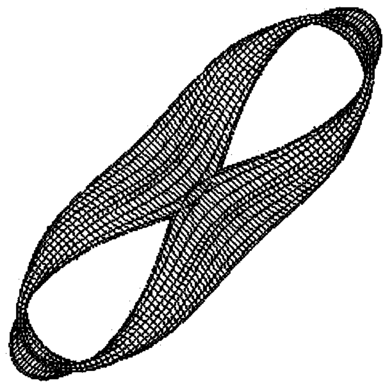

(a) Mode 1- ω_1

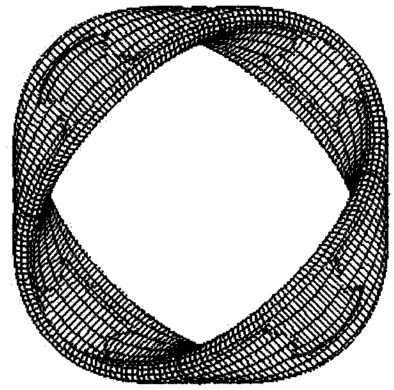

(b) Mode 2 - ω_2

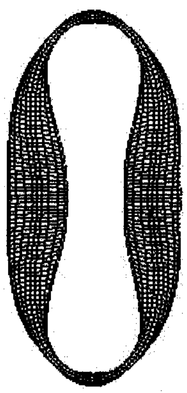

(c) Mode 3 - ω_3

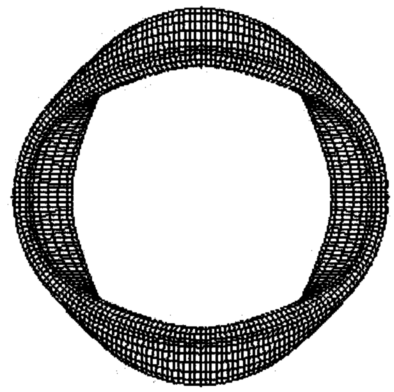

(d) Mode 4 - ω_4

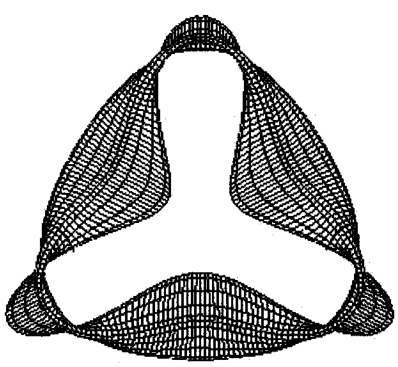

(e) Mode 5 - ω_5

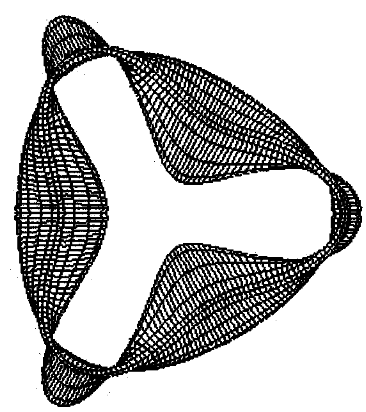

(f) Mode 6 - ω_6

Fig. 4-12 Projections on equator of mode shapes 1-6 of case 2 with 4 light rings

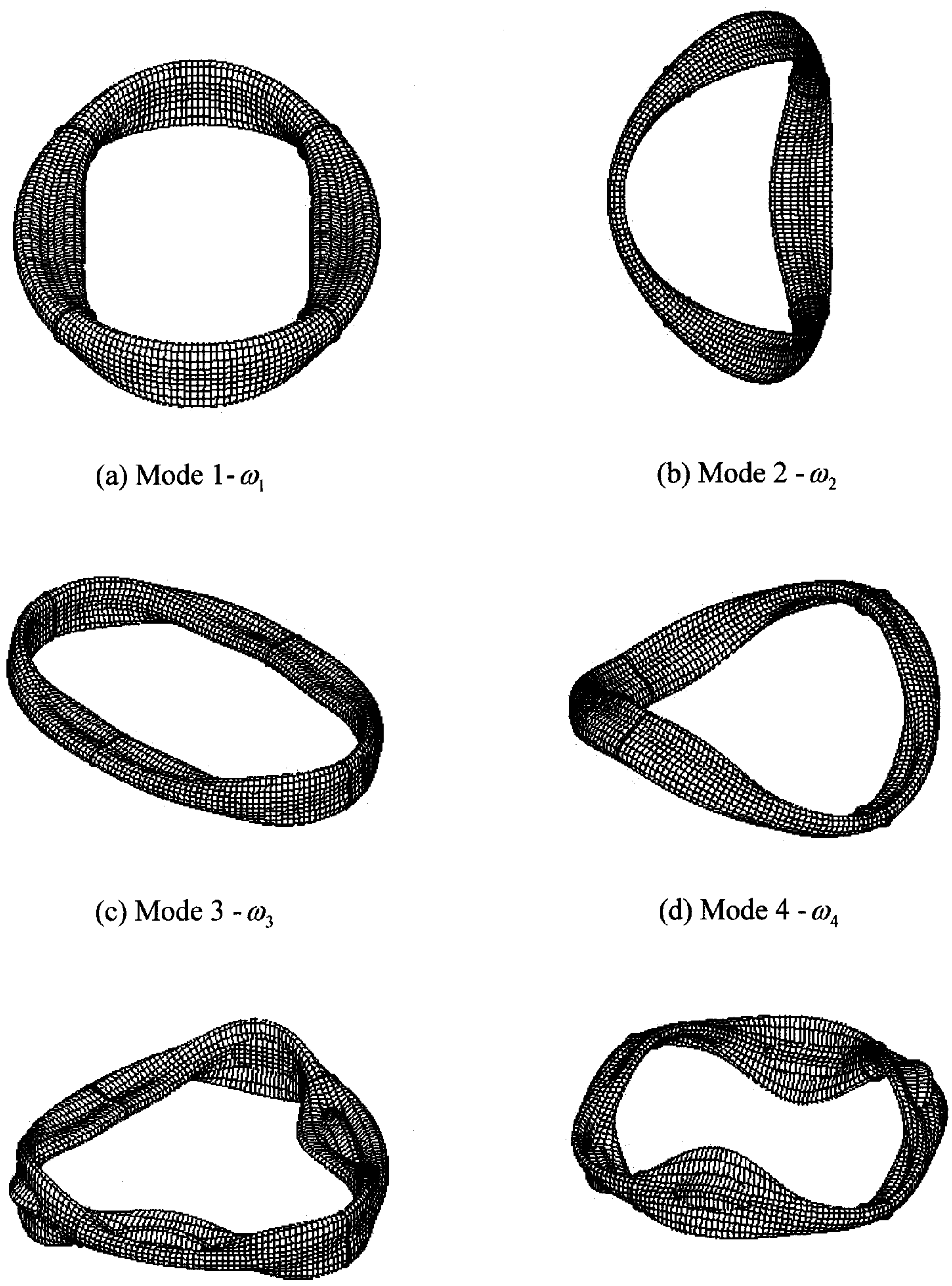

(a) Mode 1 - ω_1

(b) Mode 2 - ω_2

(c) Mode 3 - ω_3

(d) Mode 4 - ω_4

(e) Mode 5 - ω_5

(f) Mode 6 - ω_6

Fig. 4-13 Three-dimensional views of mode shapes 1-6 of case 2 with 4 heavy rings

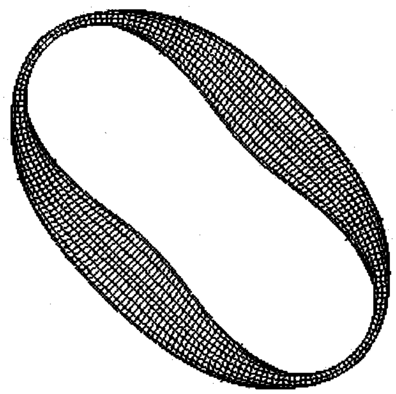

(a) Mode 1- ω_1

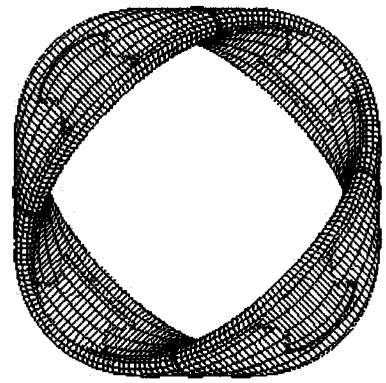

(b) Mode 2 - ω_2

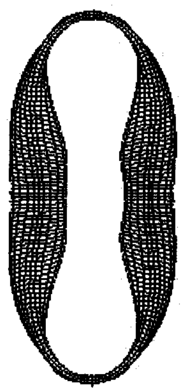

(c) Mode 3 - ω_3

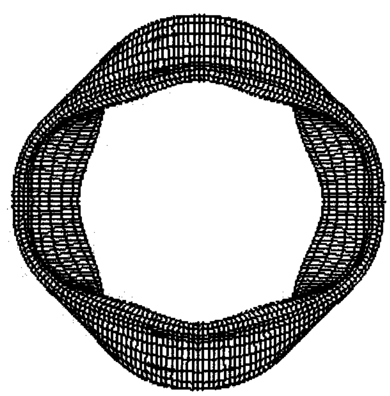

(d) Mode 4 - ω_4

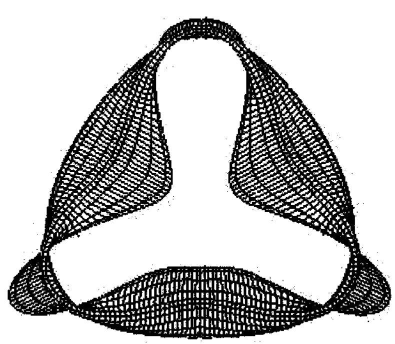

(e) Mode 5 - ω_5

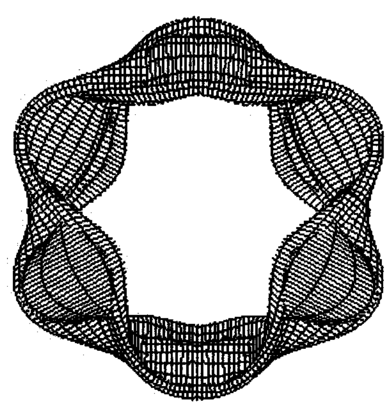

(f) Mode 6 - ω_6

Fig. 4-14 Projections on equator of mode shapes 1-6 of case 2 with 4 heavy rings

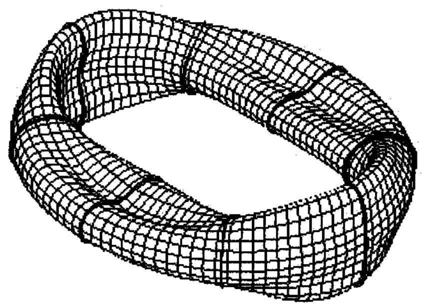

(a) Mode 1- ω_1

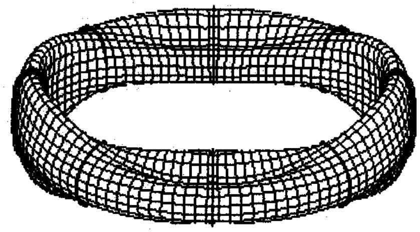

(b) Mode 2 - ω_2

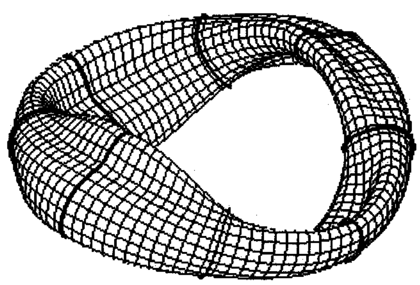

(c) Mode 3 - ω_3

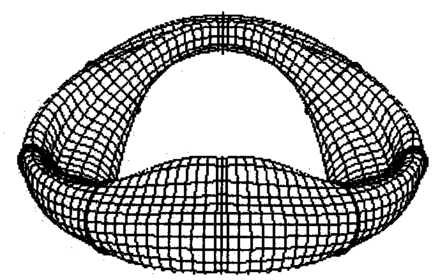

(d) Mode 4 - ω_4

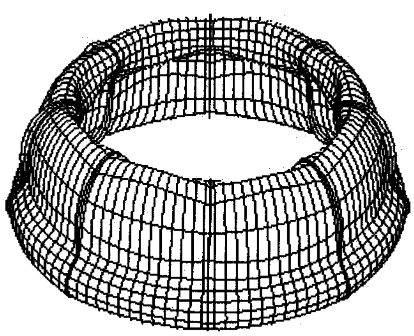

(e) Mode 5 - ω_5

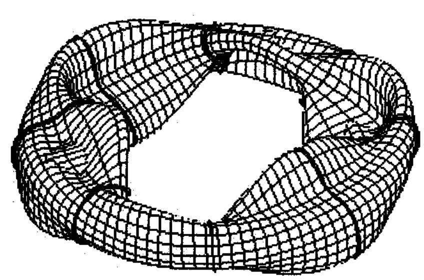

(f) Mode 6 - ω_6

Fig. 4-15 Three-dimensional views of mode shapes 1-6 of case 3 with 8 light rings

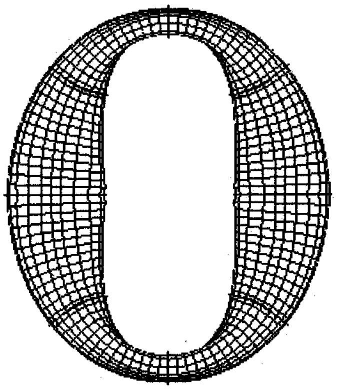

(a) Mode 1 - ω_1

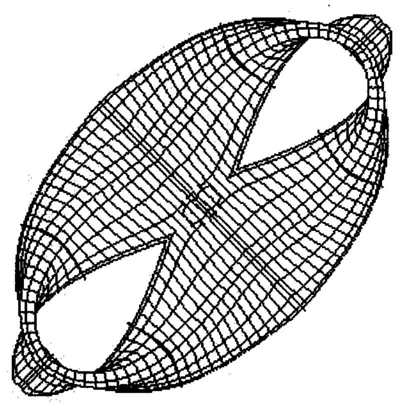

(b) Mode 2 - ω_2

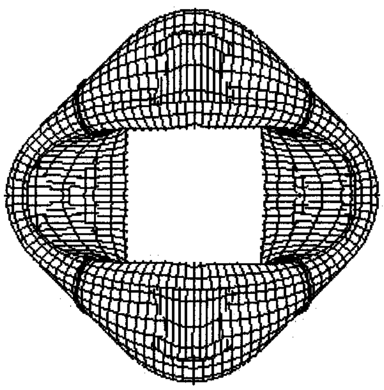

(c) Mode 3 - ω_3

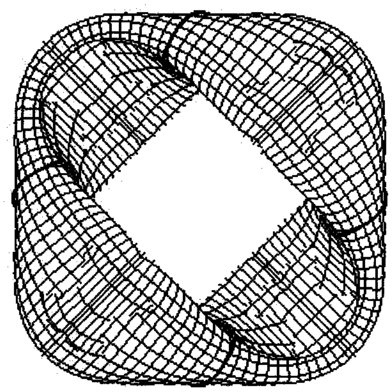

(d) Mode 4 - ω_4

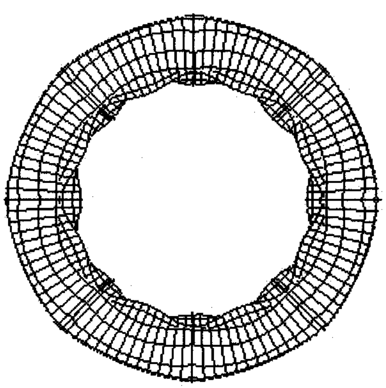

(e) Mode 5 - ω_5

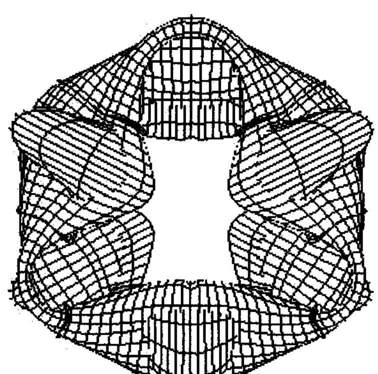

(f) Mode 6 - ω_6

Fig. 4-16 Projections on equator of mode shapes 1-6 of case 3 with 8 light rings

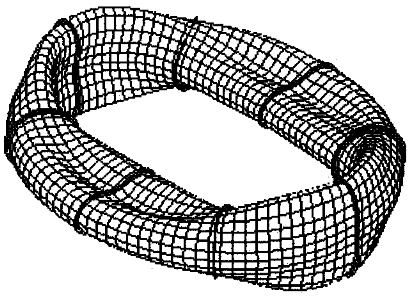

(a) Mode 1 - ω_1

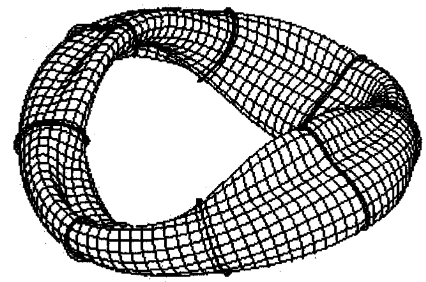

(b) Mode 2 - ω_2

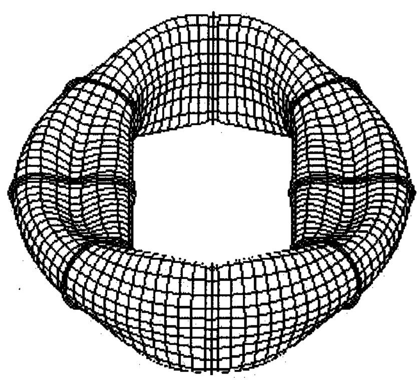

(c) Mode 3 - ω_3

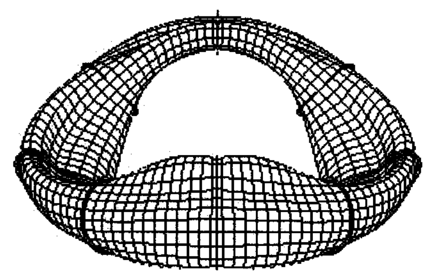

(d) Mode 4 - ω_4

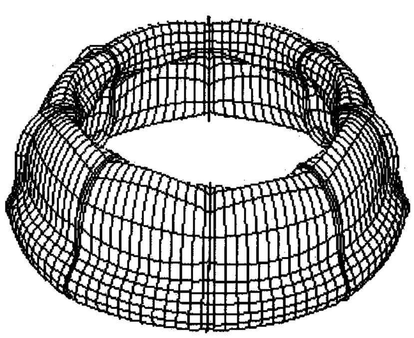

(e) Mode 5 - ω_5

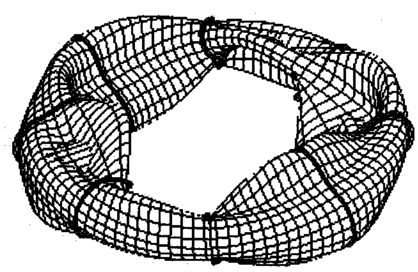

(f) Mode 6 - ω_6

Fig. 4-17 Three-dimensional view of mode shapes 1-6 of case 3 with 8 heavy rings

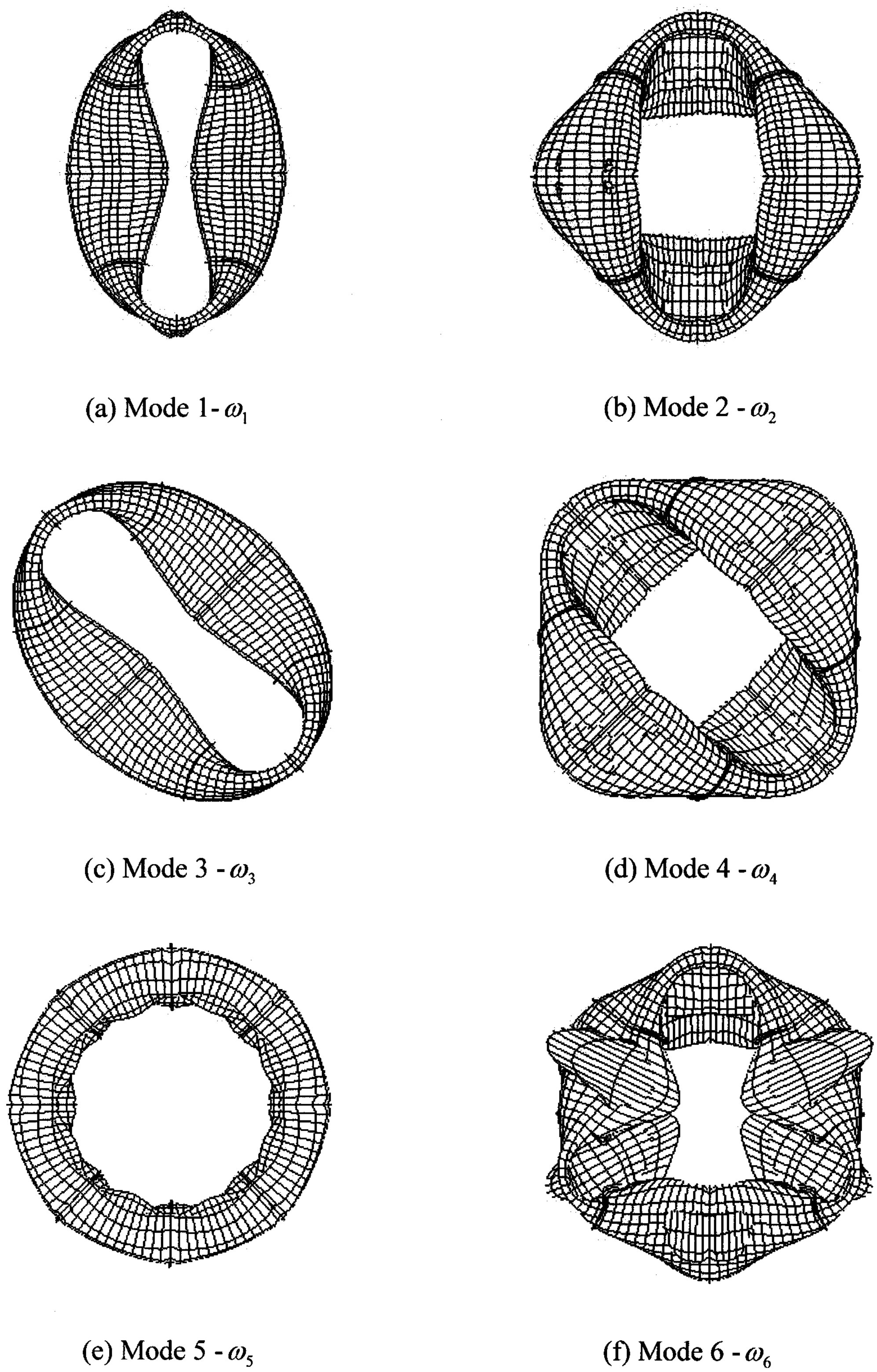

Fig. 4-18 Projections on equator of mode shapes 1-6 of case 4 with 8 heavy rings

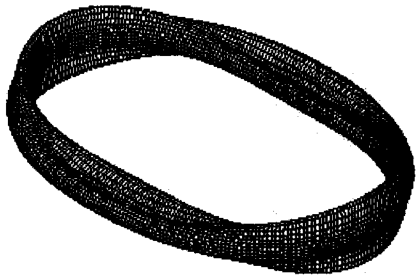

(a) Mode 1 - ω_1

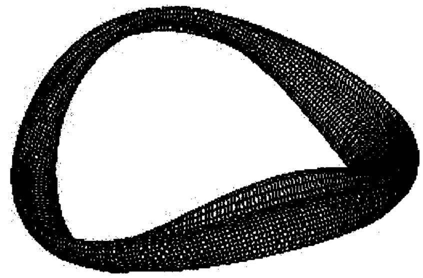

(b) Mode 2 - ω_2

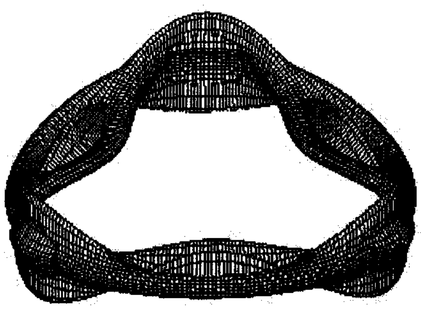

(c) Mode 3 - ω_3

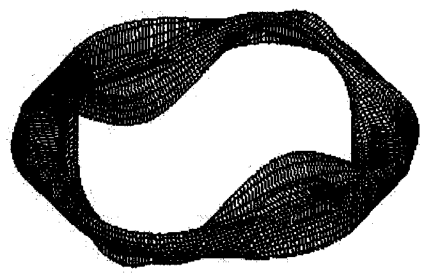

(d) Mode 4 - ω_4

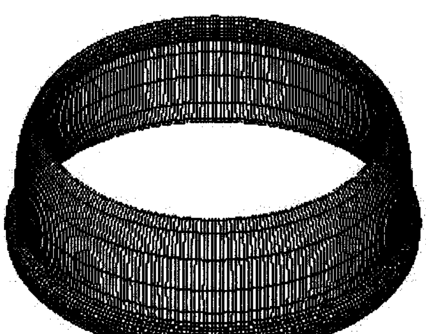

(e) Mode 5 - ω_5

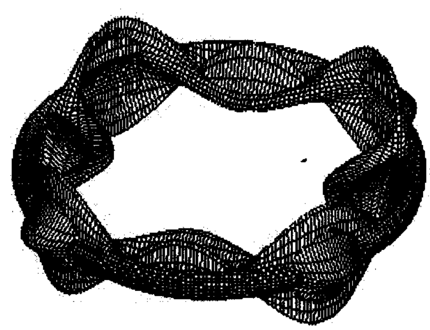

(f) Mode 6 - ω_6

Fig. 4-19 Three-dimensional views of mode shapes 1-6 of case 1 with orthotropic material M1

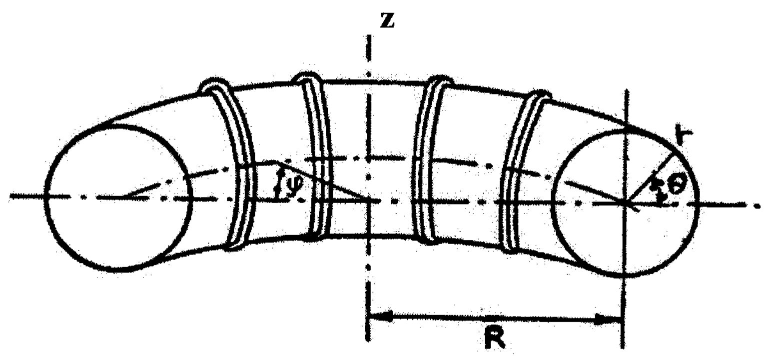

Fig. 5-1 Geometry of ring-stiffened toroidal shell

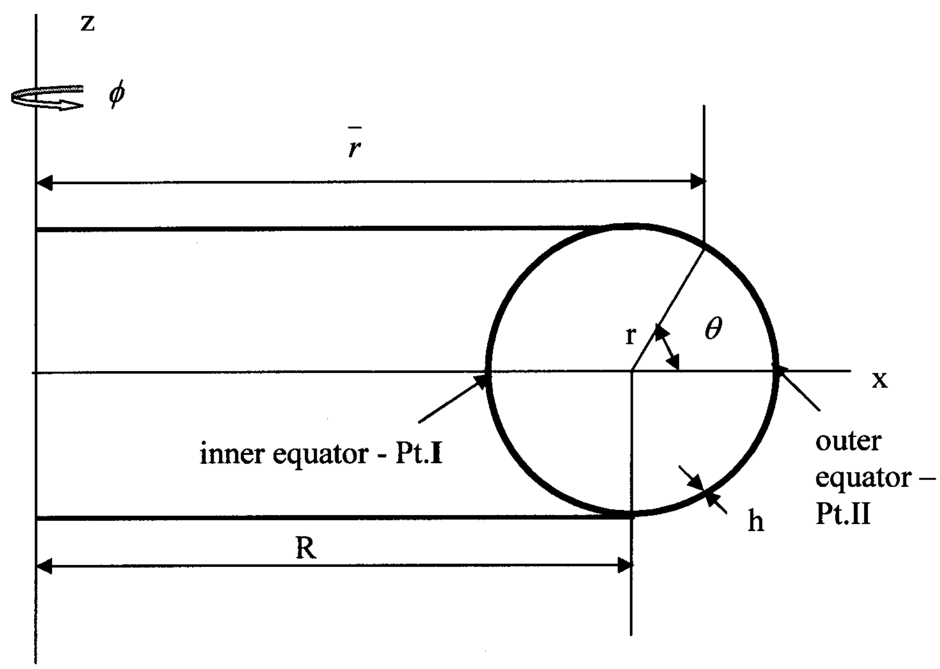

Fig. 5-2 Geometry of the toroidal shell with the boundary conditions

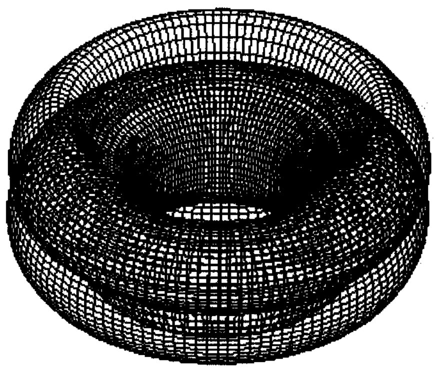

(a) Mode shape of case I

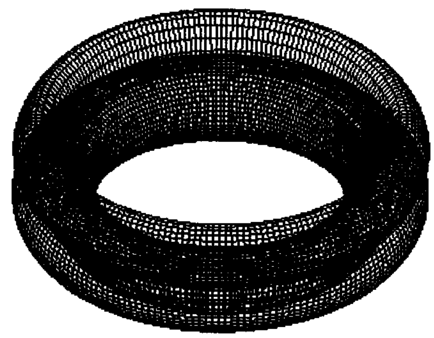

(b) Mode shape of case II

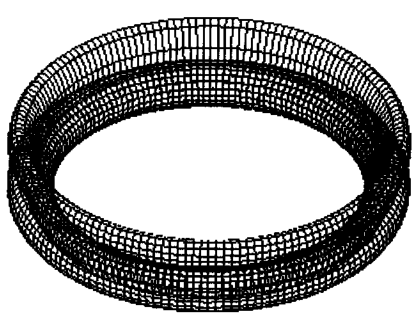

(c) Mode shape of case III

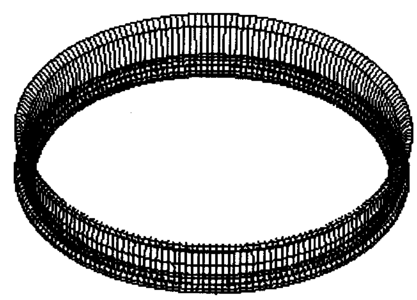

(d) Mode shape of case IV

Fig. 5-3 Three-dimensional views of mode shapes of case I-IV with original shells

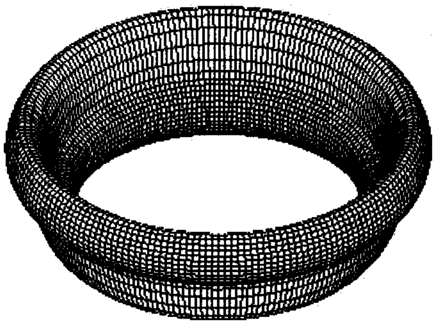

(a) Mode shape of unstiffened shell

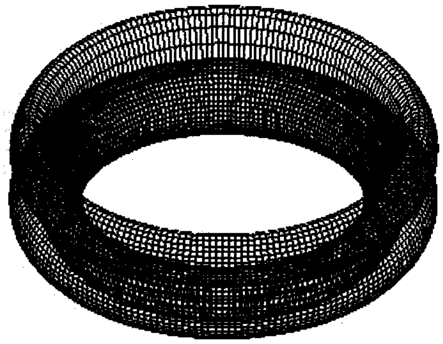

(b) Mode shape of unstiffened shell with original shell

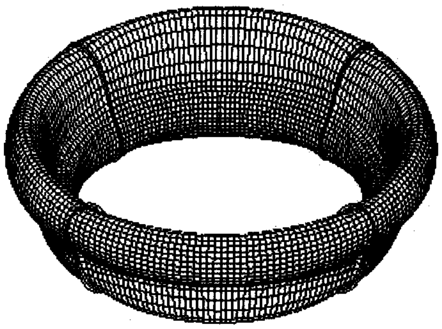

(c) Mode shape of stiffened shell with 4 light rings

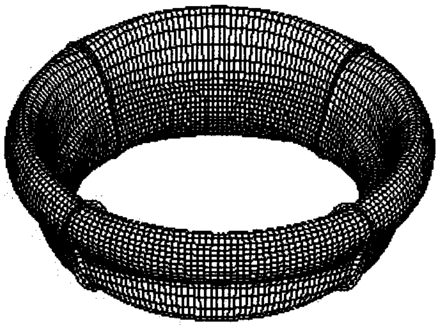

(d) Mode shape of stiffened shell with 4 heavy rings

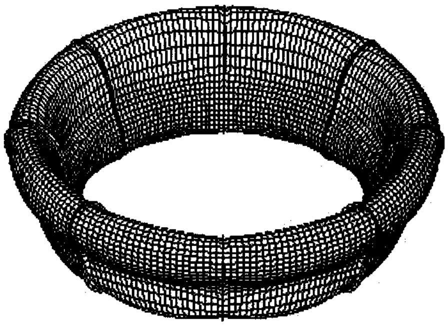

(e) Mode shape of stiffened shell with 8 light rings

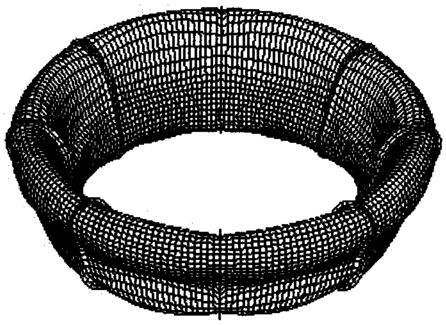

(f) Mode shape of stiffened shell with 8 heavy rings

Fig. 5-4 Three-dimensional views of mode shapes of case 1 with support at inner equator

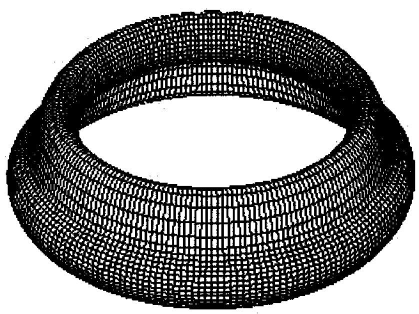

(a) Mode shape of unstiffened shell

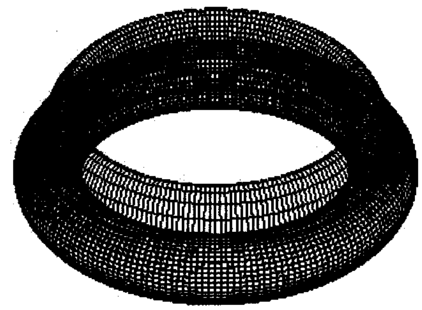

(b) Mode shape of unstiffened shell with original shell

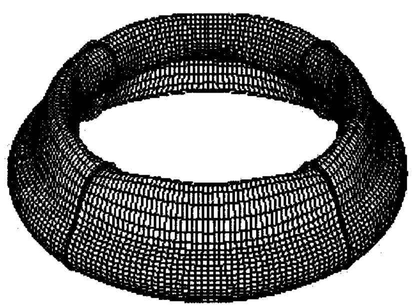

(c) Mode shape of stiffened shell with 4 light rings

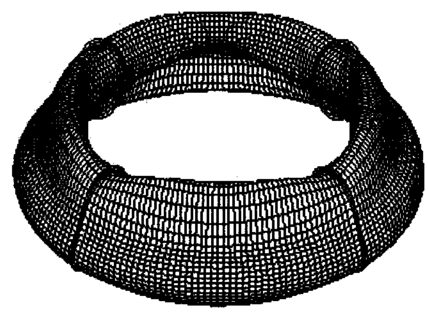

(d) Mode shape of stiffened shell with 4 heavy rings

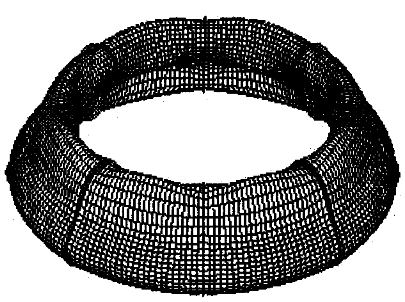

(e) Mode shape of stiffened shell with 8 light rings

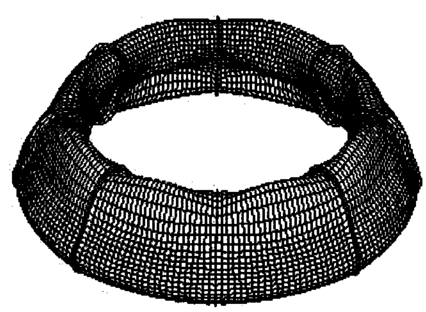

(f) Mode shape of stiffened shell with 8 heavy rings

Fig. 5-5 Three-dimensional views of mode shapes of case 1 with support at outer equator

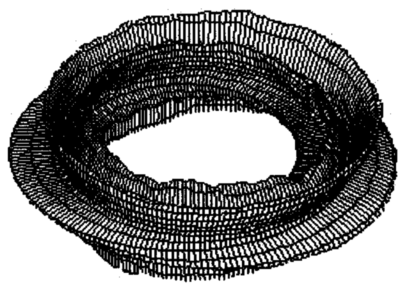

(a) Mode shape of unstiffened shell

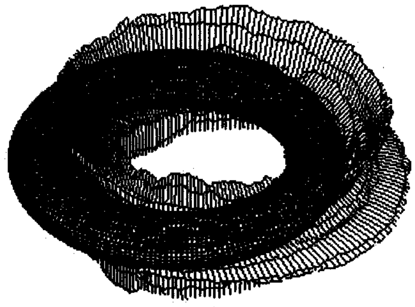

(b) Mode shape of unstiffened shell with original shell

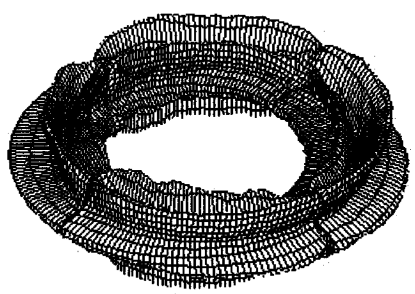

(c) Mode shape of stiffened shell with 4 light rings

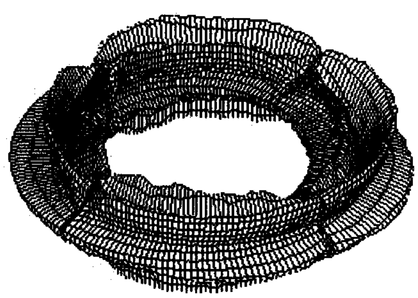

(d) Mode shape of stiffened shell with 4 heavy rings

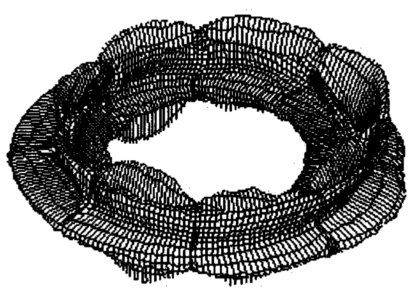

(e) Mode shape of stiffened shell with 8 light rings

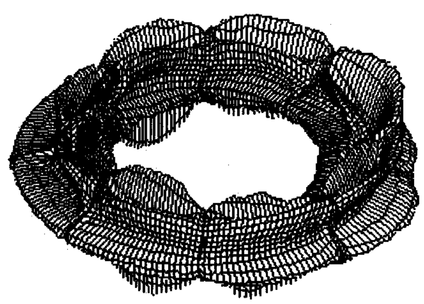

(f) Mode shape of stiffened shell with 8 heavy rings

Fig. 5-6 Three-dimensional views of mode shapes of case 1 with support at both equators

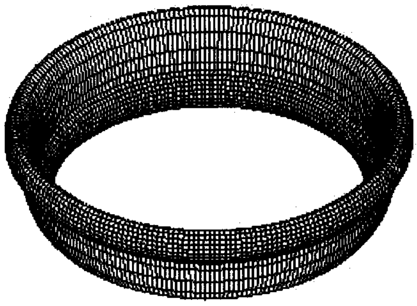

(a) Mode shape of unstiffened shell

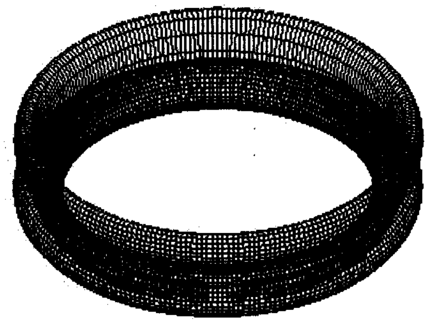

(b) Mode shape of unstiffened shell with original shell

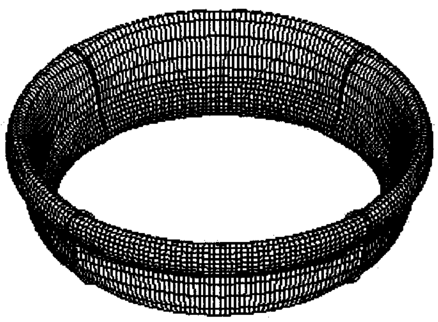

(c) Mode shape of stiffened shell with 4 light rings

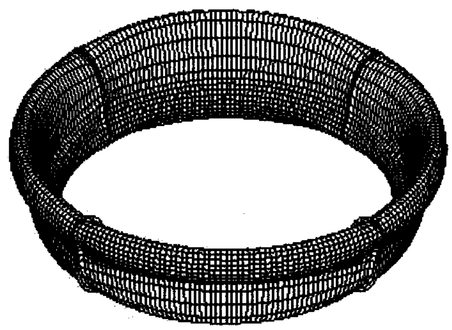

(d) Mode shape of stiffened shell with 4 heavy rings

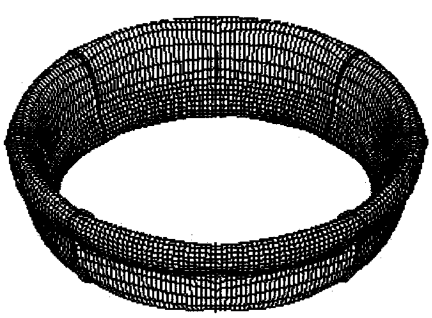

(e) Mode shape of stiffened shell with 8 light rings

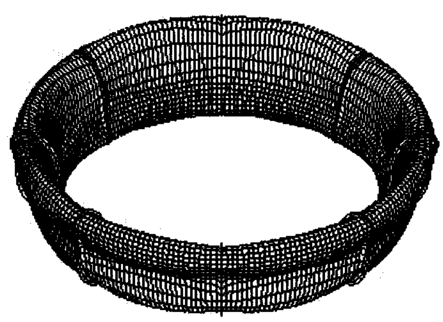

(f) Mode shape of stiffened shell with 8 heavy rings

Fig. 5-7 Three-dimensional views of mode shapes of case 2 with support at inner equator

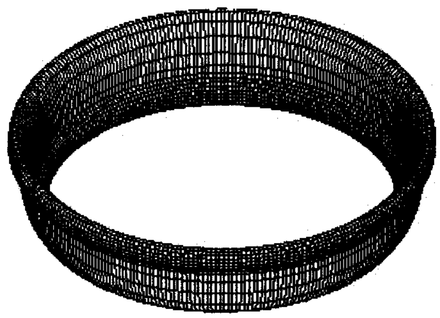

(a) Mode shape of unstiffened shell

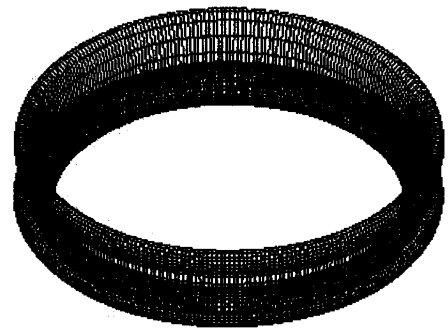

(b) Mode shape of unstiffened shell with original shell

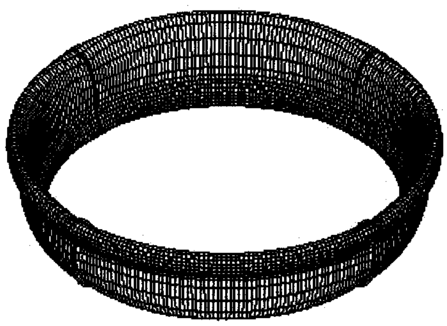

(c) Mode shape of stiffened shell with 4 light rings

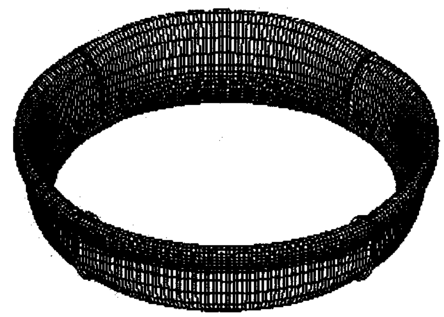

(d) Mode shape of stiffened shell with 4 heavy rings

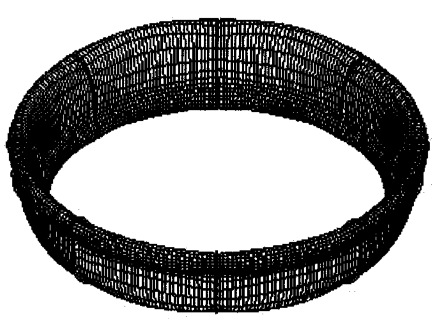

(e) Mode shape of stiffened shell with 8 light rings

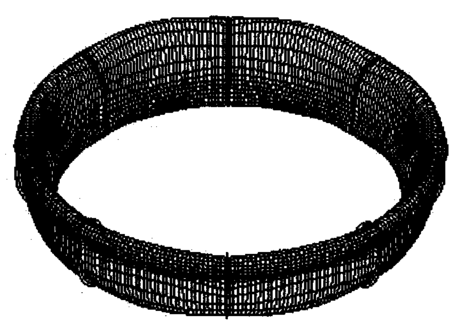

(f) Mode shape of stiffened shell with 8 heavy rings

Fig. 5-8 Three-dimensional views of mode shapes of case 3 with support at inner equator

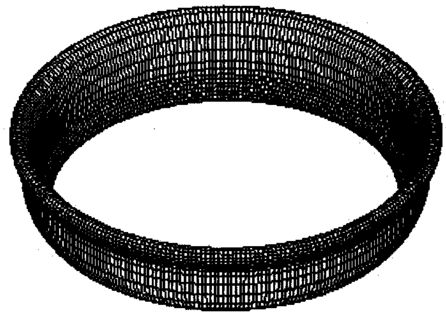

(a) Mode shape of unstiffened shell

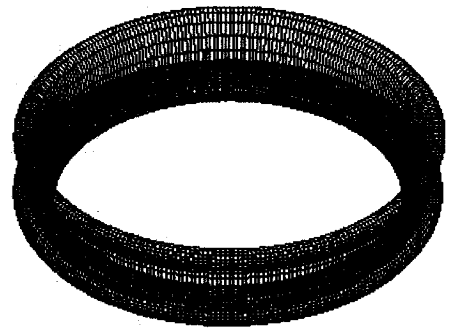

(b) Mode shape of unstiffened shell with original shell

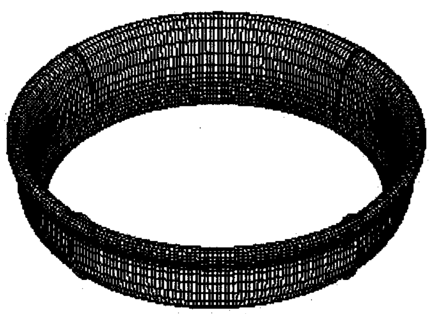

(c) Mode shape of stiffened shell with 4 light rings

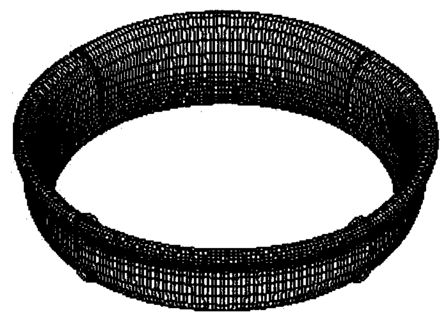

(d) Mode shape of stiffened shell with 4 heavy rings

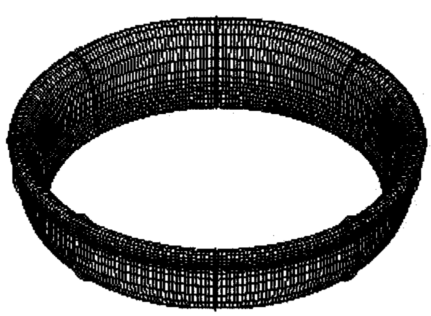

(e) Mode shape of stiffened shell with 8 light rings

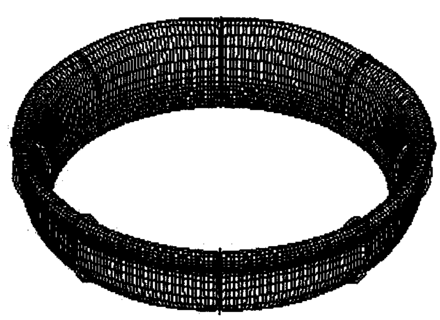

(f) Mode shape of stiffened shell with 8 heavy rings

Fig. 5-9 Three-dimensional views of mode shapes of case 4 with support at inner equator

Appendix A1-Listing of functions $a_1 - a_{42}$ of chapter 3

$a_1 = \alpha_2$;

$a_2 = \alpha_2^\bullet$;

$a_3 = -\alpha_2^\bullet$;

$a_4 = \alpha_1$;

$a_5 = 2\alpha_2'$;

$a_6 = \kappa_1\alpha_2$;

$a_7 = \kappa_1\alpha_2^\bullet$;

$a_8 = -\kappa_1\alpha_2^\bullet$;

$a_9 = \kappa_1\alpha_1 + \frac{1}{2}\alpha_1(\kappa_1 - \kappa_2)$;

$a_{10} = 2\kappa_1\alpha_1' + \frac{1}{2}\alpha_1(\kappa_1' - \kappa_2')$;

$a_{11} = -\alpha_1'$;

$a_{12} = \alpha_1$;

$a_{13} = \alpha_1'$;

$a_{14} = \alpha_2$;

$a_{15} = 2\alpha_2^\bullet$;

$a_{16} = -\kappa_2\alpha_1'$;

$a_{17} = \kappa_2\alpha_1$;

$a_{18} = \kappa_2\alpha_1'$

$a_{19} = \frac{1}{2}\alpha_2(3\kappa_2 - \kappa_1)$;

$a_{20} = 2\kappa_2\alpha_2^\bullet + \frac{1}{2}\alpha_2\kappa_2^\bullet - \frac{1}{2}\alpha_2\kappa_1^\bullet$;

$a_{21} = -\alpha_1\alpha_2\kappa_1$;

$a_{22} = -\alpha_1\alpha_2\kappa_2$;

$a_{23} = \frac{\alpha_2}{\alpha_1}$

$a_{24} = -\frac{\alpha_2\alpha_1^\bullet}{\alpha_1^2} + \frac{2\alpha_2'}{\alpha_1}$;

$a_{25} = -\frac{\alpha_1'}{\alpha_2}$;

$a_{26} = -\frac{\alpha_1^\bullet\alpha_2^\bullet}{\alpha_1^2} + \frac{\alpha_2''}{\alpha_1} + \frac{\alpha_1'\alpha_2'}{\alpha_2^2} + \frac{\alpha_1''}{\alpha_2}$

$a_{27} = -\frac{\alpha_2'}{\alpha_1}$

$a_{28} = \frac{\alpha_1}{\alpha_2}$

$a_{29} = -\frac{\alpha_1\alpha_2'}{\alpha_2^2} + \frac{2\alpha_1'}{\alpha_2}$

$a_{30} = \frac{\alpha_1^\bullet\alpha_2^\bullet}{\alpha_1^2} - \frac{\alpha_2''}{\alpha_1} - \frac{\alpha_1'\alpha_2'}{\alpha_2^2} + \frac{\alpha_1''}{\alpha_2}$

$a_{31} = 2\frac{\alpha_1'}{\alpha_1}$

$a_{32} = 2\frac{\alpha_2^\bullet}{\alpha_2}$

$a_{33} = 2$

$a_{34} = 2(\frac{\alpha_1'^\bullet}{\alpha_1} - \frac{\alpha_1^\bullet\alpha_1'}{\alpha_1^2} - \frac{\alpha_1'\alpha_2^\bullet}{\alpha_2^2} + \frac{\alpha_2''}{\alpha_2})$

$a_{35} = \alpha_2$

$a_{36} = \alpha_1$

$a_{37} = \frac{\alpha_1'}{\alpha_1\alpha_2}$

$a_{38} = -\frac{\alpha_2^\bullet}{\alpha_1\alpha_2}$

$a_{39} = \alpha_1$ $\qquad a_{41} = \dfrac{\alpha_2^{\bullet}}{\alpha_1\alpha_2}$

$a_{40} = \alpha_2$ $\qquad a_{42} = -\dfrac{\alpha_1'}{\alpha_1\alpha_2}$

where

$$(\;)^{\bullet} = \frac{\partial}{\partial\phi}(\;);;\; (\;)' = \frac{\partial}{\partial\theta}(\;)$$

$$\alpha_1 = \frac{r}{R}(R + r\cos\theta)$$

$$\alpha_1^{\bullet} = 0,\; \alpha_1^{\bullet\prime} = 0,\; \alpha_1' = -\gamma r \sin\theta,\; \alpha_1'' = -\gamma r \cos\theta$$

$$\alpha_2 = r$$

$$\alpha_2^{\bullet} = 0, \alpha_2' = 0,$$

$$\kappa_1 = \frac{1}{R_1} = \frac{\cos\theta}{R\gamma}$$

$$\kappa_1^{\bullet} = 0,\; \kappa_1' = \frac{1}{R}(-\zeta^{-2}\zeta'\cos\theta - \zeta^{-1}\sin\theta),$$

$$\kappa_1'' = \frac{1}{R}[2\zeta^{-3}(\zeta')^2\cos\theta - \zeta^{-2}\zeta''\cos\theta + 2\zeta^{-2}\zeta'\sin\theta - \zeta^{-1}\cos\theta]$$

$$\kappa_2 = \frac{1}{R_2} = \frac{1}{r}$$

$$\kappa_2^{\bullet} = 0,\; \kappa_2' = 0;$$

Appendix A2- Listing of functions $c_1 - c_{66}$ of chapter 3

$$c_1 = \frac{1}{\alpha_1}$$

$$c_2 = \frac{\alpha_1'}{\alpha_1\alpha_2}$$

$$c_3 = \kappa_1$$

$$c_4 = \frac{\alpha_2^\bullet}{2\alpha_1\alpha_2}$$

$$c_5 = \frac{1}{\alpha_2}$$

$$c_6 = \kappa_2$$

$$c_7 = \frac{1}{2\alpha_2}$$

$$c_8 = -\frac{\alpha_1'}{2\alpha_1\alpha_2}$$

$$c_9 = \frac{1}{2\alpha_1}$$

$$c_{10} = -\frac{\alpha_2'}{2\alpha_1\alpha_2}$$

$$c_{11} = \beta_1\kappa_1$$

$$c_{12} = \beta_1\kappa_1^\bullet$$

$$c_{13} = \kappa_2\beta_{12}\alpha_1'$$

$$c_{14} = -\beta_1^2$$

$$c_{15} = -\beta_1\beta_1^\bullet$$

$$c_{16} = -\beta_{12}\beta_2\alpha_1'$$

$$c_{17} = -\beta_{12}\kappa_1\alpha_2^\bullet$$

$$c_{18} = \beta_2\kappa_2$$

$$c_{19} = \beta_2\kappa_2'$$

$$c_{20} = -\beta_{12}\beta_1\alpha_2^\bullet$$

$$c_{21} = -\beta_2^2$$

$$c_{22} = -\beta_2\beta_2'$$

$$c_{23} = \frac{1}{2}\beta_2\kappa_1 - \frac{1}{4}(\kappa_2 - \kappa_1)\alpha_1\beta_{12}$$

$$c_{24} = \frac{1}{2}\beta_2\kappa_1' - \frac{1}{2}\beta_{12}\kappa_1\alpha_1' - \frac{1}{4}(\kappa_2 - \kappa_1)\beta_{12}\alpha_1'$$

$$c_{25} = \frac{1}{2}\beta_1\kappa_2 + \frac{1}{4}(\kappa_2 - \kappa_1)\alpha_2\beta_{12}$$

$$c_{26} = \frac{1}{2}\beta_1\kappa_2\kappa_2^\bullet - \frac{1}{2}\beta_{12}\kappa_2\alpha_2^\bullet + \frac{1}{4}(\kappa_2 - \kappa_1)\beta_{12}\alpha_2^\bullet$$

$$c_{27} = -\frac{1}{2}\beta_2\beta_1' + \frac{1}{2}\beta_{12}\beta_1\alpha_1'$$

$$c_{28} = -\frac{1}{2}\beta_1\beta_2^\bullet + \frac{1}{2}\beta_{12}\beta_2\alpha_2^\bullet$$

$$c_{29} = -\frac{1}{2}\beta_1\beta_2 + \frac{1}{2}\beta_{12}\beta_2\alpha_2^\bullet$$

$$c_{30} = b_1\beta_1$$

$$c_{31} = b_2\beta_{12}\alpha_2^\bullet$$

$$c_{32} = b_2\beta_2$$

$$c_{33} = b_1\beta_{12}\alpha_1'$$

$$c_{34} = b_1\kappa_1 + b_2\kappa_2$$

$$c_{35} = b_3\beta_1$$

$$c_{36} = b_4\beta_{12}\alpha_2^\bullet$$

$$c_{37} = b_4\beta_2$$

$$c_{38} = b_3\beta_{12}\alpha_1'$$

$$c_{39} = b_3\kappa_1 + b_4\kappa_2$$

$$c_{40} = \frac{1}{2}b_5\beta_2$$

$$c_{41} = -\frac{1}{2} b_5 \beta_{12} \alpha_1'$$

$$c_{42} = \frac{1}{2} b_5 \beta_1$$

$$c_{43} = -\frac{1}{2} b_5 \beta_{12} \alpha_2^{\bullet}$$

$$c_{44} = b_6 \beta_1 \kappa_1$$

$$c_{45} = b_6 \beta_1 \kappa_1^{\bullet} + b_7 \beta_{12} \kappa_1 \alpha_2^{\bullet}$$

$$c_{46} = b_7 \beta_2 \kappa_2$$

$$c_{47} = b_6 \beta_{12} \kappa_2 \alpha_1' + b_7 \beta_2 \kappa_2'$$

$$c_{48} = -b_6 \beta_1^2$$

$$c_{49} = -b_6 \beta_1 \beta_1^{\bullet} - b_7 \beta_1 \beta_{12} \alpha_2^{\bullet}$$

$$c_{50} = -b_7 \beta_2^2$$

$$c_{51} = -b_6 \beta_2 \beta_{12} \alpha_1' - b_7 \beta_2 \beta_2'$$

$$c_{52} = b_8 \beta_1 \kappa_1$$

$$c_{53} = b_8 \beta_{12} \kappa_1 \alpha_2^{\bullet} + b_9 \beta_1 \kappa_1^{\bullet}$$

$$c_{54} = b_9 \beta_2 \kappa_2$$

$$c_{55} = b_9 \beta_2 \kappa_2' + b_8 \beta_{12} \kappa_2 \alpha_1'$$

$$c_{56} = -b_8 \beta_1^2$$

$$c_{57} = -b_8 \beta_1 \beta_1^{\bullet} - b_9 \beta_1 \beta_{12} \alpha_2^{\bullet}$$

$$c_{58} = -b_9 \beta_2^2$$

$$c_{59} = -b_9 \beta_2 \beta_2' - b_8 \beta_{12} \beta_2 \alpha_1'$$

$$c_{60} = \frac{1}{2} b_{10} \beta_2 \kappa_1 - \frac{1}{4} b_{10} (\kappa_2 - \kappa_1) \alpha_1 \beta_{12}$$

$$c_{61} = \frac{1}{2} b_{10} \beta_2 \kappa_1' - \frac{1}{2} b_{10} \beta_{12} \kappa_1 \alpha_1' - \frac{1}{4} b_{10} (\kappa_2 - \kappa_1) \alpha_1 \beta_{12}$$

$$c_{62} = \frac{1}{2} b_{10} \beta_1 \kappa_2 + \frac{1}{4} b_{10} (\kappa_2 - \kappa_1) \alpha_2 \beta_{12}$$

$$c_{63} = \frac{1}{2} b_{10} \beta_1 \kappa_2^{\bullet} - \frac{1}{2} b_{10} \beta_{12} \kappa_2 \alpha_2^{\bullet} + \frac{1}{4} b_{10} (\kappa_2 - \kappa_1) \alpha_2 \beta_{12}$$

$$c_{64} = -\frac{1}{2} b_{10} \beta_2 \beta_1' + \frac{1}{2} \beta_1 \beta_{12} \alpha_1'$$

$$c_{65} = -\frac{1}{2} b_{10} \beta_1 \beta_2' + \frac{1}{2} b_{10} \beta_2 \beta_{12} \alpha_2^{\bullet}$$

$$c_{66} = -\frac{1}{2} b_{10} \beta_1 \beta_2 - \frac{1}{2} b_{10} \beta_2^{\bullet}$$

where the $b_1 - b_{10}$ are known constants of material properties, the values of α_1, α_2, κ_1, κ_2 are listed in Appendix - A1, and defined $\beta_1, \beta_2, \beta_{12}$ as

$$\beta_1 = \frac{1}{\alpha_1}, \beta_2 = \frac{1}{\alpha_2}, \beta_{12} = \beta_1 \beta_2 \text{ and } (\ )^{\bullet} = \frac{\partial}{\partial \phi}(\ ),\ (\ )' = \frac{\partial}{\partial \theta}(\ )$$

Appendix A3 - Listing of functions $e_1 - e_{41}$ of chapter 3

$$e_1 = a_4 c_{40}$$

$$e_2 = a_4(c'_{40} + c_{41}) + a_5 c_{40} + a_9(c'_{60} + c_{61}) + a_{10} c_{60}$$

$$e_3 = a_4 c_{40} + a_9 c_{60}$$

$$e_4 = -(a_5 c_{30} + a_6 c_{44})$$

$$e_5 = a_1 c_{32} + a_4 c_{42} + a_6 c_{46} + a_9 c_{62}$$

$$e_6 = a_1 c_{33} + a_4 c'_{36} + a_5 c_{42} + a_6 c_{47} + a_9 c'_{62} + a_{10} c_{62}$$

$$e_7 = a_6 c_{50} + a_9 c_{66}$$

$$e_8 = a_6 c_{51} + a_9(c'_{51} + c_{64}) + a_{10} c_{66}$$

$$e_9 = -a_6 c_{48}$$

$$e_{10} = a_1 c_{34} + a_6 c'_{49} + a_7 c_{49} + a_8 c_{57} + a_9 c'_{64} + a_{10} c_{64}$$

$$e_{11} = -(a_{12} c_{35} + a_{14} c_{40} + a_{17} c_{52} + a_{19} c_{60})$$

$$e_{12} = -(a_{11} c_{30} + a_{12} c'_{35} + a_{13} c_{35} + a_{14} c_{40} + a_{16} c_{44}$$
$$+ a_{17} c'_{52} + a_{18} c_{52} + a_{19} c_{61})$$

$$e_{13} = a_{12} c_{37} + a_{17} c_{54}$$

$$e_{14} = [a_{11} c_{32} + a_{12}(c'_{37} + c_{38}) + a_{13} c_{37} + a_{16} c_{46}$$
$$+ a_{17}(c'_{54} + c_{55}) + a_{18} c_{54}]$$

$$e_{15} = a_{11} c_{48} + a_{12} c'_{38} + a_{12} c_{38} + a_{14} \dot{c}_{43} + a_{15} c_{43} + a_{16} c_{47}$$
$$+ a_{17} c'_{55} + a_{18} c_{55} + a_{19} \dot{c}_{63} + a_{20} c_{63}$$

$$e_{16} = -(a_{14} c_{42} + a_{19} c_{62})$$

$$e_{17} = a_{17} c_{58}$$

$$e_{18} = a_{16} c_{50} + a_{17}(c'_{58} + c_{59}) + a_{18} c_{58}$$

$$e_{19} = a_{12} c_{39} + a_{16} c_{51} + a_{17} c'_{59} + a_{18} c_{59} + a_{19} \dot{c}_{65} + a_{20} c_{65}$$

$$e_{20} = -(a_{17} c_{56} + a_{19} c_{66})$$

$$e_{21} = a_{11} c_{34} + a_{12} c'_{39} + a_{13} c_{39}$$

$$e_{22} = -(a_{16} c_{48} + a_{17} c'_{66} + a_{18} c_{56} + a_{19} c_{64})$$

$$e_{23} = -(a_{28} c_{52} + a_{33} c_{60})$$

$$e_{24} = -[a_{25}c_{44} + 2a_{28}c'_{52} + a_{29}c_{52} + a_{31}c_{60} + a_{33}(c'_{60} + c_{61})]$$

$$e_{25} = a_{23}c_{44}$$

$$e_{26} = -[a_{21}c_{30} + a_{22}c_{35} + a_{23}(\ddot{c}_{44} + 2c_{45}) + a_{24}(\dot{c}_{44} + c_{60}) + a_{25}c'_{44} + a_{26}c_{44} + a_{27}(\dot{c}_{52} + c_{53}) + a_{28}\ddot{c}_{52} + a_{29}c'_{52} + a_{30}c_{52} + a_{31}c_{61} + a_{32}c'_{61}]$$

$$e_{27} = a_{28}c_{54}$$

$$e_{28} = a_{25}c_{46} + a_{28}(2c'_{54} + c_{55}) + a_{29}c_{54}$$

$$e_{29} = a_{21}c_{32} + a_{22}c_{37} + a_{23}\ddot{c}_{46} + a_{24}\dot{c}_{46} + a_{25}(c'_{46} + c_{47}) + a_{26}c_{46} + a_{27}\dot{c}_{54} + a_{28}(c''_{54} + 2c'_{55}) + a_{29}(c'_{54} + c_{55}) + a_{30}c_{54} + a_{32}c_{63} + a_{33}\dot{c}_{63}$$

$$e_{30} = -a_{23}c_{46}$$

$$e_{31} = a_{1}c_{33} + a_{22}c_{38} + a_{23}\ddot{c}_{47} + a_{24}\dot{c}_{47} + a_{25}c'_{47} + a_{26}c_{47} + a_{27}\dot{c}_{55} + a_{28}c''_{55} + a_{29}c'_{55} + a_{30}c_{70} + a_{31}\dot{c}_{63} + a_{32}c'_{63} + a_{33}\dot{c}_{63}{}' + a_{34}c_{63}$$

$$e_{32} = -a_{23}c_{47}$$

$$e_{33} = a_{28}c_{58}$$

$$e_{34} = a_{25}c_{50} + a_{28}(2c'_{58} + c_{59}) + a_{29}c_{58}$$

$$e_{35} = a_{23}\ddot{c}_{50} + a_{24}\dot{c}_{50} + a_{25}(c'_{50} + c_{51}) + a_{26}c_{50} + a_{27}\dot{c}_{58} + a_{28}(c''_{58} + 2c'_{59}) + a_{29}(c'_{58} + c_{59}) + a_{30}c_{58}$$

$$e_{36} = -(a_{23}c_{50} + a_{28}c_{56})$$

$$e_{37} = a_{23}\ddot{c}_{51} + a_{24}\dot{c}_{51} + a_{25}c'_{51} + a_{26}c_{51} + a_{27}\dot{c}_{59} + a_{28}c''_{59} + a_{29}c'_{59} + a_{30}c_{59} + a_{31}\dot{c}_{65} + a_{32}c'_{65} + a_{33}\dot{c}_{65}{}' + a_{34}c_{65}$$

$$e_{38} = -[a_{23}c_{50} + a_{25}c_{48} + 2a_{28}c'_{56} + a_{29}c_{56} + a_{31}c_{66} + a_{33}(c'_{66} + c_{64})]$$

$$e_{39} = a_{21}c_{34} + a_{22}c_{39}$$

$$e_{40} = -[a_{23}(\ddot{c}_{48} + 2\dot{c}_{49}) + a_{24}(\dot{c}_{48} + c_{49}) + a_{25}c'_{48} + a_{26}c_{63} + a_{27}(\dot{c}_{56} + c_{57}) + a_{28}c''_{56} + a_{29}c'_{56} + a_{30}c_{56} + a_{31}c_{64}]$$

$$e_{41} = -a_{23}c_{48}$$

where all a_i are given in Appendix A1, and all c_i are given in Appendix A2.

Appendix B1-Listing of function a_1- a_{80} of chapters 4 and 5

$$a_1 = \frac{1}{r}$$

$$a_2 = a_1$$

$$a_3 = -\frac{\gamma}{r\zeta}\sin\theta$$

$$a_4 = \frac{1}{r\zeta}$$

$$a_5 = \frac{\gamma}{r\zeta}\cos\theta$$

$$a_6 = \frac{1}{2r\zeta}$$

$$a_7 = \frac{\gamma}{2r\zeta}\sin\theta$$

$$a_8 = \frac{1}{2r^2\zeta}$$

$$a_9 = \frac{1}{r^2}$$

$$a_{10} = -\frac{1}{r^2}$$

$$a_{11} = -\frac{1}{Rr\zeta}\sin\theta$$

$$a_{12} = \frac{1}{R\ r\zeta^2}\cos\theta$$

$$a_{13} = \frac{1}{Rr\zeta}\sin\theta$$

$$a_{14} = -\frac{1}{r^2\zeta^2}$$

$$a_{15} = \frac{1+2\zeta}{(2r\zeta)^2}$$

$$a_{16} = \frac{1}{2r^2\zeta}(\gamma\cos\theta - \frac{1}{2})$$

$$a_{17} = \frac{2\gamma^2\sin 2\theta + (1-2\zeta)\gamma\sin\theta}{(2r\zeta)^2}$$

$$a_{18} = -\frac{1}{r^2\zeta}$$

$$a_{19} = -\frac{1}{Rr\zeta^2}\sin\theta$$

$$a_{20} = \frac{1}{r^2}$$

$$a_{21} = \frac{2}{r^2}$$

$$a_{22} = \frac{1}{r^2}$$

$$a_{23} = -\frac{\gamma}{r^2\zeta}\sin\theta$$

$$a_{24} = \frac{1}{r^2\zeta}$$

$$a_{25} = \frac{\gamma}{r^2\zeta}\cos\theta$$

$$a_{26} = -\frac{\gamma}{r^2\zeta}\sin\theta$$

$$a_{27} = \frac{1}{r^2\zeta}$$

$$a_{28} = \frac{\gamma}{r^2\zeta}\cos\theta$$

$$a_{29} = \frac{\gamma^2}{r^2\zeta^2}\sin^2\theta$$

$$a_{30} = \frac{1}{r^2\zeta^2}$$

$$a_{31} = \frac{\gamma^2}{r^2\zeta^2}\cos^2\theta$$

$$a_{32} = -\frac{\gamma}{2r^2\zeta^2}\sin\theta$$

$$a_{33} = -\frac{2\gamma^2}{r^2\zeta^2}\sin\theta\cos\theta$$

$$a_{34} = \frac{\gamma}{r^2\zeta^2}\cos\theta$$

$$a_{35} = \frac{1}{4r^2\zeta^2}$$

$$a_{36} = \frac{\gamma^2}{4r^2\zeta^2}\sin^2\theta$$

$$a_{37} = \frac{1}{4r^4\zeta^2}$$

$$a_{38} = \frac{\gamma}{2r^2\zeta^2}\sin\theta$$

$$a_{39} = \frac{1}{2r^3\zeta^2}$$

$$a_{40} = \frac{\gamma}{2r^3\zeta^2}$$

$$a_{41} = \frac{1}{r^4}$$

$$a_{42} = -\frac{1}{r^4}$$

$$a_{43} = \frac{1}{r^4}$$

$$a_{44} = -\frac{1}{Rr^3\zeta}\sin\theta$$

$$a_{45} = \frac{1}{Rr^3\zeta^2}\cos\theta$$

$$a_{46} = \frac{1}{Rr^3\zeta}\sin\theta$$

$$a_{47} = -\frac{1}{r^4\zeta^2}$$

$$a_{48} = \frac{1}{Rr^3\zeta}\sin^2\theta$$

$$a_{49} = -\frac{1}{Rr^3\zeta^2}\cos\theta$$

$$a_{50} = -\frac{1}{Rr^3\zeta}\sin\theta$$

$$a_{51} = \frac{1}{r^4\zeta^2}$$

$$a_{52} = \frac{1}{R^2r^2\zeta^2}\sin^2\theta$$

$$a_{53} = -\frac{1}{R^2r^2\zeta^3}\sin\theta\cos\theta$$

$$a_{54} = \frac{1}{R^2r^2\zeta^4}\cos^2\theta$$

$$a_{55} = \frac{1}{R^2r^2\zeta^2}\sin^2\theta$$

$$a_{56} = \frac{1}{r^4\zeta^4}$$

$$a_{57} = -\frac{2}{R^2r^2\zeta^2}\sin^2\theta$$

$$a_{58} = \frac{2}{R^2r^2\zeta^3}\sin\theta\cos\theta$$

$$a_{59} = \frac{1}{Rr^3\zeta^3}\sin\theta$$

$$a_{60} = -\frac{1}{Rr^3\zeta^4}\cos\theta$$

$$a_{61} = -\frac{1}{Rr^3\zeta^3}\sin\theta$$

$$a_{62} = \frac{(1+2\zeta)^2}{(2r\zeta)^4}$$

$$a_{63} = \frac{(1+2\zeta)(\gamma\cos\theta - \frac{1}{2})}{4r^4\zeta^3}$$

$$a_{64} = \frac{(\gamma\cos\theta - \frac{1}{2})^2}{4r^4\zeta^2}$$

$$a_{65} = \frac{\left(2\gamma^2\sin 2\theta + (1-2\zeta)\gamma\sin\theta\right)^2}{(2r\zeta)^4}$$

$$a_{66} = \frac{1}{r^4\zeta^2}$$

$$a_{67} = -\frac{1}{Rr^3\zeta^3}\sin\theta$$

$$a_{68} = \frac{1}{R^2r^2\zeta^4}\sin^2\theta$$

$$a_{69} = \frac{(1+2\zeta)\left(2\gamma^2\sin 2\theta + (1-2\zeta)\gamma\sin\theta\right)}{8r^4\zeta^4}$$

$$a_{70} = \frac{(\gamma\cos\theta - \frac{1}{2})\left(2\gamma^2\sin 2\theta + (1-2\zeta)\gamma\sin\theta\right)}{4r^4\zeta^3}$$

$$a_{71} = -\frac{\left(2\gamma^2\sin 2\theta + (1-2\zeta)\gamma\sin\theta\right)}{4r^4\zeta^3}$$

$$a_{72} = -\frac{\sin\theta\left(2\gamma^2\sin 2\theta + (1-2\zeta)\gamma\sin\theta\right)}{2Rr^3\zeta^4}$$

$$a_{73} = \frac{2\sin\theta}{Rr^3\zeta^2}$$

$$a_{74} = \frac{1}{R^2r^2\zeta^3}\sin^2\theta$$

$$a_{75} = -\frac{1}{r^4\zeta^2}(\gamma\cos\theta - \frac{1}{2})$$

$$a_{76} = -\frac{\sin\theta}{Rr^3\zeta^3}(\gamma\cos\theta - \frac{1}{2})$$

$$a_{77} = -\frac{1}{r}$$

$$a_{78} = \frac{1}{r}$$

$$a_{79} = -\frac{1}{r\zeta}$$

$$a_{80} = \frac{\gamma}{r\zeta}$$

Appendix B2 – Listing functions of $K_{ij}, K_{kij}, M_{ij}, G_{ij}$ of chapters 4 and 5

$$K_{uv}(j,n) = -A_{12}\, j\, n\, f_9 + A_{22}\,\gamma\,\mu_m\, f_{10} + \frac{A_{66}\,\mu_m\,(\gamma\, f_{11} - n\, f_{12})}{4}$$
$$-\frac{D_{12}\, j\,\mu_m\, f_{13}}{R\,r} + \frac{D_{22}\,\mu_m\, f_{14}}{R^2} + \frac{2D_{66}\,\mu_m\,(-2n\, f_{15} + n\, f_{16} + 8 f_{17})}{8r^2}$$

$$K_{uw}(j,n) = A_{11}\, j\,(f_{18} + f_{19}) + A_{12}\,(j\, f_{20} - f_{21}) - A_{22}\,\gamma^2 f_{22}$$
$$+\frac{D_{11}\, j\, n^2 f_{23}}{r^2} + D_{12}\left(-\frac{j\, n\, f_{24}}{R\,r\,\gamma} + \frac{j\,\mu_m^{\,2} f_{25}}{r^2} - \frac{n^2 f_{26}}{R\,r\,\gamma}\right)$$
$$+ D_{22}\left(\frac{n\, f_{27}}{R^2} - \frac{\mu_m^{\,2} f_{28}}{R\,r}\right) + D_{66}\,\mu_m^{\,2}\left(\frac{n\, f_{29}}{r^2} - \frac{f_{30}}{R\,r}\right)$$

$$K_{vv}(j,n) = A_{22}\,\mu_m^{\,2} f_{31} + \frac{A_{66}\,(f_{32} - j\, f_{33} - n\, f_{34} + j\, n\, f_{35})}{4} + \frac{D_{22}\,\mu_m^{\,2} f_{36}}{R^2}$$
$$+\frac{D_{66}\,(4\, j\, n\, f_{37} - 4\, j\, n\, f_{38} + j\, n\, f_{39} + 4 f_{40} - 8n\, f_{41} - 8\, j\, f_{42})}{4r^2}$$

$$K_{vw}(j,n) = -A_{12}\,\mu_m\, f_{43} - A_{22}\,\gamma\,\mu_m\, f_{44} - \frac{D_{12}\, n^2\,\mu_m\, f_{45}}{R\,r} + D_{22}\,\mu_m\left(\frac{n\, f_{46}}{R^2} - \frac{\mu_m^{\,2} f_{47}}{R\,r}\right)$$
$$+\frac{D_{66}\,(-2R\, j\, n\,\mu_m f_{48} + 2R\, n\,\mu_m f_{49} - 2r\mu_m f_{50} + R\, n\,\mu_m\, f_{51} - r\mu_m f_{52} + 2rj\mu_m f_{53})}{R\,r^2}$$

$$K_{ww} = A_{11}\,(f_{54} + f_{55}) + 2A_{12} f_{56} + A_{22} f_{57} + \frac{D_{11} j^2 n^2 f_{58}}{r^2}$$
$$+ D_{12}\left(\frac{-jn^2 f_{59}}{R\,r\,\gamma} + \frac{n^2\mu_m^{\,2} f_{60}}{r^2} + \frac{j^2\mu_m^{\,2} f_{61}}{r^2} - \frac{j^2\, n\, f_{62}}{R\,r\,\gamma}\right)$$
$$+ D_{22}\left(\frac{j\, n\, f_{63}}{R^2} + \frac{\mu_m^{\,4} f_{64}}{r^2} - \frac{n\mu_m^{\,2} f_{65}}{R\,r} - \frac{j\mu_m^{\,2} f_{66}}{R\,r}\right)$$
$$+ 4\, D_{66}\,\mu_m^{\,2}\left(\frac{j\, n\, f_{67}}{r^2} - \frac{n\, f_{68}}{R\,r} - \frac{j\, f_{69}}{R\,r} + \frac{f_{70}}{R^2}\right)$$

$$K_{kuu}(j,n) = A_1 (1 + \frac{e_k}{r})^2 j^2 n^2 f_{71} + \frac{G_1}{r^2}(1 + \frac{e_k}{r})^2 \mu_m^{\,2}\, j\, n\, f_{72}$$

$$K_{kuw}(j,n) = -\frac{A_1 e_k}{r}(1 + \frac{e_k}{r})\, j\, n^2 f_{73} - \frac{G_1 e_k}{r^3}(1 + \frac{e_k}{r})\mu_m^{\,2}\, j\, n^2 f_{74}$$

$$K_{kvv}(j,n)=(E_3+G_3)f_{75}$$

$$K_{kvw}(j,n)=\frac{E_2}{r}\mu_m j^2 f_{76}+(E_3+G_3)(\frac{\mu_m e_k}{r}j\,nf_{77}-\frac{e_k\mu_m}{R}j_{78}f)$$

$$K_{kww}(j,n)=\frac{E_1}{r^2}\mu_m f_{79}-\frac{E_2 e_k\mu_m}{r^2}(j^2+n^2)f_{80}-\frac{2E_2 e_k\mu_m}{Rr}(jf_{81}+n\,f_{82})$$
$$+(E_3+G_3)e_k\mu_m\left[\frac{j\,n}{r^2}f_{84}+\frac{1}{R^2}f_{85}-\frac{1}{Rr}(n\,f_{86}+j\,f_{87})\right]$$
$$-E_3(j^2+n^2)f_{88}+E_3 j^2 n^2 f_{89}+\frac{A_1 e_k{}^2}{r^2}j^2 n^2 f_{90}$$
$$+\frac{G_1 e_k{}^2}{2r^4}j^2 n^2\mu_m{}^2 f_{91}$$

$$M_{uu}(j,n)=f_{18}$$

$$M_{vv}(j,n)=f_{19}$$

$$M_{ww}(j,n)=f_{19}$$

$$G_{uu}(j,n)=f_{95}$$
$$G_{uw}(j,n)=-\frac{1}{2}f_{96}+\frac{1}{2}n\,f_{97}+\frac{j}{2}f_{98}$$
$$G_{vv}(j,n)=f_{99};$$
$$G_{vw}(j,n)=-\mu_m\,f_{100}$$
$$G_{ww}(j,n)=f_{101}+2\,f_{102}$$

where the values of f_1-f_{102} are listed in Appendix – B3

Appendix B3 - Listing of integrating function $f_1 - f_{102}$ of chapters 4 and 5

$$f_1 = \int_0^{2\pi} \cos j\theta \cos n\theta \, d\theta$$

$$f_2 = \gamma \int_0^{2\pi} \cos\theta \cos j\theta \cos n\theta \, d\theta$$

$$f_3 = \int_0^{2\pi} \frac{1}{\zeta} \sin j\theta \cos n\theta \, d\theta$$

$$f_4 = \int_0^{2\pi} \zeta \cos j\theta \cos n\theta \, d\theta$$

$$f_5 = \gamma \int_0^{2\pi} \sin\theta \sin j\theta \cos n\theta \, d\theta$$

$$f_6 = \gamma \int_0^{2\pi} \sin\theta \sin n\theta \cos j\theta \, d\theta$$

$$f_7 = \int_0^{2\pi} \frac{1}{\zeta} \sin^2\theta \sin j\theta \cos n\theta \, d\theta$$

$$f_8 = \int_0^{2\pi} \frac{(1+2\zeta)^2}{\zeta^3} \sin j\theta \sin n\theta \, d\theta$$

$$f_9 = f_1$$

$$f_{10} = \int_0^{2\pi} \frac{1}{\zeta} \sin\theta \sin j\theta \cos n\theta \, d\theta$$

$$f_{10} = f_{11}$$

$$f_{12} = \int_0^{2\pi} \sin j\theta \sin n\theta \, d\theta$$

$$f_{13} = \int_0^{2\pi} \frac{1}{\zeta} \cos\theta \cos j\theta \cos n\theta \, d\theta$$

$$f_{14} = \int_0^{2\pi} \frac{1}{\zeta^2} \sin\theta \cos\theta \sin j\theta \cos n\theta \, d\theta$$

$$f_{15} = \int_0^{2\pi} \frac{(1+2\zeta)}{\zeta^2} \cos\theta \sin j\theta \sin n\theta \, d\theta$$

$$f_{16} = \int_0^{2\pi} \frac{(1+2\zeta)}{\zeta^2} \sin j\theta \sin n\theta \, d\theta$$

$$f_{17} = \int_0^{2\pi} [\frac{1+2\zeta}{4\zeta^3}\gamma^2 \sin 2\theta + \frac{(1-4\zeta^2)}{8\zeta^3}\gamma \sin\theta] \sin j\theta \cos n\theta \, d\theta$$

$$f_{18} = f_1; \; f_{19} = f_2 = f_{20}; \; f_{21} = f_5$$

$$f_{22} = \int_0^{2\pi} \frac{1}{\zeta} \sin\theta \cos\theta \sin j\theta \cos n\theta \, d\theta$$

$$f_{23} = f_4; \; f_{24} = f_6$$

$$f_{25} = \int_0^{2\pi} \frac{1}{\zeta} \cos j\theta \cos n\theta \, d\theta$$

$$f_{25} = f_5; \; f_{27} = f_7$$

$$f_{28} = \int_0^{2\pi} \frac{1}{\zeta^2} \sin\theta \sin j\theta \cos n\theta \, d\theta$$

$$f_{29} = f_{16}$$

$$f_{30} = \int_0^{2\pi} \frac{(1+2\zeta)}{\zeta^2} \sin\theta \sin j\theta \cos n\theta \, d\theta$$

$$f_{31} = f_{25}$$

$$f_{32} = \int_0^{2\pi} \frac{\gamma^2 \sin^2\theta}{\zeta} \cos j\theta \cos n\theta \, d\theta$$

$$f_{33} = f_5; \; f_{34} = f_6$$

$$f_{35} = \int_0^{2\pi} \zeta \sin j\theta \sin n\theta \, d\theta$$

$$f_{36} = \int_0^{2\pi} \frac{1}{\zeta^3} \cos^2\theta \cos j\theta \cos n\theta \, d\theta$$

$$f_{37} = \int_0^{2\pi} \frac{\gamma^2 \cos^2\theta}{\zeta} \sin j\theta \sin n\theta \, d\theta$$

$$f_{38} = \int_0^{2\pi} \frac{\gamma \cos\theta}{\zeta} \sin j\theta \sin n\theta \, d\theta$$

$$f_{39} = f_3$$

$$f_{40} = \int_0^{2\pi} [\gamma^4 \sin^2 2\theta + \gamma^3 (1-2\zeta) \sin\theta \sin 2\theta + \frac{1}{4}\gamma^2 \sin^2\theta (1-2\zeta)^2] \cos j\theta \cos n\theta \, d\theta$$

$$f_{41} = \int_0^{2\pi} [\frac{(\gamma\cos\theta - 1/2)}{2\zeta^2}\gamma^2 \sin 2\theta + \frac{(\gamma\cos\theta - 1/2)(1-2\zeta)}{4\zeta^2}\gamma \sin\theta] \sin n\theta \cos j\theta \, d\theta$$

$$f_{42} = \int_0^{2\pi} [\frac{(\gamma\cos\theta - 1/2)}{2\zeta^2}\gamma^2 \sin 2\theta + \frac{(\gamma\cos\theta - 1/2)(1-2\zeta)}{4\zeta^2}\gamma\sin\theta]\sin j\theta\cos n\theta\, d\theta$$

$f_{43} = f_1$; $f_{44} = f_{45} = f_3$

$$f_{46} = \int_0^{2\pi} \frac{1}{\zeta^2}\sin\theta\cos\theta\sin n\theta\cos j\theta\, d\theta$$

$$f_{47} = \int_0^{2\pi} \frac{1}{\zeta^3}\cos\theta\cos j\theta\cos n\theta\, d\theta$$

$$f_{48} = \int_0^{2\pi} \frac{(\gamma\cos\theta - 1/2)}{\zeta}\sin j\theta\sin n\theta\, d\theta$$

$$f_{49} = \int_0^{2\pi} \frac{\gamma^2}{\zeta^2}\sin 2\theta\sin n\theta\cos j\theta d\theta$$

$$f_{50} = \int_0^{2\pi} \frac{\gamma^3}{\zeta^3}\sin\theta\sin 2\theta\cos j\theta\cos n\theta d\theta$$

$$f_{51} = \int_0^{2\pi} \gamma\frac{(1-2\zeta)}{\zeta^2}\sin\theta\cos\theta\sin n\theta\, d\theta$$

$$f_{52} = \int_0^{2\pi} \gamma\frac{(1-2\zeta)}{\zeta^3}\sin^2\theta\cos j\theta\cos n\theta\, d\theta$$

$$f_{53} = \int_0^{2\pi} \frac{(\gamma\cos\theta - 1/2)}{\zeta^2}\sin\theta\sin j\theta\cos n\theta\, d\theta$$

$f_{54} = f_1$; $f_{55} = f_2$; $f_{56} = f_2$

$$f_{57} = \int_0^{2\pi} \frac{\gamma^2\cos^2\theta}{\zeta}\cos j\theta\cos n\theta\, d\theta$$

$f_{58} = f_4$; $f_{59} = f_5$; $f_{60} = f_{25}$; $f_{61} = f_{25}$; $f_{62} = f_6$; $f_{63} = f_7$

$$f_{64} = \int_0^{2\pi} \frac{1}{\zeta^3}\cos j\theta\cos n\theta\, d\theta$$

$$f_{65} = \int_0^{2\pi} \frac{1}{\zeta^2}\sin\theta\sin n\theta\cos j\theta\, d\theta$$

$f_{66} = f_{28}$

$$f_{67} = \int_0^{2\pi} \frac{1}{\zeta}\sin j\theta\sin n\theta\, d\theta$$

$f_{68} = f_{65}$; $f_{69} = f_{28}$

$$f_{70} = \int_0^{2\pi} \frac{\sin^2\theta}{\zeta^3} \cos j\theta \cos n\theta \, d\theta$$

$f_{71} = f_{12}$; $f_{72} = f_{64}$; $f_{73} = f_1$; $f_{74} = f_{64}$; $f_{75} = f_{12}$

$f_{76} = f_{25}$; $f_{77} = f_3$; $f_{78} = f_{28}$; $f_{79} = f_{64} = f_{80} = f_{64}$

$$f_{81} = \int_0^{2\pi} \frac{\sin\theta}{\zeta^3} \sin j\theta \cos n\theta \, d\theta$$

$$f_{82} = \int_0^{2\pi} \frac{\sin\theta}{\zeta^3} \sin n\theta \cos j\theta \, d\theta$$

$$f_{83} = \int_0^{2\pi} \frac{(r + R\cos\theta + r\sin^2\theta)}{\zeta^4} \cos j\theta \cos n\theta \, d\theta$$

$$f_{84} = \int_0^{2\pi} \frac{1}{\zeta^2} \sin j\theta \sin n\theta \, d\theta$$

$$f_{85} = \int_0^{2\pi} \frac{\sin^2\theta}{\zeta^4} \cos j\theta \cos n\theta \, d\theta$$

$f_{86} = f_{82}$; $f_{87} = f_{81}$; $f_{88} = f_{89} = f_{90} = f_1$; $f_{91} = f_{64}$

$f_{92} = f_{35}$; $f_{93} = f_{94} = f_{98} = f_4$; $f_{95} = f_{97} = f_{35}$

$f_{96} = f_5$; $f_{99} = f_{102} = f_2$; $f_{100} = f_{101} = f_1$

Appendix C – Listing of functions b_1- b_{20} of chapter 5

$$b_1 = \frac{E_k I_{zk}}{2(r+e_k)} \frac{R^2}{r^2(R+r\cos\theta)}$$

$$b_2 = \frac{E_k I_{zk}}{r(r+e_k)^2} \frac{1}{(1+r\cos\theta)}$$

$$b_3 = -\frac{E_k I_{zk}}{r^2(r+e_k)^2} \frac{e_k}{(1+r\cos\theta)^2}$$

$$b_4 = \frac{E_k I_{zk}}{R\ r\ (r+e_k)^2} \frac{e_k \sin\theta}{(1+r\cos\theta)^3}$$

$$b_5 = \frac{E_k I_{zk} e_k}{R^2 r\ (r+e_k)^2} \frac{(r+R\cos\theta+r\sin^2\theta)}{(1+r\cos\theta)^2}$$

$$b_6 = \frac{E_k I_{zk}}{2(r+e_k)^3} + \frac{G_k\ J_k}{2(r+e_k)^3}$$

$$b_7 = [\frac{E_k I_{zk}}{2(r+e_k)^3} + \frac{G_k J_k}{2(r+e_k)^3}] \frac{e_k}{r(1+\gamma\cos\theta)}$$

$$b_8 = [\frac{E_k I_{zk}}{2(r+e_k)^3} + \frac{G_k J_k}{2(r+e_k)^3}] \frac{e_k^2 \sin^2\theta}{R^2\zeta^4}$$

$$b_9 = [\frac{E_k I_{zk}}{(r+e_k)^3} + \frac{G_k J_k}{(r+e_k)^3}] \frac{e_k}{r\zeta}$$

$$b_{10} = [\frac{E_k I_{zk}}{(r+e_k)^3} + \frac{G_k J_k}{(r+e_k)^3}] \frac{e_k \sin\theta}{R\zeta^2}$$

$$b_{11} = [\frac{E_k I_{zk}}{(r+e_k)^3} + \frac{G_k J_k}{(r+e_k)^3}] \frac{e_k^2 \sin\theta}{Rr\zeta^3}$$

$$b_{12} = \frac{E_k I_{\eta k}}{2(r+e_k)^3} + \frac{G_k\ A_k}{2(r+e_k)}$$

$$b_{13} = \frac{E_k I_{\eta k}}{(r+e_k)^3}$$

$$b_{14} = \frac{E_k I_{\eta k}}{2(r+e_k)^3}$$

$$b_{15} = \frac{E_k A_k (r + e_k)}{2r^2}$$

$$b_{16} = \frac{E_k A_k e_k}{r^2}$$

$$b_{17} = \frac{1}{2} \frac{E_k A_k}{r + e_k} \frac{e_k^2}{r^2}$$

$$b_{18} = \frac{1}{2r^2} \frac{G_k J_k}{r + e_k}$$

$$b_{19} = \frac{G_k J_k}{r^4}$$

$$b_{20} = \frac{1}{2r^4} \frac{G_k J_k}{r + e_k}$$

Appendix D - Buckling Analysis of Ring-Stiffened Toroidal Shell Using ADINA-4rings

Preprocessing:

ADINA-AUI-ADINA

Control-Heading-Name (example: stiffened toroidal shell)

Control-Degrees of Freedom-ok

Control-Analysis Assumption-Large Deflection

Geometry-Points	x1	x2	x3
1	16	0.0	0.0
2	20	-4	0.0
3	24	0.0	0.0
4	15.643	0.0	0.0
5	24.357	0.0	0.0
6	20	4	
7	20	4.357	0.0
8	20	-4.357	0.0

Geometry-Lines-Define-

-Add
Line Number: 1
Type: Circle
Points: 1, 2, 3

-Add
Line Number: 2
Type: Straight
Points: 4, 1

-Add
Line Number: 3
Type: Straight
Points: 3, 5

-Add
Line Number: 4
Type: Arc
Points: 1, 3, 6

-Add
Line Number: 5
Type: Arc
Points: 4, 5, 7

-Add
Line Number: 6
Type: Arc
Points: 1, 3, 2

-Add
Line Number: 7
Type: Arc
Points: 4, 5, 8

-ok-

Geometry-Surface-Define-

-Add
Surface Number: 1
Type: Revolve
Initial Line: Line 1-Angle of Rotation-360^0

-Add
Surface number: 2
Type: Patch
Lines: 2, 4, 3, 5

-Add
Surface number: 3
Type: Patch
Lines: 2, 6, 3, 7

-Add
Surface Number: 4
Type: Transform
Initial Surfaces: 2, 3
Copies of Surfaces: 4
Transform Number-Add-Angle of Rotation-90^0

-ok-

Model-Material-Elastic-Isotropic-

-Add
Young's Modulus: E=0.207e12
Poisson Ratio: $\nu=0.3$ -ok-

(applying for the orthotropic material, see an example in the end of this program)

Meshing-Element Groups-
-Add
Group Number: 1
Type: Shell-Save

-Add
Group Number: 2
Type: Shell

-ok-

Meshing-Mesh Density-Surface 1
-Method-Use Number of Divisions
-Number of Subdivisions
u: 40 v:200

Meshing-Create Mesh-Surface
-Type: Shell
-Element Group: 1
-Nodes per Element: 9
-Surface Number: 1

Meshing-Mesh Density-Surface 2
-Method-Use Number of Divisions
-Number of Subdivisions
u: 2 v:20
-Also Sign the Surfaces: 3-11

Meshing-Create Mesh-Surface
-Type: Shell
-Element Group: 2
-Nodes per Element: 9
-Surface Number: 2-11

-ok-

Model-Boundary Conditions-Apply on the Nodes
-Count the Nodes along the Inner Equator
-Nodes: 1-7961(step: 40)
-Apply: Fixed to the above Nodes

-ok-

Model-Loading-Apply
-Type: Pressure-Define
-Add
Pressure Number: 1
Magnitude: -1

-ok-

Model-Loading-Apply Load
-Apply to: Surface
-Site Number: 1

Analysis-In dialog box beside ADINA box, select the analysis.
-Type: Linearized Buckling
-Click Icon of Analysis Option (Right of Analysis Type Dialog)
-Number of Modes: type the number of the modes

Processing of File:

Solution-Data File/Run
-File Name: buckling1
-Save
(ADINA Runs)
-ok-close-close

Postprocessing:

ADINA-PLOT-File-Open: buckling1.por

Definitions-Response-
-Type: Mode Shape
-Number: 1
-Select: xyz view for the three-dimensional view from the command, then save as BMP file.
-Clear
-Mesh Plot
-Select: xz view for the projection view, then save as BMP file.
-Click "movie icon" to see animation.

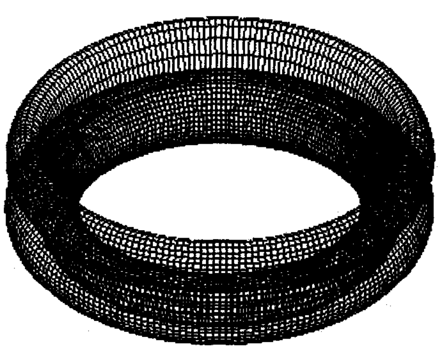

(a) Mode shape of unstiffened shell with the original shell

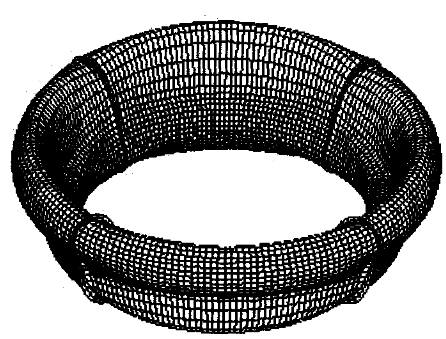

(b) Mode shape of stiffened shell with 4 rings

Example of applying the orthotropic material using ADINA

A composite material is chosen for this example. The material properties are based on [Wang, 1999] and taken as

$$E_1 = 7.44\times10^8\ Pa\,;\ E_2 = 3.47\times10^9\ Pa$$
$$\nu_{12} = 0.192\,;\ \nu_{21} = 0.45$$
$$G_{12} = 2.04\times10^9\ Pa; G_{13} = 0.099\times10^9; G_{23} = 0.137\times10^9$$
$$\rho = 700\ Kg/cm^3$$

The following procedures are the steps to apply for the orthotropic material

Model-Orthotropic Axes Systems-Define
- -Add
- -System Number: 1
- -Defined by: Surface

-ok-

Model-Orthotropic Axes Systems-Assign (material)
- -Add
- -Surface Site: 1
- -Axes System: 1
- -Click the icon next to the axes system
- -Choose: a direction from Local x (2 direction)
  b direction from Local y (1 direction)

-ok-

Model-Material-Elastic-Orthotropic
- -Add
- -Apply: at this step, input the values of the material properties given above

-ok-